

UAV for Medical Equipment Distribution

Final Design Review Report

June 9, 2021



Presented to

Vertical Flight Society

Prepared By

Brandon Halebsky
Justin Slavick
Logan Christensen
Richard Barakat

Mechanical Engineering Department
California Polytechnic State University
San Luis Obispo
Spring 2021

Statement of Disclaimer

Since this project is a result of a class assignment, it has been graded and accepted as fulfillment of the course requirements. Acceptance does not imply technical accuracy or reliability. Any use of information in this report is done at the risk of the user. These risks may include catastrophic failure of the device or infringement of patent or copyright laws. California Polytechnic State University at San Luis Obispo and its staff cannot be held liable for any use or misuse of the project.

Abstract

This Final Design Review document overviews the senior design project participating in the Vertical Flight Society's 38th Annual Student Design Competition sponsored by The Boeing Company. The goal of this project and competition is to develop an unmanned vertical lift for medical equipment distribution capable of safely delivering a 50 kg payload over distances up to 200 km. This system must be autonomous and have a backup plan to land if any part of the system malfunctions. We discuss the research and justification that drove the selection of the aircraft configuration, a winged quadcopter with a rear propeller. Furthermore, we document our reasoning and analysis for sizing and shaping of the rotors, propeller, and wings, selecting a hybrid-electric turbogenerator for the powerplant, designing the payload release mechanism, and sizing and shaping of the semi-monocoque structure. We provide analysis that numerically verifies our UAV's ability to meet the requirements for payload capacity, range, mission time, and geometric envelope.

Table of Contents

1. Introduction	1
2. Background	1
2.1 Customer Research.....	1
2.2 Product Research.....	2
2.3 Technical Research.....	5
3. Objectives.....	9
3.1 Customer Wants and Needs	9
3.2 Quality Function Deployment.....	10
3.3 Engineering Specifications.....	10
3.4 Specification Risks.....	12
4. Concept Design	12
4.1 Ideation.....	13
4.2 Idea Refinement and Selection.....	14
4.3 Preliminary Design.....	16
5. Critical Design.....	27
5.1 Design Description.....	27
5.2 Design Justification	39
5.3 Safety, Maintenance, and Repair Considerations.....	54
5.4 Cost Analysis.....	54
6. Final Design	56
6.1 Design Changes.....	56
6.1.1 Component Layout.....	57
6.1.2 Payload Release Mechanism Weight Reductions.....	57
6.1.3 Fuselage Shape and Structure	59
7. Manufacturing	61
7.1 Full-System Manufacturing Plan	61
7.1.1 Material and Part Procurement	61
7.1.2 Manufacturing Operations	62
7.1.3 Assembly Story.....	62
7.1.4 Outsourcing	63
7.2 Prototype Manufacturing	64
7.2.1 Manufacturing Operations	65
7.2.2 Part Procurement and Cost Analysis.....	66
7.2.3 Prototype Assembly	66
8. Design Verification	68
8.1 Evaluation of Specifications.....	68
8.2 Testing.....	70
8.3 Data Collection and Analysis.....	71
8.4 Design Performance	73
9. Project Management.....	74
10. Conclusion.....	75
References	76

1. Introduction

In the medical world, there are many roadblocks that prevent responders from reaching a patient during emergencies. Whether responders are getting stuck in traffic, scaling mountains, driving on hilly highways, or scrambling past icy roads, patients commonly fail to receive their much-needed medical treatment. A quicker and more reliable method of transportation is to avoid the roads altogether, a feat that can be achieved through means of a medical supply delivery drone.

This idea is one that Boeing sees potential in and is making an effort to bring it to life by sponsoring the 2025 Unmanned Vertical Lift for Medical Equipment Distribution design competition. Boeing is one of the world's largest aerospace companies with a history of manufacturing airplanes, rotorcraft, satellites, rockets and more. They are sponsoring this student design competition to promote interest in the vertical flight industry and find solutions for the issues faced by medical responders regarding efficient delivery of urgent medical treatment.

The goal of this report is to outline the work done in our efforts to design a vertical unmanned aerial vehicle capable of delivering medical supplies to a specific site. We will design it with the intent to meet requirements described in the design competition, as well as to meet any needs and wants we discover through customer-focused research and relevant case studies.

Our team consists of Brandon Halebsky, Justin Slavick, Logan Christensen, and Richard Barakat, 4 senior mechanical engineering students enrolled at California Polytechnic State University, San Luis Obispo. This report will include the following sections: Background which describes the relevant product and technical research, Objectives which describes the customer requirements and corresponding engineering specifications, Project Management which outlines the timeline of the project, Concept Design which overviews our ideation, idea selection, and preliminary design, and Conclusion which summarizes our project goals and progress.

2. Background

Our design research focused on the customers' wants and needs, existing products that meet some of the customer needs, and technical research regarding the governing engineering principles and design features of a UAV. The primary sources of information were the Vertical Flight Society's website, online articles interviewing customers of services that fulfill a similar need, websites of companies that create a similar product and existing U.S. patents, and textbooks and an interview for technical information regarding UAVs.

2.1 Customer Research

The host of the design competition, the Vertical Flight Society, has outlined a list of design specifications for the unmanned vertical lift that define the desired range, payload carrying capacity, dimensional limits, speed, and safety requirements [1]. Based on these design constraints, we were able to define the framework of engineering specifications that our design must lie within in order to satisfy the requirements of the design competition.



To better understand the customer needs, we researched articles that included interviews from medical professionals and patients who have benefited from delivery of medical supplies by UAV. A 2017 Times article covered the use of Zipline medical drones that deliver blood to hospitals in Rwanda. The implementation of delivery drones to transport medical supplies, particularly blood, across a distance of 100 km led to a reduction in delivery time from three hours to fifteen minutes. According to the head surgeon, he does not care how the blood arrives, as long as he receives it in less than fifteen minutes [2].



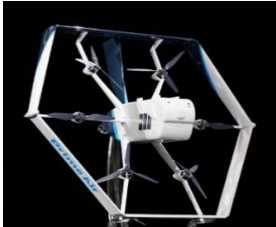
A 2018 article published by Rural Reporters also covered the use of Zipline drones in Rwanda and featured an interview with the Head of Biomedical Services at the Rwanda Biomedical Center, Dr. Jean Baptize, who revealed that they lose 6 percent of blood due to overstocking and that drone-deliveries can reduce the need for overstocking and thus reduce wasted medical supplies. Additionally, he outlined goals to cover 80 percent of Rwanda with blood deliveries by drone and expand the deliveries to other supplies such as anti-rabies vaccines. Lastly, he also described two possible uses of drone-deliveries by hospitals: routine deliveries for hospitals equipped with freezers that can store blood from 2-8°C, and emergency deliveries for hospitals without enough freezer capacity [3].

2.2 Product Research

To gauge the existing solutions to the demands of customers and the design competition, we looked for products and services on the market that provide unmanned aerial delivery of medical supplies or other payload with an emphasis on vertical take-off and landing aircraft. Five existing UAVs that can deliver a payload are shown and compared in Table 1.

Table 1: Performance comparison of existing drone-delivery products and services.

Product	Range	Max Payload	Cruise Speed	Vertical Takeoff (yes / no)
Zipline Drone [4] 	160 km	2 kg	101 km/h	no
DHL Parcelcopter [5] 	65 km	4 kg	130 km/h	yes





Product	Range	Max Payload	Cruise Speed	Vertical Takeoff (yes / no)
Griff 135 [6] 	-*	50 kg	-	yes
VoloDrone [7] 	40 km	200 kg	80 km/h	yes
Amazon Prime Air Drone [8] 	24 km	2.3 kg	-	yes

* 25-30 minutes of flight time with 30 kg payload

The existing UAVs displayed in Table 1 provide unique solutions that meet some of the needs expressed by the customers. The Zipline drone provides the best range by far but is not able to lift heavy payloads and does not takeoff vertically. The DHL Parcelcopter is the fastest drone out of the five and features a unique combination of propellers and airfoils but has a limited range and payload carrying capacity. The Griff 135 can lift a payload up to 50 kg and has vertical takeoff capability but is only capable of flying for 25-30 minutes with a 30 kg payload. The VoloDrone can lift the heaviest payload out of the five UAVs as it can generate a large lift force with 18 propellers but has a limited range of 40 km. The Amazon Prime Air drone features propellers whose angle relative to the vertical axis can be adjusted to vary the amount of lift and thrust generated based on the demands of the flight path and conditions. Although the Amazon Prime Air drone satisfies the vertical takeoff requirement, its range is the worst of the five UAVs and is unable to lift heavy payloads.

To capture a wider range of existing products, we also researched vertical takeoff (VTOL) aircraft that do not necessarily deliver a payload and may carry a human passenger. Several existing VTOL aircraft are shown and compared in Table 2.

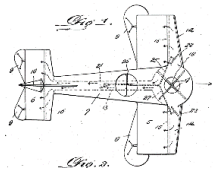
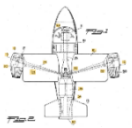
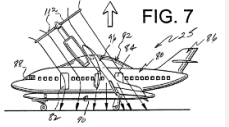
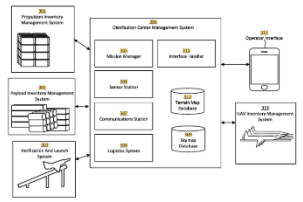
Table 2: Performance comparison of existing VTOL aircraft.

UAV	Range / Flight Time	Max Payload	Power Source
Wisk Cora [9] 	40 km (22 NM)	180 kg (400 lb)	battery + 12 motors
SCHIEBEL Camcopter S-100 [10] 	200 km	50 kg	engine
BETA ALIA-250 [11] 	463 km (250 NM)	635 kg (1400 lb)	battery + 4 motors
Joby Aviation VTOL Aircraft [12] 	240 km	-	motors

The SCHIEBEL Camcopter S-100 uses an unmanned, single rotor helicopter configuration to meet two of the major requirements of the design competition: 200 km range and up to 50 kg payload capacity. However, the fuselage of the Camcopter is too small to package the required payload sizes. The Wisk Cora and Beta Alia-250 both use similar winged quadcopter designs with rear propellers combined with fully electric propulsion to achieve payload capacities well above our target of 50 kg. However, the Wisk Cora can only reach a range of 40 km while the Beta Alia-250 can fly up to 463 km; this difference may be due to difference in battery technology and motor efficiency as both manufacturers make their powerplants in-house. Furthermore, differences in the overall size of the aircrafts as well as the number and size of rotors may be contributing factors as the Cora has 12 relatively small rotors while the Alia-250 has four large rotors in a quadcopter configuration.

In addition to researching existing UAVs, we also researched existing patents related to UAVs, vertical takeoff and landing aircraft, and management systems of remote aircraft. Several patents with relevant technologies are summarized in Table 3.

Table 3: Patents pertaining to vertical lift aircraft.

Patent Name	Patent No.	Description	Illustration
Aircraft propulsion and control [13]	US 1491954 A	<ul style="list-style-type: none"> Adapts standard airplane design to enable hovering Fan blows high speed air across the top surface of the wings and generate more lift 	
Unmanned aerial vehicle with vertical takeoff and landing capability [14]	CA 2929254 C	<ul style="list-style-type: none"> UAV with left and right airfoil-shaped wings that generate lift in forward flight Thrust generating devices attached to wings and fuselage 	-
Airplane for vertical take-off in horizontal attitude [15]	US 2780424 A	<ul style="list-style-type: none"> Aircraft capable of landing or taking-off vertically Jet motors able to rotate relative to fuselage 	
Vertical takeoff and landing aircraft [16]	US 6896221 B1	<ul style="list-style-type: none"> Wings and engines that can pivot about fuselage Can land vertically or horizontally on runway 	
Unmanned aerial vehicle management system [17]	US 1039554 B2	<ul style="list-style-type: none"> UAS provides real-time information about flight route to UAV UAV dynamically updates mission based on received information 	

These patents highlight existing technologies related to vertical takeoff and landing systems that enable both vertical and horizontal flight. The first patent in Table 3 titled “Aircraft propulsion and control” was granted in 1924 and provides a simple but unique method of generating more lift with a traditional airplane design by blowing high-speed air along the top of the wings. The fourth patent in the table is a more contemporary concept that involves changing the propeller angle to generate lift and thrust as needed, similar to the Amazon Prime Air Drone included in Table 1. The fifth patent in Table 3 was granted to Zipline for their aerial management system that outlines how the UAV receives and adapts its flight path based on information received from the aerial system. This is relevant technology that essentially behaves as a feedback loop for the UAV to adjust its path based on information provided in real-time which allows for safe and efficient travel.

2.3 Technical Research

The objective of this competition is to design an aircraft capable of unmanned vertical lift. The aircraft needs to be able to travel autonomously, meaning that all flight control must come from electronic intelligence and a control subsystem, rather than a manned crew. Typically, this is

achieved in the form of an Unmanned Aircraft System (UAV) or a drone aircraft. In his book, *Unmanned Aircraft Systems: UAVS Design, Development, and Deployment*, Reg Austin distinguishes a difference between the two types of aircraft. A drone is defined by non-communicative flight, where the drone would fly a pre-programmed mission and return to the launch site with no input from a ground control crew. A UAV, on the other hand, contains communications and radio transmission subsystems that allow it to send and receive data, as well as take corrective action if systems get damaged [18]. A UAV is often paired with a ground crew forming a complete Unmanned Aircraft System (UAS). For the purposes of this project, we will be considering both aircraft types in our design.

A drone aircraft typically comprises of three systems: navigation, payloads, and the aircraft itself. On top of these, UASs also contain systems for communications, a control station, and launch and recovery, with others included as needed.

- The navigation system exists to tell the plane, and any control crew, where the aircraft is at a given time during autonomous flight. While Inertial Navigation Systems (INS) have been used in the past, most modern aircraft use a Global Positioning System (GPS) [19].
- The payload system is any weight carried by the aircraft that does not directly contribute to flight or control. The payload for this aircraft will be 50kg of medical equipment, but other typical payloads include cameras and radar systems.
- The aircraft provides the means of carrying the payload to a location specified in the mission. To achieve this task, it relies on the use of many sub-systems. These typically include stabilization/control systems, power plant, electrical, airframe structure, and other mechanisms required for the mission [20].

However, this project specifically requires the use of a Vertical Take-Off and Landing (VTOL) aircraft. The first main benefit to such an aircraft is the ability to hover over a single location and to fly at low speeds, while the second benefit is the ability to take-off and land over small clearance areas [18]. The latter of which is beneficial to the concept of delivering medical equipment to those in need at isolated areas.

For a low-speed aircraft, typically one that travels below 150 knots (173 mph) at any given time, the most efficient VTOL configuration would be that of a helicopter due to its superior hover efficiency and insensitivity to turbulent flow [21]. Most helicopter configurations control the horizontal and vertical position of the aircraft by pitching the direction of the rotor. Each helicopter rotor is powered by an engine connected to a transmission that can control the cyclic and collective pitch of the rotors. Cyclic pitch control works by tilting the hub, or the top of the spinning axis at which the blades connect, toward the direction of thrust desired. The rotor speed is then increased to maintain altitude and the helicopter accelerates in that direction [23]. Collective pitch control works by pitching each rotor blade up or down equally and simultaneously. Pitching the blades up increases the angle of attack of the airfoils and causes the helicopter to gain altitude, while pitching the blades down decreases altitude. Collective pitch exists to keep the helicopter at a steady height without needing to change the rotor speed or power [23]. It is often paired with control from a

governor, which keeps the helicopter blades spinning at a constant speed when hovering or moving.

Helicopters can come in many rotor configurations but the most common include single rotor, tandem rotor, intermeshing rotor, coaxial rotor, multirotor, and compounded [18]. The singular rotor on a single-rotor helicopter causes the body to spin in the opposite direction of rotor spin due to the conservation of angular momentum. In response to this undesired outcome, most single-rotor configurations have a tail rotor to provide yaw control [23]. While this configuration is the most used, the asymmetric tendencies bring disadvantages in the form of the tail rotor requiring non-propulsive power and being dangerous at times to those near it.

The tandem configuration consists of two rotors that move in opposite directions to prevent body rotation. As a result, these configurations do not need a tail rotor to control yaw or spinning [23]. The dual rotors cover a large disc area and are most used for very heavy helicopters that become too unstable with just one large rotor. For smaller scale tandem helicopters, the rotors would need to be mounted on pylons that can create undesired structural loads [18].

Intermeshing rotors follow the tandem configuration but have the rotor blades discs mesh through each other to save space. These helicopters see the benefits of a tandem configuration without needing to worry about the structural integrity of mounting rotors on pylons. However, it can be difficult to control the rotors in a way to ensure the blades never collide.

Coaxial rotors consist of two rotors on top of each other, spinning in opposite directions. When the two rotors are spaced ideally, the air accelerated downward from the top rotor can make this configuration more efficient than that of a single rotor [23]. The costs of this configuration are the need of a complex transmission system to provide separate cyclic and collective controls on a single axis, and higher maintenance difficulty from the increased structural height required.

The multirotor configuration differs from the rest in that there is no cyclic or collective pitch control. These helicopters consist of multiple fixed rotors connected to electric motors, that each spin at different speeds to control position and rotation on each of the three axes. The lack of need for a transmission system makes this configuration the easiest to build, but the hardest to develop an algorithm for to control flight [18].

Finally, compounded helicopter designs, when a wing and sometimes a horizontal propulsion system is added, can help a helicopter increase cruise speed and efficiency. This helicopter configuration can cause the helicopter to achieve up to 300 knots (345 mph) at the cost of a severe reduction in payload weight and endurance [18].

Convertible helicopter designs allow for a vertical take-off mechanism to tilt and become a fixed-wing aircraft, allowing for fixed-wing flight speed combined with VTOL hovering and claustrophobic landing capabilities. However, this configuration in general creates a severe payload weight penalty that is much worse than that of any helicopter or fixed-wing aircraft [18]. Some examples of convertible helicopter designs include tiltrotor, tiltwing, tilt-body, ducted fan, and jet-life. Tiltrotor and tilt-wing aircraft work by mounting the rotors or wings with rotors attached on a rotating shaft. This allows the aircraft to take-off and hover vertically, but cruise like

that of a fixed-wing aircraft. Tiltrotor aircraft do not include wings and are more efficient in hover while tiltwing aircraft often need multiple smaller rotors and are more efficient in cruise. The engines can either tilt with the rotor, or remain fixed with the body, but both configurations lead to a complicated fuel and oil system [18]. Tilt-body aircraft allow the body of the aircraft to tilt with the wings/rotors when transitioning from hover to cruise or vice versa. However, air separation creates a high likelihood that this aircraft will stall in the transition phase. As a result, stronger rotors and larger wings are required to keep the aircraft from losing altitude, but this will lead to an increase in weight. In addition to this design consideration, a low wing aspect-ratio (short small span to top wing area ratio) and flow attachment devices such as vortex generators and leading/trailing edge-flaps will also be required [18]. Ducted fan aircrafts work by using a coaxial fan as a thruster, or a device that pushes large and fast amounts of air away from the direction of motion, instead of a rotor generating lift. Currently these are hard to control and do not travel very quickly but do make it much easier to transition from hover to cruise [18]. Finally, jet life aircraft use large jets of air to keep the aircraft in flight and smaller jets of air to provide roll and pitch control. The engine power and cost required to use this configuration, however, is extremely high and makes the aircraft not suited for low-speed operations [18].

The goal of designing any aircraft is to reduce the total drag while gaining as much lift as possible. The total drag of an aircraft is a component of three types of drag: induced, parasitic, and profile drag. Induced drag is drag that is caused by vortexes generated at wing or rotor tips during lift, where the high-pressure air under the airfoil travels up to the low-pressure air above the airfoil. Therefore, it is a drag that directly correlates to the amount of lift an aircraft produces. In particular, induced drag is a function of the lift squared. As slower aircraft require wings or rotors to have a high angle of attack to generate more lift, induced drag tends to decrease as flight velocity increases [21]. Parasitic drag is drag caused by non-lift-generating surfaces. This can include drag on the fuselage or body, any type of interference of the air, depressurization in a cabin, etc. Parasitic drag is a function of the aircraft velocity squared [21].

Profile drag is characterized by any drag that is directly caused by the wing or rotor during flight. It can be reduced to two types: form and skin drag. Form drag is caused when air streamlines around the airfoil of a wing or rotor separate from the surface. A low-pressure wake is created along the back edges of the airfoil, and the pressure differential with the high-pressure front of the wing or rotor causes a high drag force [21]. Skin drag is drag caused by the friction of air on the surface of the wing or rotor. Turbulent, or chaotic, flow around a wing or rotor tends to create more skin friction than laminar, or streamlined, flow. However, the lack of inertial forces in laminar flow cause it to separate earlier than turbulent flow would, creating more form drag [21]. Profile drag tends to not vary with flight velocity, but instead with the properties of the air. In rotary-wing aircraft, profile drag affects the speed and torque of rotor rotation rather than the velocity and thrust in horizontal flight, like that of fixed-wing aircraft [22]. It is therefore important to calculate profile power, or the rotational power required to overcome profile drag, in design. Since relative velocity varies with radius, and is asymmetric in forward flight, this must be done with numerical analysis on the computer.

3. Objectives

Medical professionals need a way to transport medical supplies quickly and precisely, in emergency situations, while avoiding the delays that come with ground transportation. The Vertical Flight Society (VFS) is tasking teams to develop an unmanned vertical lift concept capable of delivering a 50kg payload to a range of up to 200km in a safe and efficient manner [1].

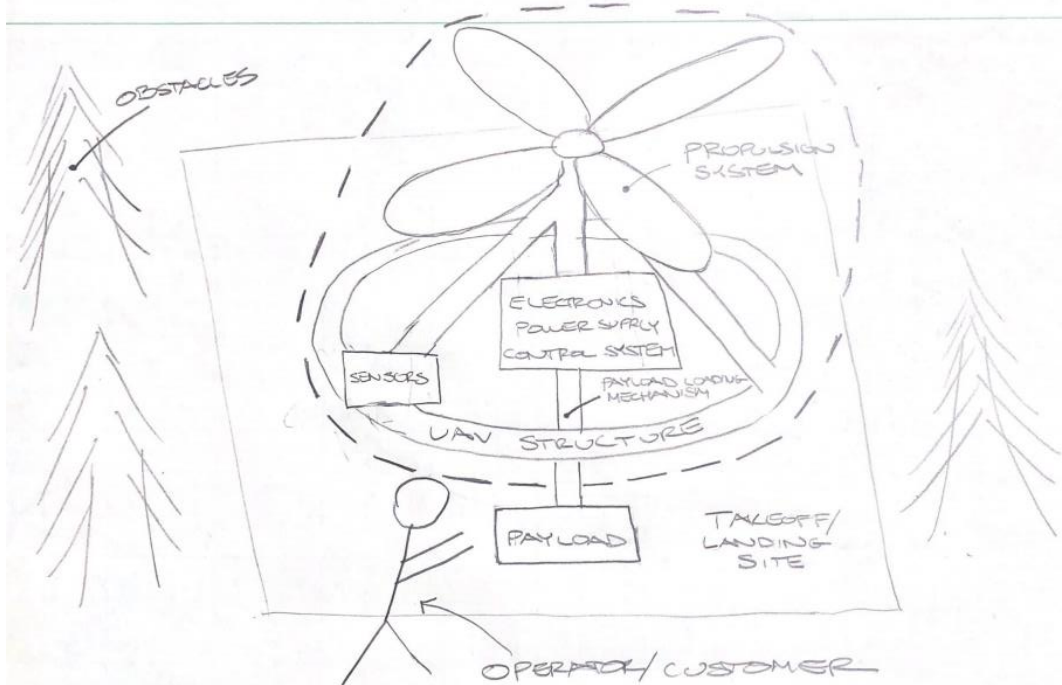


Figure 1. Boundary diagram of planned project scope.

In the boundary diagram, Figure 1, the dotted line visually represents the system that we can design and modify as we see fit, anything outside of the dotted line is out of our control. Objects outside of the dotted system such as the payload and takeoff/landing site need to be considered when we design our system.

3.1 Customer Wants and Needs

To effectively produce a design, we need to determine what is necessary and what is an added functionality based on the customer wants and needs determined during background research. In Table 4, the customer needs are the necessary design capabilities and the customer wants are the additional functionalities that improve customer satisfaction.

Table 4: Customer Wants and Needs

Customer Needs	Customer Wants
Able to reach far distances	Easy to troubleshoot and repair
Vertical Takeoff	Accessible and cost-efficient materials
Fast enough to reach patients in need	Durable
Obstacle detection and avoidance	Vehicle not too big
Controlled landing during failure	Ergonomic loading of payload

Table 4 describes the customer's needs and wants; this was derived from the Request for Proposal document [17] given to us by the Vertical Flight Society and the background research conducted on similar products. The customer want of, "vehicle not too big," is both a need and a want, the Vertical Flight Society has a requirement that the system must not be bigger than 20 feet by 20 feet with no constraint on height, but also has a recommendation of not designing a system larger than 15 feet by 15 feet with no constraint on height [1]. When we are designing the system, we expect to include the customer wants in the design. If the customer needs cause complications with the customer wants, we will prioritize the customer needs.

3.2 Quality Function Deployment

The purpose of Quality Function Deployment is to determine the best specifications to meet the needs and wants of our targeted customers with assigned ratings of importance all in one easy-to-navigate matrix. The goal is to respond to these customer requirements and produce the best possible design that fulfills the important criteria displayed on the matrix. Our House of Quality can be found in Appendix B with the main sections being divided up into descriptions for our project's *who*, *what*, *how*, *now*, and *how much*. The *who* consists of the people whose opinions we would want to base our design around. This includes medical professionals, medical dispatchers, receivers of supplies, and manufacturers. As for the *what*, we listed 16 different requirements that would be of value to the targeted customers. These requirements were very general and easily understood by any population. The *how* includes the engineering specifications, which is essentially a collection of parameters that could be used to measure the customer requirements. These measurable qualities are then described with roughly estimated numerical values in the *how much* section to really get a clearer picture of the measurements we are aiming for in our design. Lastly, the *now* section lists similar current products that can be judged based off the customer requirements we have listed on the matrix. Overall, the quality function deployment is an important tool that allows us to determine correlations between requirements and the targeted customers. We can also compare what metrics are relevant to the needs and wants of these customers and visualize which numerical values will be important when considering certain designs during our ideation process.

3.3 Engineering Specifications

Table 5 visually shows the specifications from the quality function deployment that must be met to successfully complete the project. The specification column briefly describes the criteria we are analyzing. The requirements are the numeric values associated with the specifications. The tolerance describes whether the numeric values in the requirements column are a minimum value or maximum value. The risk tells how high of a priority each specification is, H being high, M being medium, and L being low. The compliance column describes how we will test each specification to each requirement. A stands for analysis, this would be various engineering calculations to prove each specification is in its acceptable range. I stands for inspection, this would be something like taking a measurement or weighing a component. S stands for simulation, which could include performing FEA and CFD simulations.

Table 5: Engineering Specifications

#	Specification	Requirement	Tolerance	Risk	Compliance
1	Range	200km	Min	M	A,S
2	Pay Load Dimensions	70cmx70cmx70cm or 50cmx50cmx140cm	Min	L	A,I
3	Payload Mass	50kg	Min	L	A,I
4	System Dimensions	20'x20'	Max	L	A,I
5	Number of Collisions With Obstacles	0 collisions	Max	M	A
6	Required Delivery Site Area	50'x50'	Max	L	A,I
7	Vertical Lift Time	2 minutes	Max	H	A
8	Time to Reach Destination	108 km/h or 160 km/h	Max	H	A
9	Vertical Lift Angle	+/- 9.5° off vertical	Max	M	A,S
10	Control System Inputs	20m object avoidance distance	Min	M	A,S
11	Blade Guard	Guard gap of 1cm	Max	L	A,I
12	Max Impact Force	100,000 Newtons	Min	H	A
13	Lift Force	> Weight of payload + weight of system	Min	H	A
14	Thrust Force	> Drag force of air + Force to speed	Min	M	A
15	System Weight	<500 lb.	Max	M	A,I
16	Number of Subsystems	≤ 10 subsystems	Max	L	I,S

To prove our design will function as intended we will need to test each engineering specification. Listed below are descriptions of each specification and how we will test each specification.

1. The range is the distance the system will need to fly. This will be tested by performing an analysis on the system at its maximum weight capacity.
2. The payload dimensions are the outer dimensions of the payload the system will carry. This will be tested by measuring the inner dimensions of the cargo space.
3. The payload weight is the weight of the payload the system will carry. This will be tested by an engineering analysis to ensure the cargo space will have the required strength to hold the payload without fracturing.
4. The system dimensions are the outer dimensions of the entire system. This will be tested by measuring the outer dimensions of the entire system.
5. The number of collisions with obstacles is how many obstacles the system collides with. This will be tested by running simulations to test the accuracy of the design control system.
6. The required delivery site area is the area the system will have to land and deliver the payload. This will be tested by running simulations to test the accuracy of the design control system.
7. The vertical lift time is the time the system takes to climb to its flying height. This will be tested by performing engineering calculations on the lift force needed to overcome gravity and make a quick ascent.

8. The time to reach destination is the speed needed to fly to the destination in the required amount of time. This will be tested by performing engineering calculations on the thrust force needed to accelerate our system to reach the desired velocity.
9. The vertical lift angle is the maximum angle from normal to the ground that the system can take off at with the given take off zone. This will be tested by performing a simulation on the take-off control system.
10. The control system inputs are the sensors and code that will detect whether an object is close to the system. We will test this by performing a simulation to see whether the sensors and code work as intended.
11. The blade guard is a safety feature for any spinning blades which would prevent fingers or limbs from being injured. We will test this by measuring the gap of the blade guard.
12. The max impact force is the maximum impact for the system should have to withstand. We will test this by doing an engineering analysis on the system in freefall with the selected failsafe mechanisms.
13. The lift force is the force needed to change the systems vertical position. This will be tested by performing an engineering analysis of the lift force at the systems max weight.
14. The thrust force is the force needed to move the system horizontally. This will be tested by performing an engineering analysis on the thrust force at the maximum system weight.
15. The system weight is the total weight of the entire system. This will be tested by weighing either the entire system or each component of the system and adding each component weight up.
16. The number of subsystems is the number of different control systems (ex: GPS, collision avoidance, etc). This will be tested by counting each subsystem.

3.4 Specification Risks

In this design there are crucial specifications that may be difficult to achieve due to a variety of reasons, these are labeled with a risk of H or High in table 5. The first two high risk specifications are the vertical lift time and the time to reach destination. These are inherently connected because the best products for each of these categories operate with vastly different systems. If we choose to focus on the best methods on the market currently to achieve either a fast vertical-lift time or time to reach the destination, the one we did not choose will suffer [21]. We will choose to focus on designing a system that has a good middle ground. The max impact force is another high-risk specification. This is because at a free fall the impact force will be substantially higher than the 100,000 N we are aiming for. To achieve this, we will design our system so that it has a way of knowing it is failing and be able to slow itself down autonomously. The last high-risk specification is the lift force. This will be difficult to achieve because this system will be heavy and needs to be able to climb vertically to its flying altitude while moving quickly and then transition to moving horizontally quickly.

4. Concept Design

The concept design process entailed a functional decomposition of the system, developing ideas through brainstorming and prototyping, evaluating concepts based on relevant criteria, and selecting a concept that will define our design direction.

4.1 Ideation

The selection process of a concept design began with the ideation stage which included outlining the functions the system must perform and brainstorming many ways to achieve these functions. The existing ideas were developed through the creation of physical ideation models that were used to verify key functions and further communicate our ideas.

4.1.1 Functional Decomposition

The first step of the idea creation stage was creating a functional decomposition of the system that outlines the major functions and sub-functions required to meet the customer needs. The functional decomposition is shown in Figure 2.

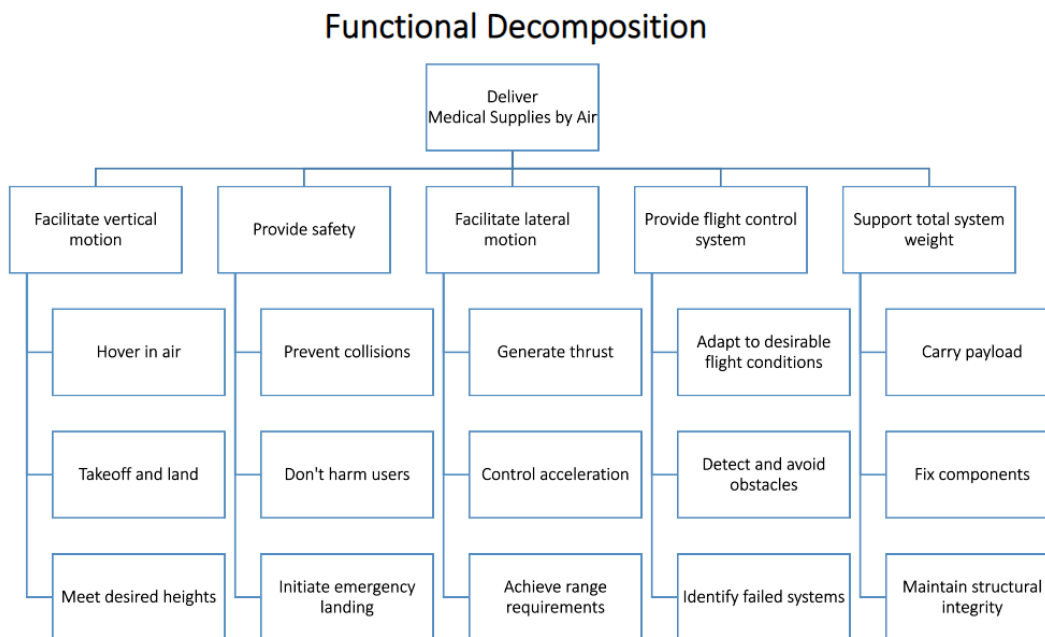


Figure 2. Functional decomposition diagram outlining major functions and sub-functions of system.

The major functions listed across the top of Figure 2 are the basic actions the system must perform to deliver medical supplies by air. The sub-functions derived from each major function are the actions the system must perform to meet each respective major function. The functional decomposition diagram was used to direct our ideation efforts as we brainstormed many different ways to achieve the major functions as shown in Appendix C.

4.1.2 Ideation models

After brainstorming many possible ideas, we built physical models to test the viability of critical features of our alternative designs. These models were used to conceptualize existing ideas, generate new ideas, and verify basic functions. Twenty physical models of potential ideas for one the major or sub-functions were created using prototyping materials such as foam board, straws, cardboard, paper, string, and hot glue. The functions modeled included propulsion systems such

as a quadcopter and fixed-wing configurations as well as payload delivery systems such as parachute and unwinding chain configurations. The potential solutions for the functions modeled were primarily derived from the ideas created in the function trees shown in Appendix C. The ideation models are shown in Figure C.5 of Appendix C.

4.2 Idea Refinement and Selection

After concluding the ideation stage, the next step in our preliminary design development was to compare the design ideas and combine the best ideas to create full-system concepts. For each major function, the function designs were evaluated based on the design criteria and compared against one another. The best performing concept ideas for each function were combined interchangeably to generate full-system concepts. The full-system concepts were assessed and compared using matrices that considered the importance of each design specification and the performance of the concept design.

4.2.1 Pugh Matrices

In order to choose a concept design to move forward with, we had to conduct a series of idea refinement and selection sessions. We began this process by first generating Pugh matrices, which is a procedure that is done to produce an assortment of design ideas for each specific function. Each function was evaluated according to certain criteria that were established before the designs were chosen. In addition, each concept was to be compared to a datum, where a rating of “+” would be assigned to any design choice’s criteria performance that was advantageous over the datum. A design that was determined to be worse than the datum’s performance for a criterion would be assigned a rating of “-”. The functions we chose to do Pugh matrices for were the payload loading and unloading function, the structure or geometry of the drone, the ability to engage in vertical and horizontal motion, and the specified power system. We selected different criteria for each Pugh matrix depending on what parameters might best evaluate how well our designs perform our desired functions. All Pugh matrices for each function can be found in Appendix D.

4.2.2 Morphological Matrix

The next step in the idea development process was to assemble the top 4-5 ideas that performed well for each function into one Morphological matrix. This matrix lays out all the best ideas in a one place which assisted with creating the Weighted Decision matrix. As shown in Figure 3, the top ideas for each function are displayed with the design name and a basic sketch included.


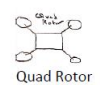


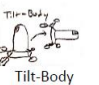

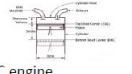







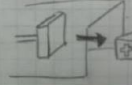


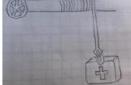
Functions	Idea 1	Idea 2	Idea 3	Idea 4	Idea 5
Move Vertically/Laterally	 Tandem Rotor	 Quad Rotor	 Tiltwing	 Tiltrotor	 Tilt-Body
Power Vehicle	 Car Battery	 IC engine	 Lithium Ion Battery	 Supplemental solar power	
Structure	 Truss	 Monocoque	 Semi-monocoque	 Composite	
Loading/Unloading Payload	 Sliding Door	 Piston	 Retractable Arms	 Parachute Drop	 Unwinding Chain

Figure 3. Morphological matrix displays best designs for each Pugh matrix function.

4.2.3 Weighted Decision Matrix

The final idea selection approach was to select a few combinations of function designs and evaluate them against engineering specs that would best help us identify our final preliminary design. Our engineering specs included parameters such as cost, manufacturability, weight, lift/hover capability, and safety to name a few that would do well to evaluate the performance of a delivery drone. Each engineering spec was assigned a weight based off how essential they would be to the functionality and customer requirements for our project. For example, we considered the cost of our drone to be of utmost importance and therefore assigned it a weight of 5. On the other hand, durability was less significant in the grand scheme of things, so we allocated a weight of 2 for it. Each member of the team was responsible for choosing their own concept designs, while we also selected function design combinations for the most practical and the highest rated for each function on the Pugh matrices. The Weighted Decision matrix can be found in Figure 4.

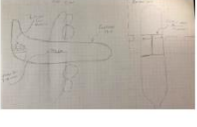


Team F56 UAV	10/29/2020	Idea 1		Idea 2		Idea 3	
		>Tilt Wing >Composite body >Sliding door >Lithium ion batteries		>Quad propulsion system >lithium ion / solar >composite body >unwinding chain payload		>Quad propulsion system >lithium ion / solar >composite body >parachute payload	
Specification	Weight						
		Score	Total	Score	Total	Score	Total
Low Cost	2	2	4	5	10	5	10
Manufacturability	3	1.5	4.5	5	15	5	15
Weight	4	3	12	4	16	5	20
Lift/Hover	4	2.5	10	5	20	5	20
Safety	5	3	15	4	20	3	15
Range	5	5	25	3	15	3	15
Delivery Speed	4	5	20	2	8	2	8
Durability	2	1	2	1	2	1	2
Payload Capacity	5	2	10	4	20	4	20
		Totals	102.5	4	126		125

Figure 4. Weighted Decision Matrix





Team F56 UAV	Idea 4	Idea 5	Idea 6	Idea 7				
	>Quad/tilt rotor/fixed-wing >hybrid engine >composite body >unwinding chain payload	>Coaxial Helicopter >fully electric >monocoque >horizontal sliding door payload	>Semi-Monocoque body >Tandem Rotor Design >Human opened doors >Reciprocating (helicopter) engines	>Quadcopter/fixed-wing >lithium ion >composite body >unwinding chain				
Specification								
	Score	Total	Score	Total	Score	Total	Score	Total
Low Cost	1	2	3	6	4	8	1.5	3
Manufacturability	2	6	3.5	10.5	4	12	3	9
Weight	2.5	10	3.5	14	3.5	14	3	12
Lift/Hover	5	20	3	12	4	16	4	16
Safety	3	15	4	20	4	20	3	15
Range	4.5	22.5	4	20	3	15	4.5	22.5
Delivery Speed	5	20	3	12	3	12	2.5	10
Durability	3	6	2.5	5	3	6	3.5	7
Payload Capacity	4	20	4	20	4	20	3	15
Totals		121.5		119.5		123		109.5

Figure 4. Weighted Decision Matrix

4.3 Preliminary Design

After ideating, evaluating, and comparing several concepts, a preliminary design was chosen using our weighted decision matrix. The preliminary design will have a quad propulsion system with lithium-ion batteries. The body will be made of a composite material. The payload will be delivered to the receiver using an unwinding chain.

4.3.1 Preliminary Design Description

This design is comprised of four different subsystems: the control system, the propulsion system, the payload release system, and the airframe. To ensure that this design meets the competition and customer requirements, the team finds it necessary estimate the general weight and shape of the components for each subsystem using currently developed models. Total aircraft weight is necessary to calculate the rotor power for hover, climb, and forward flight while component geometry and location is necessary to determine the lofted shape of the fuselage. Figure 5 contains the CAD model of the aircraft showcasing part sizes. The payload release mechanism is covered in more detail in section 4.3.2.

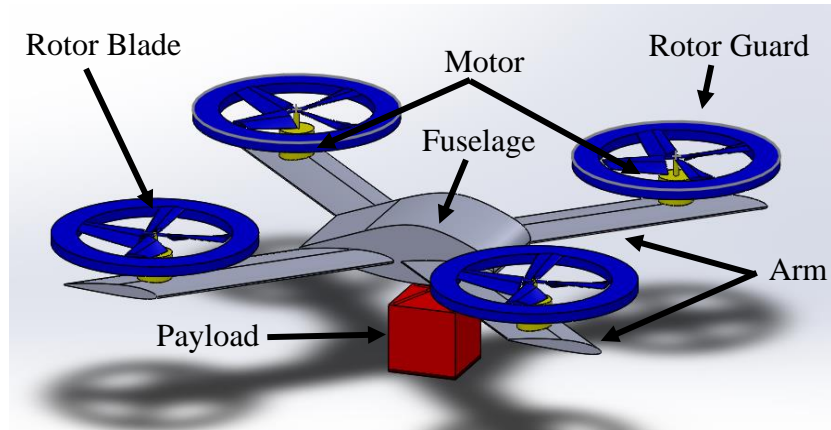


Figure 5. Conceptual CAD Model. The four subsystems are in gray, blue, yellow, and red for airframe, propulsion, control system, and payload, respectively.

The on-board control system will consist of four main components: a printed circuit board, antenna, sensor configuration, and wire array, all located in the body of the system. The printed circuit board will be implemented as a microcontroller development board, such as an Arduino, to control the system. The antenna will be used to execute the program to fly the aircraft on its mission from a remote ground control location, and to communicate with ground control on its deliver status and location. The sensors can be encompassed all-in-one with a GPS that contains altimeters and accelerometers for position, stability, waypoint, and obstacle-avoidance control. Finally, the wires will run inside each arm and will be sized large enough to limit resistance and power to the motors.

The propulsion system will consist of the motors spinning the propellers and the batteries powering the motors. The design of the propulsion system is largely impacted from the gross aircraft weight and flight performance, detailed table 6 and section 4.3.4 respectively. The analysis has resulted in choosing to use four 20 hp motors with a max RPM of around 1775. These motors will be mounted on each arm to easily provide six degree-of-freedom control to the aircraft by allowing the controller to slightly alter each motor's individual RPM. To power these motors, we chose to use one 500 watt-hour battery. This will be sufficient to get the aircraft to the destination at the right speed without needing to recharge. The battery will be located near to the center of gravity of the whole system.

The main design features modeled by the airframe are the airfoil-shaped rotor arms and the streamlined shape of the fuselage. The arm shape is critical as our engineering judgement and market research suggests that aircraft that can induce lift with features that do not require power will improve endurance performance. The fuselage consists of a blunt and rounded design lofted over the location and geometries of the payload release mechanism and control system components. Daniel P. Raymer, author of *Aircraft Design: A Conceptual Approach*, suggests that fuselages of this configuration will minimize the parasitic drag experienced by the aircraft while in motion [25].

A concept prototype of the preliminary design was created to provide a physical representation of the major components and how they will fit together by 3D printing the major components. The

major components models were the fuselage, rotor arms, and propeller disks as shown in Figure 6.

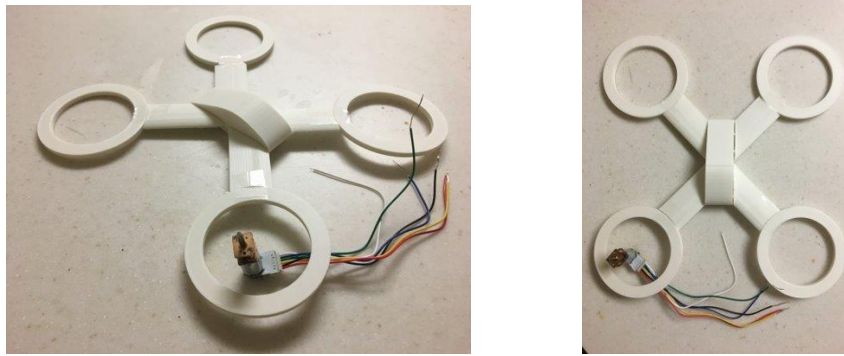


Figure 6. 3D-printed concept prototype featuring major components of the concept design.

We used our concept prototype to observe how adding additional weight at various locations affects the center of gravity of the entire system. We also are reconsidering the way the propellers are attached to the rotor arms as slightly longer rotor arms with propellers mounted above may provide more lift despite the added weight. A single motor is shown in the images above in one of the propeller disks; going forward, we plan on fastening four motors to the prototype with 3D-printed rotor blades with the aim of using the prototype to experiment with various control techniques.

This design excels in many areas desired by potential customers that give it major benefits over the other concepts that were considered. A large benefit to this design is the simplicity of the rotor system. Most VTOL concepts that perform at this forward flight speed and efficiency contain rotor transmission systems that contain hundreds of moving parts. Not only does this make it hard for medical professionals and emergency workers with little engineering experience to maintain their product, but the fatigue and dynamic stresses severely drop the life of these tiny components. This design eliminates any excessive bearings or hinges in favor of a simple motor with varying RPM. Additionally, this design can perform a vertical take-off better and more efficiently than other designs since the four propellers are all pointing downward. This could cause some problems for the speed we need to achieve to fulfill the mission requirements. Another great feature of this design is the use of airfoils to produce lift to reduce the power consumption needed to keep the system flying. These airfoils may allow us to use some of the power saved from generating lift to increase the thrust therefore increasing the speed. The composite body will allow for more weight to be used for battery capacity while maintaining the structural strength needed to complete the mission. Since this is a one-time build making a mold for the body may be extremely inefficient, but if this design were to be mass produced this could cut down on manufacturing time. The major drawback of this design would be the power consumed to distance traveled ratio. A fixed wing design would be much more power efficient. A detailed breakdown of the mass estimate for each of the component is shown in Table 6.

Table 6: Subsystem Component Mass and Dimension Estimations

Sub-System	Component	Number	Similar Model	Mass (kg)	Dimensions
Airframe	Fuselage	1	N/A	43	2m chord, 1m span
	Arms	4	N/A	24	0.5588m chord, 2.540m span
Airframe	Rotor Guards	4	N/A	19	1.25m OD
Propulsion	Battery	1	CyberPower SmartApp	35	431 x 820 x 264mm
	Motors	4	Marathon Motors 20hp	42	268mm diameter x 535mm height
	Rotor Blades	16	N/A	2	0.25m chord, 1m span
Payload	Payload	1	N/A	50	70 x 70 x 70mm
	Chain	1	N/A	12	2m long
	Crank	1	N/A	3	203.2mm diameter x 203.2mm height
	Crank Motor	1	Dayton ¼ hp motor	3	150mm diameter x 200mm height
Control	Circuit Board	1	Arduino	25e-3	68.6mm x 53.4mm
	Antenna	1	Vexxis GNSS-802	507e-3	176mm diameter x 55mm height
	GPS	1	Advanced Navigation Certus	280e-3	78 x 115 x 34mm
	Wires	8	N/A	0.5	0.005m diameter x 3m length
Total Mass				523	

4.3.2 Payload Release Mechanism

The ability to deliver the payload reliably and quickly is an important aspect of the mission. Therefore, a system is needed to carry and drop the heavy box at the delivery site. The system proposed is an unwinding chain that will let the payload hang from the below the drone during flight and hover. A servo-actuated motor will be responsible for winding and unwinding the chain, causing the payload to raise or lower in height. The chain will split into four sections towards the end that will each latch onto clips on the corners of the payload.

This payload release system includes the following major benefits:

- A Smaller and Denser Fuselage. Large reductions in efficiency in an aircraft come from the drag across the fuselage and the lack of space for lift generating surfaces to operate. With a smaller and more compact fuselage, the rotor size can be increased while the

parasitic drag can be reduced, assuming the payload can be stored within the fuselage envelope during forward flight.

- **Impact Reduction.** With a separate motor lowering the payload while the aircraft is in hover, the chance of damaging the payload is reduced when compared to being housed inside the aircraft during landing. Additionally, any complete power shutdown in the drone will allow the impact to occur at two separate times. The payload hitting the ground before the drone will have less impact force than a combined impact.
- **Ergonomic Loading and Unloading.** Dropping the payload directly on the ground while the aircraft is still in hover allows for very efficient handling of the critical medical equipment. The action of clipping and unclipping a chain will take less than a second at each corner.

The potential drawbacks of this system include increased weight and complexity, difficult obstacle avoidance, and increased drag and vibrational loads on the payload and chain.

4.3.3 Concept Design Updates

Aerial vehicle design is a field that requires constant concept iteration and trade studies to determine an aircraft configuration that will meet the desired mission requirements at the lightest weight. In the conceptual design stage, the aircraft shape and inclusion of major components is determined largely by prior performance knowledge, rough statistical estimation of performance metrics, and thorough aerodynamic research. Once a shape and configuration are chosen to satisfy the design requirements, the performance metrics must be redetermined. Often, there is discrepancy between the initial estimates and recalculated values, and the aircraft design must be adjusted to account for the new values.

Section 5.1.1 outlines how the size and shape of the rotors were designed for optimum efficiency in climb, the most power-consuming stage of either mission. Upon design of these motors, estimates for the rotor thrust, lift, and drag were able to be applied to forward flight. With these results, our group determined that changes to the design layout could be made to increase our cruise speed and performance in forward flight without a critical weight penalty by making the following changes:

- **Lift-Generating Wings.** At high forward flight speeds, the rotor drag is greatly reduced when the rotor blades no longer need to spin to produce lift. Adding fixed wings reduces the large drag and the Mach number at the advancing blade tips in favor of a smaller drag created by the wings and a non-critical increase in weight at these high speeds. Less drag has a large impact on the decrease of delivery time.

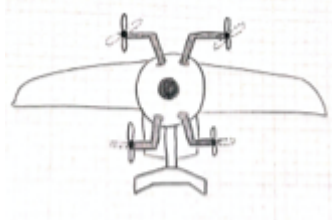


Figure 7. Quadrotor with Wings and Tail/Empennage

- Empennages for Stability. In fixed-wing forward flight, rotor RPM differential is no longer an option in aircraft control. A vertical and horizontal tails or empennages need to be added with deflectable control surfaces to allow the aircraft to remain stable and perform maneuvers. In addition to stability, the empennages can provide structural support to the rotors and allow the aircraft to glide to a safe landing without a parachute.
- A Horizontal Propulsion System. As the rotors can no longer tilt to provide thrust in forward flight, a separate horizontal propulsion system is needed to provide the thrust needed in cruise. While there are many types of horizontal propulsion for aircraft, including turbojets, turbofans, and vectored thrust, propellers represent the most efficient method for light, subsonic aircraft. Figure 8 exemplifies this configuration with the inclusion of pusher propellers on the wings.



Figure 8. Quadrotor Configuration with Wings and Pusher Propellers

4.3.4 Alternate Designs

- A Single or Double-Rotor Helicopter. Rotor efficiency is proportional to the rotor radius in general. The large rotor-disc area for a single, tandem, intermeshing, or coaxial helicopter design may prove to be much more efficient than a quadcopter configuration for an aircraft of this size. For the quadcopter benefits listed above, this change should only be considered if the reduction in efficiency is significant. Figure 9 showcases a coaxial helicopter design.



Figure 9. Coaxial Helicopter

- A Tiltrotor or Tiltwing Configuration. This design change will be considered if both the horizontal speed and powerplant efficiency are not satisfactory to meet the mission requirements. At the cost of high complexity and weight, this configuration could provide the best of rotary-wing hovering and fixed-wing flight. Figure 10 provides an example of a tiltrotor.



Figure 10. Tiltrotor with Rotating Arms and Fuselage

4.3.5 Preliminary Analysis

Some of the major performance requirements for the UAV including climbing a vertical distance of 150 m and flying a lateral distance of 200 km in less than 75 minutes. These specifications can be used in conjunction with a simplified engineering model to calculate rough estimations for the minimum thrust force and power required to complete the mission.

A free-body diagram (FBD) of a simplified UAV model with front and rear propellers in forward flight was created as shown in Figure 11. The FBD was used to determine the equations of motion for the UAV in forward flight and solve for the thrust force required to achieve a terminal velocity that will achieve the requirement of flying 200 km in less than 75 minutes. The hand calculations and final expression for thrust force and pitch angle can be found in Appendix E.

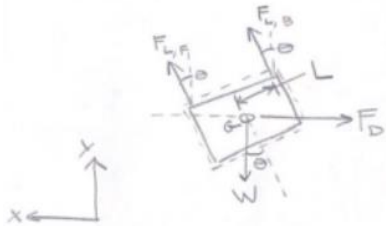


Figure 11. FBD of simplified UAV in forward flight.

A terminal velocity of 50 m/s was used to solve for expressions for thrust force as

$$F_L = \sqrt{[(C_D A) \left(\frac{1}{2} \rho\right) V_t^2]^2 + W^2} \quad (1)$$

and pitch angle as

$$\theta = \cos^{-1} \left(\frac{W}{F_L} \right) \quad (2)$$

and plot thrust and pitch against system mass in MATLAB as shown in Figure 12. The drag coefficient, C_D , was assumed to be 1, and the frontal area, A , was assumed to be 0.8 m². The MATLAB code is attached in Appendix G.

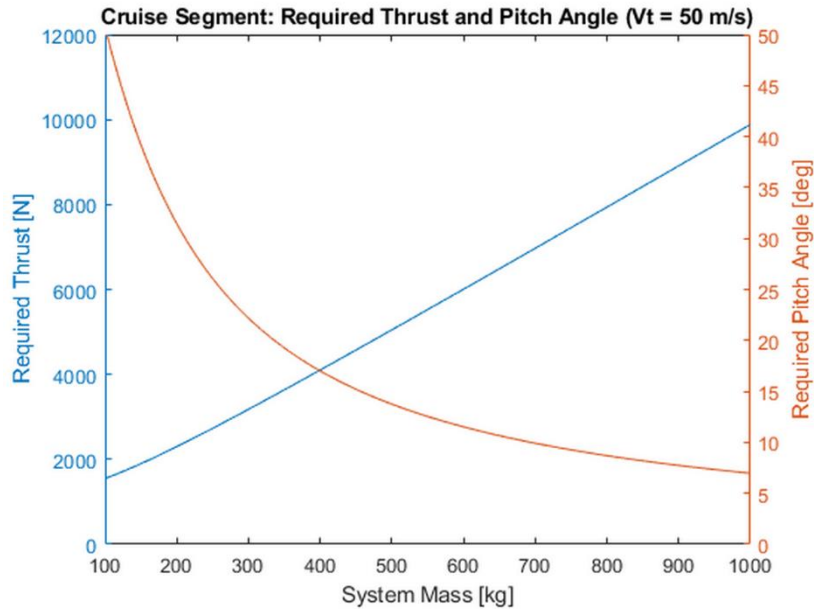


Figure 12. Thrust force and pitch angle during steady, forward flight plotted against system mass.

The plot in Figure 12 provides an estimate for the thrust force the UAV will need to generate during steady, forward flight based on initial estimations for the system mass. Additionally, the thrust force was necessary for calculating the power required during forward flight. The estimate for the pitch angle at steady, forward flight will be important for designing the structure to minimize drag.

The ideal power required per rotor to climb vertically was calculated using conservation of momentum and conservation of energy principles to solve for power required to hover as

$$P = \frac{T^3}{\sqrt{2\rho A}} \quad (3)$$

with full hand calculations attached in figure E.3 of Appendix E, and analytical expressions for climb power as a function of hover power [22] as

$$\frac{P}{P_h} = \frac{V_c + v_i}{v_h} = \frac{V_c}{v_h} + \frac{v_i}{v_h} \quad (4)$$

The results for ideal climb power required per rotor assuming 4 rotors with equal thrust force, a climb velocity of 2.5 m/s, and several different rotor radii are plotted in Figure 13.

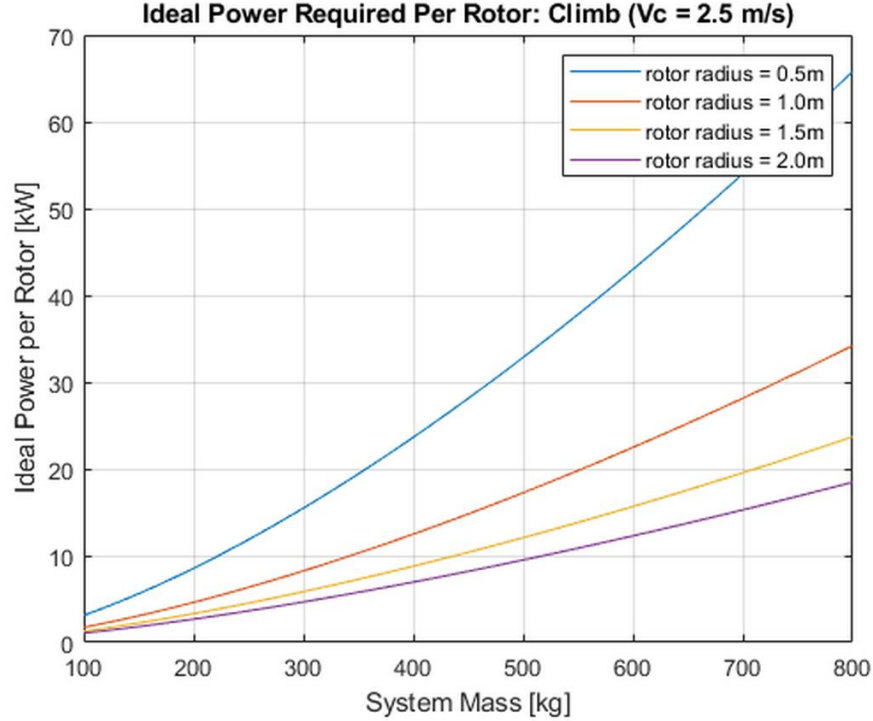


Figure 13. Ideal power per rotor require to climb at 2.5 m/s assuming four rotors exerting equal thrust force. The data for various rotor sizes are shown.

The results in Figure 13 highlight the importance of minimizing the system mass in reducing the power required to complete the mission. Furthermore, there is a significant reduction in required power between a rotor radius of 0.5 m and 1.0 m, but less improvement between 1.5 m and 2.0 m; this suggests that increases in rotor size become less important when the rotors are already relatively large and that the mass increase associated with increases in rotor size should be closely analyzed.

The results for required thrust force during steady, forward flight shown in Figure 12 were used to calculate the induced velocity, v_i , by solving

$$T = 2\rho A v_i \sqrt{(V_\infty \cos \alpha)^2 + (V_\infty \sin \alpha + v_i)^2} \quad (5)$$

where V_∞ is the terminal velocity and α is the pitch angle [22]. Then, the induced velocity was used to solve for the ideal power required per rotor for forward flight [22] as

$$P = T(V_\infty \sin \alpha + v_i) = T V_\infty \sin \alpha + T v_i. \quad (6)$$

The ideal power per rotor was solved assuming four rotors and various rotor sizes and plotted in Figure 14.

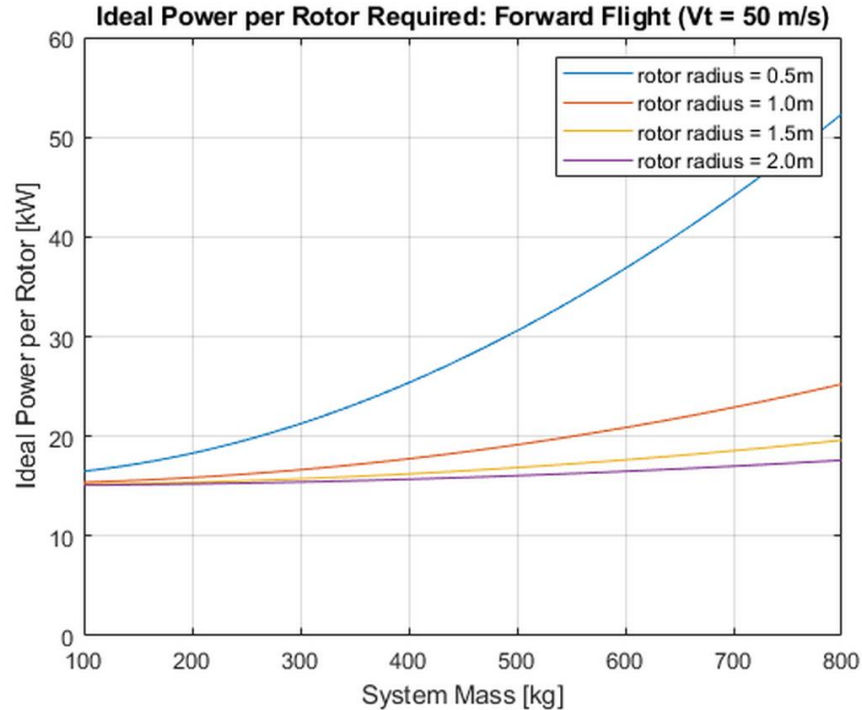


Figure 14. Ideal power required per rotor during forward flight at 50 m/s assuming four rotors exerting equal thrust force. The data for various rotor sizes are shown.

The estimated ideal power per rotor for steady, forward flight shown in Figure 14 further highlights the large reduction in required power from a rotor radius of 0.5 m to 1.0 m. There is little improvement between increases in rotor radius after 1.0 m which is consistent with the climb power results in Figure 13. Lastly, the ideal power required for the rotor radii greater than 0.5 m are all in the 15-20 kW range for most masses which provides a rough estimate for the ideal motor power required to meet the delivery time requirements.

4.3.6 Design Hazards and Risks

There are several major design hazards with the concept design that pose safety concerns to users and bystanders in the vicinity of the operating UAV as summarized in Appendix F. The UAV has inherently dangerous characteristics as it is a large mass moving at high speed at a high altitude and thus will possess large amounts of potential and kinetic energy. During steady, forward flight, the UAV is susceptible to collisions with both stationary and moving obstacles that may cause significant damage depending on the mass and velocity of the obstacles which could lead to full system failure by breaking a critical component or disturbing the UAV to an extent where it is unable to recover. This scenario could result in free fall of the UAV with a significant amount of potential energy that would lead to a very large impact force that could cause injury or death to bystanders and catastrophic failure of the UAV. We plan on mitigating this critical design hazard by installing proximity that can detect nearby objects and signal the control system to divert its path. In the case of an uncontrolled free fall, we plan on equipping the UAV with an emergency parachute that can reduce the velocity upon impact; this will first require hand calculations to validate the efficacy of parachute for UAV operating at an altitude of 150 m.

There are also major safety concerns for users, particularly operators and medical professionals who will be close to the UAV at the takeoff and landing sites respectively. The concept design features sharp propellers that will be rotating at high speeds. We plan on equipping the UAV with proximity sensors near the rotors to ensure they do not turn on when an operator or customer is near the propellers. Additionally, we plan on designing guards around the propellers to provide additional protection to users; this will likely hinder efficiency but is still a design tradeoff we plan on overcoming due to the high importance of user safety.

The design features lithium-ion batteries which are prone to exploding at very high temperatures. We will mitigate this safety concern by designing a heatsink around the battery to quickly conduct heat away in the event of overheating. Furthermore, we will include a circuit breaker that will break the circuit in the event of a short circuit which will prevent the battery from overheating and causing damage to the battery's internal separator.

A major manufacturing risk is associated with this design as it features a composite body. Although the material has not been selected yet, a strong material candidate is carbon fiber whose dust is unhealthy for humans to inhale. Therefore, if we use a carbon fiber material for the UAV structure, we will take the necessary precautions during the manufacturing stage of this project when sawing and handling any carbon fiber components.

One of the major design risks is the intent to streamline the fuselage and shape the rotor arms as airfoils. The UAV will be operating at downward pitch angle; therefore, the airfoils and fuselage will have to be aerodynamically designed for this operating pitch angle. However, this angle is subject to change based on the terminal velocity requirements as described in our preliminary analysis, so it is possible that the airfoils may reduce efficiency at velocities that deviate from the designed operating velocity during forward flight. A potential solution may be incorporating tilting rotor arms that can change the angle of attack of the airfoil-shaped rotor arms. However, this will add complexity and weight to the design so a detailed analysis of the airfoil performance may be necessary before making any major design changes. If our analysis suggests that the airfoils have little or negative effect on the aerodynamic performance, we may explore using rotor arms that are lighter only provide structural support and do not induce lift which may require an increase in increase in power and battery life.

4.3.7 Outstanding Challenges

In the current design the biggest challenge will be to meet the distance requirement of 200 km on a single charge with a speed of 160 km/h in order to meet the time requirement. In order to achieve this range and speed a large battery will be used. This adds excess weight which may prevent the system from flying. When we came up with the current design, we were using a methodology typically used by mechanical engineers, after continuing our research we found an aircraft design textbook which laid out a plan to design a fixed wing aircraft. Currently our plan is to use the methodology that the aircraft design textbook provided to adapt and refine our current design. If time permits, we will use the methodology from the aircraft design textbook to come up with a design from scratch and compare it to the current design.

Another challenge which is a crucial part of this design is the weight. Currently we are using estimated weights for the whole system. As we start narrowing down the components, we will use we will be able to accurately update the entire system weight. In the worst-case scenario this could cause our estimated total system weight to increase to a weight that is not capable of getting off the ground. The best-case scenario, which is more likely because we attempted to overestimate the total system weight, is the case where the weight decreases. If this is the case, we are able to decrease weight from the battery.

A smaller challenge will be adapting a control system from other similar quadcopters to meet the needs of our design. If we find out that this control system will not work with our design, we will need to create our own control system. This may not be manageable with our team of 4 undergrad students seeing as none of us have designed a control system for a flying object.

A requirement for the VFS student design competition is that all technologies should be from the current year (2020) in order to support an initial entry into service in 2025. It may be a small challenge to find these current technologies.

Another challenge will be if we decide to build a scaled down functional model of our design. We are planning on making the outer shell out of a composite material. This will require us to create a mold to create the outer shell.

5. Critical Design

5.1 Design Description

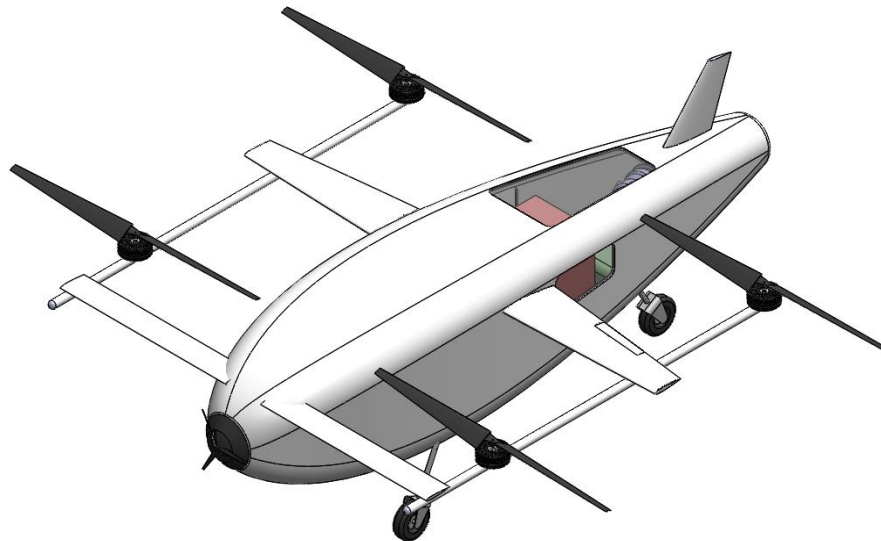


Figure 15. UAV design featuring four rotors, front propeller, and wings.

The aircraft design shown in figure 15 represents a hybrid between a VTOL quadcopter and a fixed-wing airplane. The four rotors are mounted at locations equidistant from the center of gravity

to provide balanced hover. An autonomous control system directly controls the voltage and current input into electric motor to adjust the torque and RPM of the rotors for pitch, roll, and yaw stability. This control system is guided using many sensors to calculate altitude, geographical position, orientation, and atmospheric parameters and is all powered by a turbogenerator. Upon take-off, the rotor blades will cause the aircraft to climb straight above the launch site at around 1.25 m/s until it reaches an altitude of 150 m. The control system will then add power to a tractor propeller in the front of the aircraft to provide horizontal thrust. As the aircraft gains forward-flight speed, the horizontal wings will begin to provide more and more lift. This allows power to be slowly taken from the rotors and transferred to the propeller, further increasing the cruise speed. Once the rotors no longer spin, the aircraft will reach its max cruise speed and stability and control will be provided by the aileron, elevator, and rudder flaps on the wings and empennages. Deceleration to the landing site location will occur in the opposite manner, until the aircraft is operating completely as a quadcopter.

Autonomous drop-off and rapid loading of the payload is completed with the use of an automatic ramp and cart assembly. The payload sits on a cart with rollers that is locked and fixed to the fuselage throughout the duration of the flight. Upon landing, linear actuators cause the ramp to lower to the ground. The cart is then released and rolls along a track until it is completely on the ground. When loading, the cart can be pushed onto the track with little effort until the locking mechanism activates. The ramp will then raise automatically upon launch.

This UAV design offers many benefits compared to traditional fixed-wing aircraft and quadcopters of a similar size. The notable advantage when compared to fixed-wing aircraft is the ability for the aircraft to launch vertically and hover. However, the wing and cruise control surface design also provide many advantages when compared to those of other fixed-wing aircraft. As the rotors supplement the lift during horizontal acceleration, the wings are designed to operate at cruise speed alone. The wings could, therefore, be designed to operate at the lowest area, weight, and drag to provide the lift during cruise and turning maneuvers. Other traditional fixed-wing aircraft are constrained in design to take-off and landing where low aircraft speeds necessitate a large wing coefficient of lift, increased weight, and higher induced drag. The rotors are also able to be designed without forward-flight constraints, as must be considered with other quadcopters. Specifically, a large blade twist angle and taper ratio can be used to increase hover figure-of-merit without worry of retreating blade stall, large profile drag, or blade slap in forward flight. Drag divergence and noise concerns also become less of an issue as the advancing blade tip will not increase in Mach number or enter the compressible flow regime.

5.1.1 Propulsion System Design

The geometric layout of the rotor blade is provided in figure 16. The rotors were designed to provide maximum efficiency in hover using a combined blade-element theory (BET) and disk-actuator momentum theory.

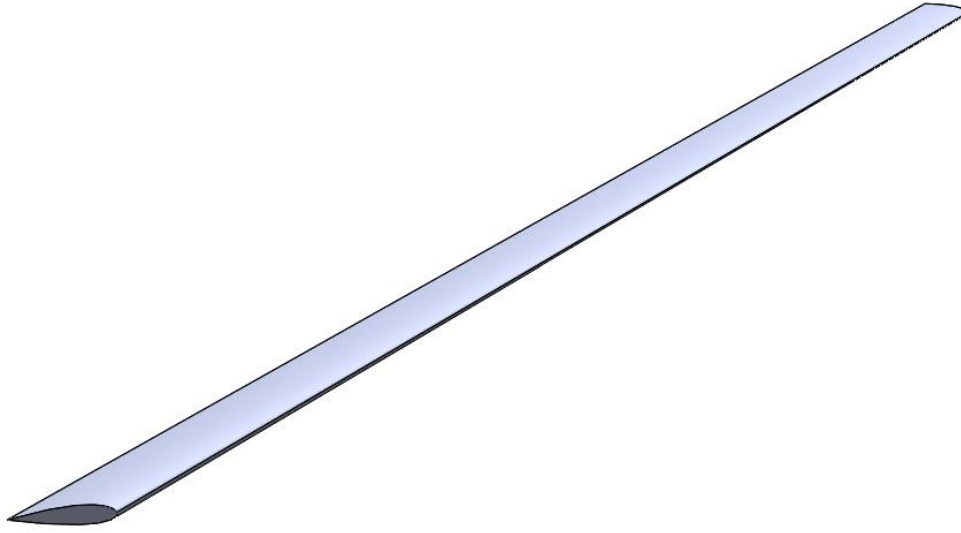


Figure 16. Rotor Blade Geometry

The larger a rotor blade is, the less it needs to spin to provide lift. This directly impacts the non-dimensional thrust coefficient, defined as

$$C_T = \frac{T}{\rho * A * V_{tip}^2}, \quad (7)$$

where T is the rotor thrust, ρ is the air density, A is the rotor disk area, and V_{tip} is the rotor tip velocity. Reducing the tip velocity will reduce the power loading, P/T, up to a certain thrust coefficient. The change in power loading is very small around the minimum coefficient of thrust so the blade area was able to be designed small enough to prevent excessive downwash interference with the fuselage or wings.

A helicopter or quadcopter rotor provides lift as air is sucked through the rotating rotor-disk by spinning airfoils. For non-twisted, rectangular blades, the amount of air, or inflow, across the blade is not constant across the radius. As rotor efficiency is characterized by approaching a uniform inflow distribution, changes to the rotor shape are necessary to improve rotor performance. Twisting the rotor blades allows the inflow to approach this value. The ideally twisted blade calls for an inverse twist distribution where the twist angle approaches infinity at the root. As this is impossible, a linear twist provides a sufficient approximation. However, a twist also tends to create a large amount of induced drag due to the high lift distribution. Linear taper in the blade chord from root to tip will reduce the tip vortices that cause this drag. Figure 17 shows the application of the blade element momentum theory to determine the combination of twist and taper that will provide the maximum rotor figure of merit, defined as the ratio between the ideal rotor power and actual rotor power.

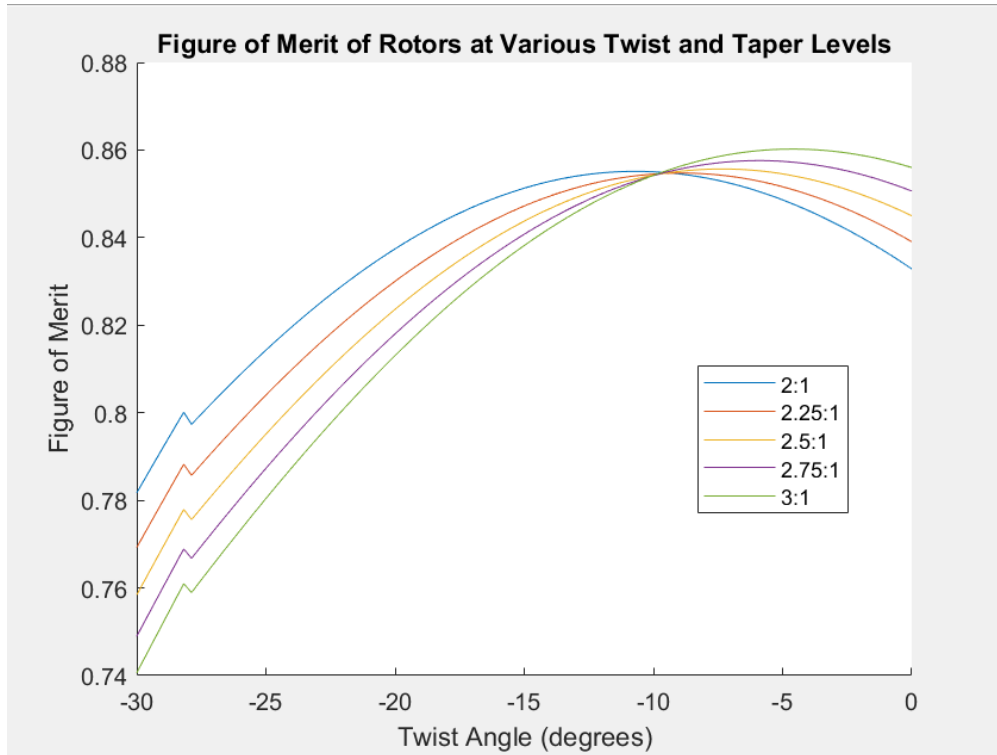


Figure 17. Rotor Blade Twist and Taper Analysis

The geometric configuration of the propeller is given in figure 18.

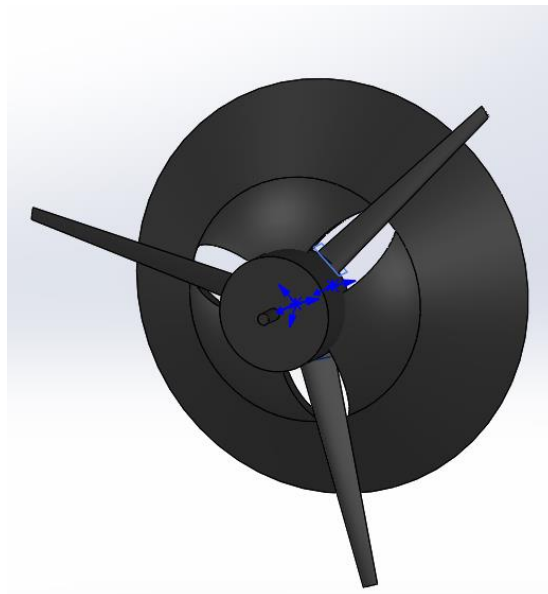


Figure 18. Propeller Configuration

The propeller was also designed using combined blade element and momentum theory. Since the inflow is much greater due to the addition of forward flight speed, the propeller disk area was able

to get much smaller to yield the best figure of merit. The same sizing, twist, and taper analysis as the rotors was applied and the results are shown below in figure 19.

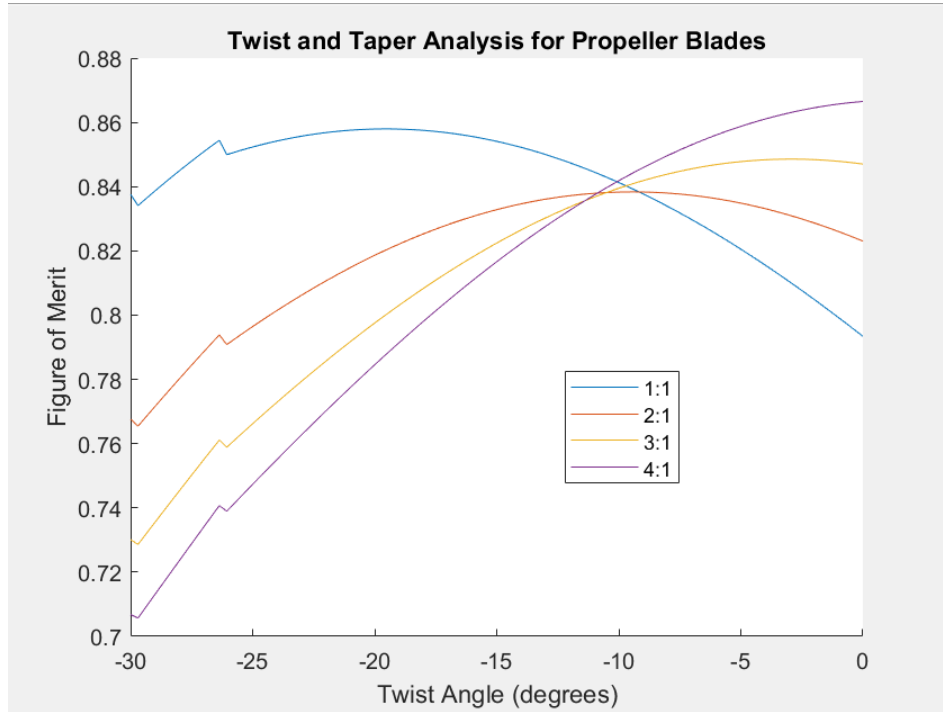


Figure 19. Propeller Design Trade Study

The geometric configuration of the main wings is given in figure 20. It has a span of 3m, a root chord length of 0.42m, aspect ratio of 6, taper ratio of 0.4, twist of 3 degrees, and utilizes a NACA 0012 airfoil. The aspect ratio, twist, taper, and airfoil was selected based on previous design successes.

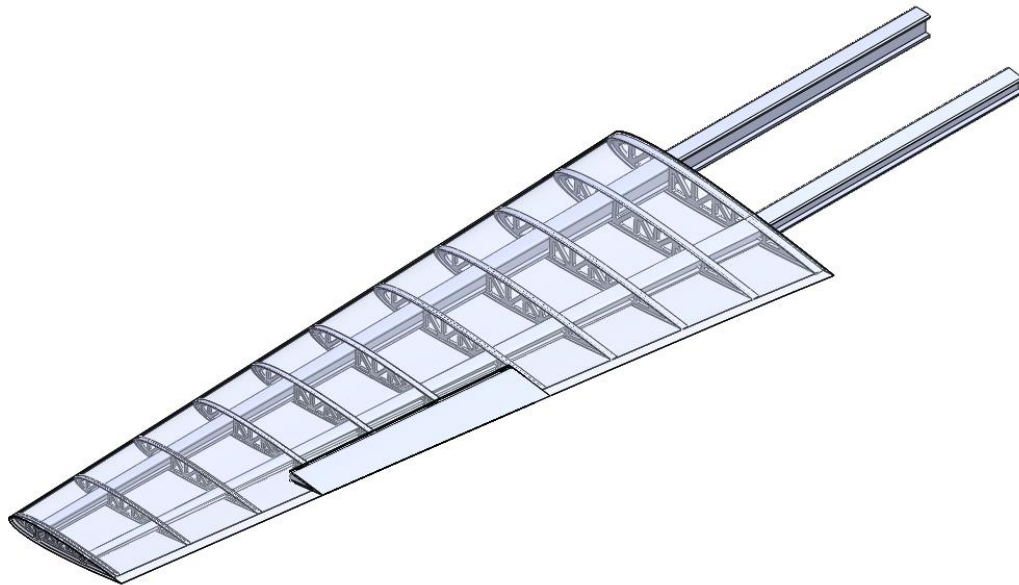


Figure 20. Wing Geometry

As the aircraft is meant to be flown at the cruise velocity that provides a maximum lift-to-drag ratio (and maximum range), the wings can be sized to operate at and drive this speed to an ideal performance value of 100 m/s. This metric is defined by the wing loading, the ratio between the aircraft weight and the reference wing area. For a rough estimate, Raymer provides an equation to determine the wing loading at maximum cruise range:

$$\frac{W}{S} = q * \sqrt{\pi * AR * e * CD_0}, \quad (8)$$

where W is the aircraft weight in Newtons, S is the wing area in m^2 , q is the dynamic pressure, AR is the wing aspect ratio, CD_0 is the aircraft drag coefficient, and e is a wing efficiency value determined from the wing induced drag coefficient [25]. The wings were designed with this area, S , and the aspect ratio was carefully selected to give the wings the structural integrity needed to hold the rotor and wing-lift loads while being long enough to reduce induced drag. The twist and taper of the wings were selected based on performance benefits from similar-sized aircraft. Rough estimates for the drag and the empennage and control surface sizing and locations were also applied from statistical methods from Raymer's *Aircraft Design: A Conceptual Approach*. Trade studies still need to conduct to determine an ideal wing loading, twist, taper, and sizing to reduce weight as much as possible.

5.1.2 Powerplant and Electronics Design

The first design decisions that had to be completed for the powerplant and electronic subsystem was to determine the type of propulsion system we wanted to use for our UAV. There are numerous types of propulsion that have been used throughout history in the aerospace industry. Some concepts like the gas turbine have been thoroughly researched and implemented in the designs of the most common aircraft. On the other hand, there are breakthrough technologies such as nuclear-powered propulsion, ion propulsion, and solar panels that give us hints at what the future might look like. We narrowed the various types of propulsion down to internal combustion engines (ICE), fully electric propulsion, and hybrid-electric propulsion because of their simplicity in design, feasibility compared to other concepts, and wide use in industry. A few pros and cons of each propulsion system can be found in Table 7.

Table 7: Pros and cons of the three propulsion systems under consideration.

Propulsion System	Pros	Cons
Internal Combustion Engine (ICE)	<ul style="list-style-type: none"> • Ideal for long range travel • Very high power density (power output per kg of fuel) • Enables long range missions with limited fuel 	<ul style="list-style-type: none"> • High carbon emission • 3/4 to 2/3 of fuel energy wasted as heat or via exhaust • Not suitable for multirotor application because of extreme engine weight

<p style="text-align: center;">Fully Electric</p>	<ul style="list-style-type: none"> • Potential for zero carbon emissions • Electric motors much quieter than engines • Electric drivetrains capable of reaching 90% efficiency (ICE efficiency is around 40%) 	<ul style="list-style-type: none"> • Really poor energy density (around 1% of ICE energy density) • Would require massive batteries to supply power for a UAV of our size • Requires much more energy to reach the speeds ICEs can achieve
<p style="text-align: center;">Hybrid-Electric</p>	<ul style="list-style-type: none"> • Optimizes energy consumption by altering power outputs depending on flight demands • Turbine powering a generator creates much more power than a battery alone would be able to provide • Battery can get recharged during cruise mode and provides backup power in case of turbine or generator failure 	<ul style="list-style-type: none"> • Much less research done and less existing aircraft utilizing hybrid-electric • Complex voltage control system for distributing among batteries, motors, and avionics

Regarding internal combustion engines, we certainly could have designed a helicopter and met all of our mission and competition requirements. However, we were intent on designing a quadcopter and so using engines to spin 4 motors would add a massive amount of weight. We also would have lost points in the competition for a lack of creativity as helicopters are quite standard. We were pretty familiar with fully electric propulsion and aware of its higher efficiency, low carbon emissions, and reduced noise. We knew it was the best propulsion system for smaller drones, but for a drone of our size, the energy density of batteries would be much too low to meet the range and velocity requirements of the mission. Hybrid-electric propulsion made the most sense for our propulsion system because we could alter power output based on which stages of the mission were the most demanding. The combination of having a gas-powered turbine and an engine to convert the mechanical power to electrical power would optimize energy consumption while also having a much lighter and more efficient design.

Going forward with hybrid-electric propulsion, we studied current aircraft and the components that were needed within our UAV. Figure 21 below showcases the most essential electronic components and how everything connects within the powerplant.

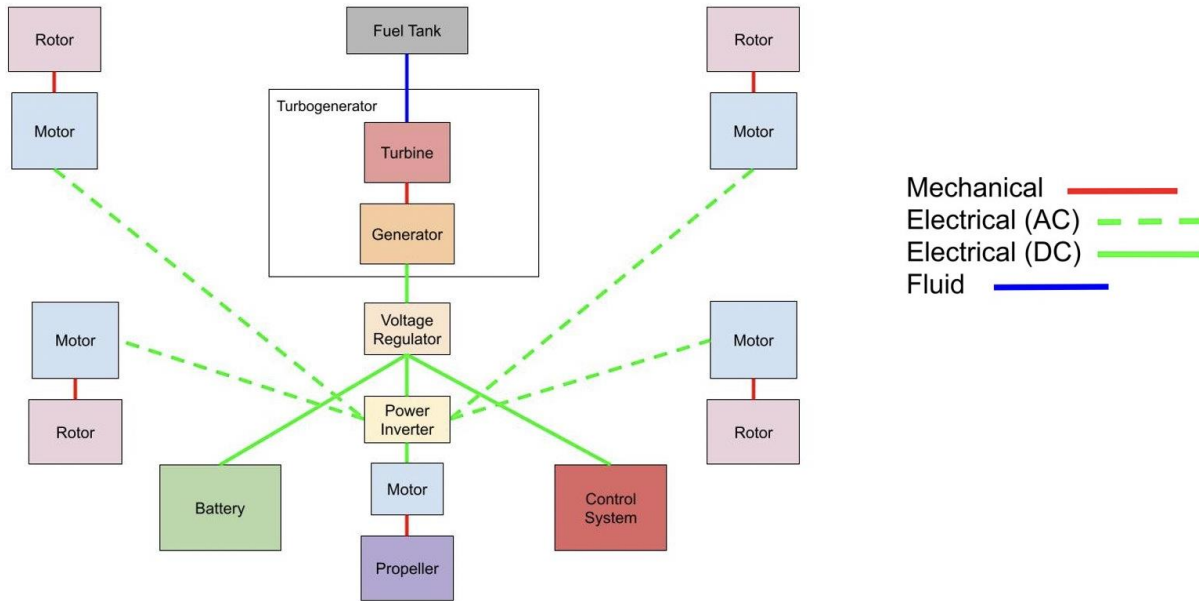


Figure 21. Diagram of the electronics subsystem and electrical connections between various components.

The fuel tank will feed the turbogenerator where the turbine will use the fuel to produce mechanical power. The generator will convert this mechanical power to electrical power and provide voltage to the motors. Because the turbogenerator outputs in DC voltage, we need a power inverter to convert it to AC voltage for our axial flux motors. The voltage regulator will be our means of distributing voltage among the turbogenerator, battery, motors, and control systems.

5.1.3 Payload Release Mechanism Design

The payload mechanism release design is composed of a ramp and a cart. The ramp and cart design was chosen because it would be reliable and lightweight. They both will primarily be built from 1/8in aluminum 6061. The payload release mechanism changed from the concept design because it was initially thought that the payload hanging beneath the UAV would create less drag because the UAV shell would be more aerodynamic. As more analysis was done it was discovered that even with a fairing covering the payload the design would not be able to fly.

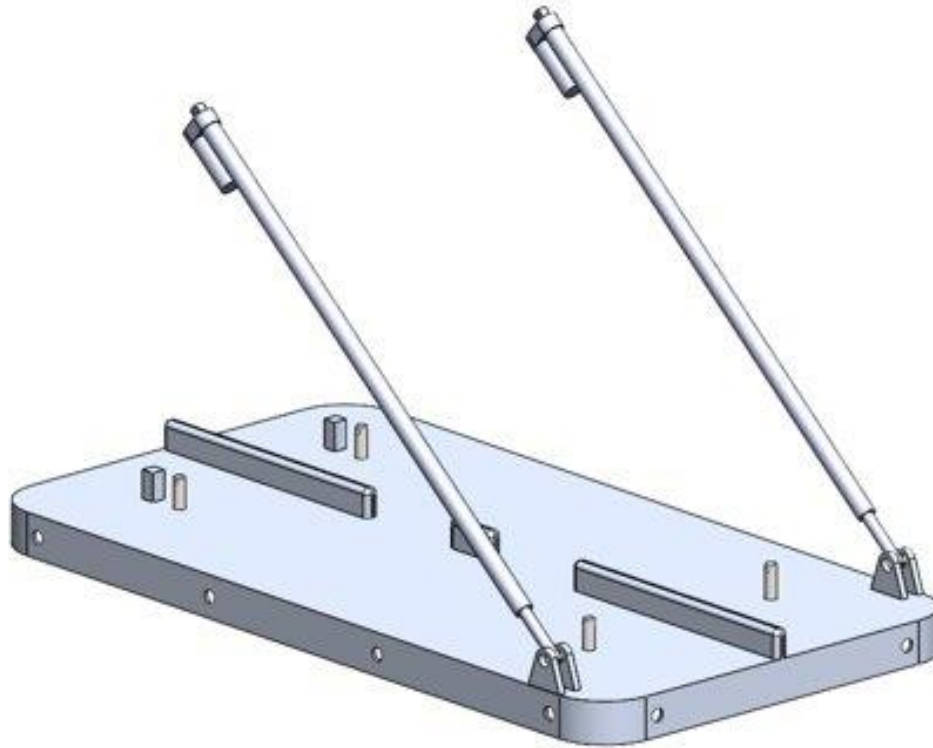


Figure 22. Payload Ramp

Above you will see the payload ramp, this will be mounted on the shell of the UAV at 12 points around the edge of the ramp. In the center of the ramp there is a 2 inch x 1 inch x 2 inch guide rail for loading and unloading the cart. The cart will be stopped by the square cart stoppers which are made from 1 inch by 1 inch aluminum 6061 bar stock on the far end of the ramp. The cart will also be locked into place with 4 small linear actuators which move normal to the top of the ramp.

There will also be two large linear actuators which will control the movement of the ramp. The connection brackets on the ramp will be plasma cut from $\frac{1}{2}$ inch aluminum 6061. Each of these large linear actuators are rated to move a load of 625N, and by assuming symmetry we can say there is a total lifting force of 1250N. It is important to note that the linear actuators will be mounted directly above the attachment points when the linear actuators are closed, this allows for the most possible force to be distributed along the axis of movement for the linear actuators.

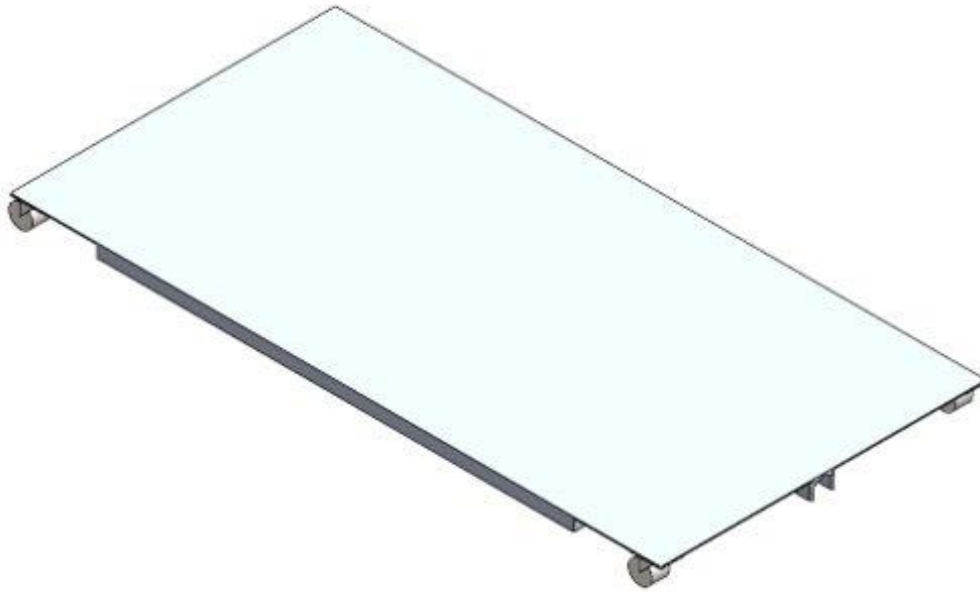


Figure 23. Payload Cart

Above you can see the payload cart. It is quite a simple design consisting of 4 castor wheels, a guidance channel and square tubing to reinforce the platform of the cart. The reason this is being built instead of purchasing a cart is the size. A cart which is 1.4m long and 0.8m wide while only being 3 inches tall is not standard. The tolerances required for the UAV to fly made designing a cart a necessity.

5.1.4 Structure Design

The primary function of the UAV structure is to support and package the external propulsion components and all the internal components in a lightweight and streamlined envelope. Additionally, the structure must be able to withstand the forces applied by the propellers and wings during all stages of the missions, especially during vertical takeoff and forward flight. The UAV structure is comprised of the fuselage, wings, rotor beams, and intake meshes as shown in Figure 24.

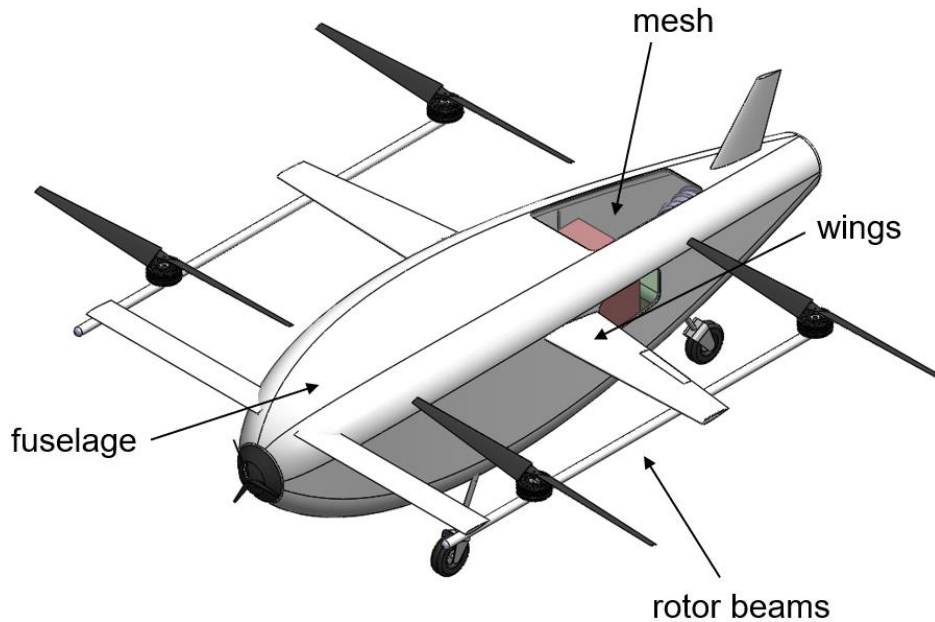


Figure 24. Major structural components of the UAV.

The largest structural component is the fuselage, which is responsible for packaging the powerplant, fuel tank, payload, and electronics in lightweight shell. The fuselage is a monocoque carbon fiber reinforced polymer which will withstand the loads on the UAV without the need for an internal frame. A carbon fiber monocoque is advantageous as carbon fiber reinforced polymers (CFRP) have an excellent strength-to-weight and stiffness-to-weight ratio when compared with other composites and alloys such as steel and aluminum. As a result, the mechanical properties of carbon fiber make it the lightest material that can achieved the required strength and stiffness for the fuselage. Furthermore, the lack of a frame in a monocoque fuselage allows for further weight reductions as the skin of the fuselage will take the majority of the static and flight loads on the UAV. In addition to being strong, stiff, and light, the fuselage must also be as streamlined as possible to reduce the drag on the UAV. The lower the frontal area and drag coefficient on the fuselage, the lesser the power and energy required to complete the mission and the greater the best range speed. The symmetrical, streamlined shape of the UAV is shown in Figure 25.

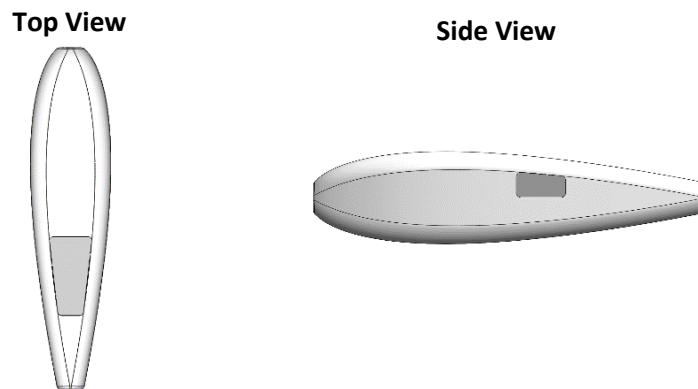


Figure 25. Streamlined shape of the fuselage based on symmetrical NACA airfoil.

The symmetrical shape of the streamlined fuselage was modeled using the equation for a symmetrical NACA airfoil,

$$y_t = 5t [0.2969\sqrt{x} - 0.1260x - 0.3516x^2 + 0.2843x^3 - 0.1015x^4] \quad (7)$$

where t is the maximum chord thickness, x is the horizontal distance from the front to the back of the airfoil, and y_t is contour line of the airfoil [26]. The streamlined shape of the fuselage is especially critical as the fuselage features cutouts covered with a structural mesh that allow air to pass into the compressor of the turbogenerator. These meshes will disrupt the boundary layer over the surface of the fuselage which will increase profile drag. We are still considering alternatives to the mesh, such as an intake duct that sticks out slightly on the surface of the fuselage, but that option will also lead to disruption of the boundary layer. As a result, modeling the fuselage to be as streamlined as possible is very important to compensate for the air intake features required by the turbogenerator.

Another major component of the UAV structure is the rotor and wing frame that features the wing spars and rotor beams as shown in Figure 26. The rotor beams run along the direction of air flow and will support two of the rotors each. The wing spars run horizontally from tip-to-tip of the two wings and will take the bending loads induced by the rotors and wings.

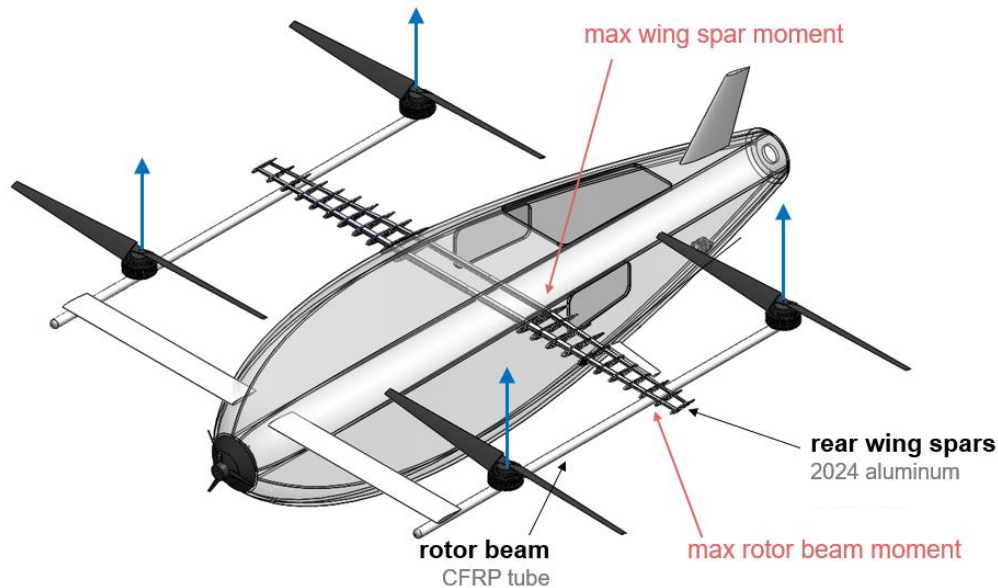


Figure 26. Rotor and wing frame that supports the propellers and wings.

One of the main advantages of this rotor and wing frame is that each member can be modeled as simply supported so the joints do not have to take moments to support the structure. Additionally, the wing spars, one in the front (not shown in the figure) and two in the back, which are perpendicular to the air flow in forward flight will be covered by airfoils which will reduce the drag on the frame. For the rotor beams which are designed to withstand bending loads induced by the rotors, we selected a CFRP tube due to its high strength and stiffness and low density.

Furthermore, the tube will allow wiring and coolant tubes to be routed inside the tubes for efficient packaging. The wing spars are aluminum I-beams which run from tip-to-tip of the wings. In the rear main wing, there two spars in order to reduce the bending moment each spar. We selected aluminum for the spars because of its ability to be forged into an I-beam which allows for the spars to be thin enough to fit inside the wings. We designed the wing spars to run from wing-to-wing so that spars will withstand the bending moments and the skin of the fuselage will withstand the shear forces where the wings attach to the fuselage. This load path is preferable because we do not want to exert bending loads on the fuselage, especially because it is made of CFRP which performs best when loaded in-plane.

5.2 Design Justification

To justify the viability of adding a propeller and wings to our design, we redid the analysis performed in section 4.3.4 using updated calculations which are attached in Appendix E. We derived the following equations for vertical rotor thrust, T_v , and horizontal propeller thrust, T_h ,

$$T_v = \frac{W - C_L A_s (\frac{1}{2} \rho V_t^2)}{N} \quad (8)$$

$$T_h = C_D A (\frac{1}{2} \rho V_t^2) \quad (9)$$

Where T_v is the difference between the weight and lift generated by the wings divided by the number of rotors, and T_h is equal to the drag force. A_s is the wing surface area and N is the number of rotors. The following analyses were performed assuming a drag coefficient of 0.2, frontal area of 1 m², a constant lift coefficient for all velocities, and four rotors. The vertical and horizontal thrust required with respect to cruise velocity is shown in Figure 27.

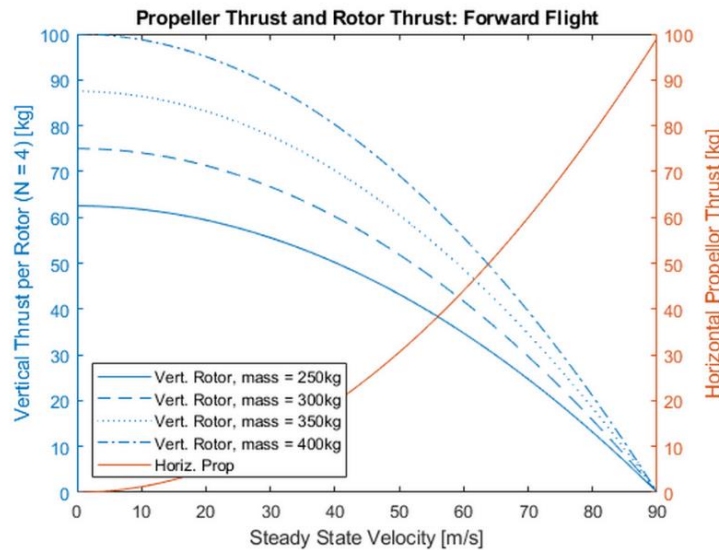


Figure 27. Vertical and horizontal propeller thrust plotted against cruise speed.

As the cruise speed increases and the wings provide more and more lift, the thrust required by the vertical rotors decreases towards zero at the speed where the lift provided by the wings equals the weight of the UAV. These estimates for thrust also provide a baseline for what thrust should be expected when measuring the thrust provided by the selected motor and propellers.

The thrust calculated in Figure 27 and momentum theory analysis (equations 5 and 6) was used to calculate the power required by the rotors and propellers during forward flight. The results of these calculations are shown in Figure 28.

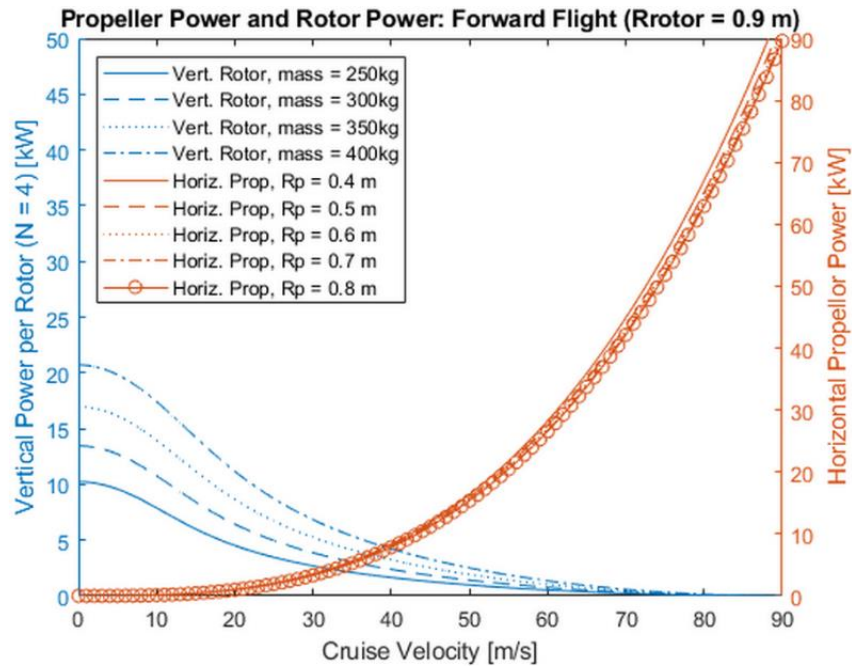


Figure 28. Vertical and horizontal power required during forward flight. Vertical power is calculated per rotor assuming $N = 4$ rotors.

The power calculations in Figure 28 indicate that larger rotor diameters reduce the power required vertical rotors. Additionally, we observe that the horizontal propeller power required does not vary much with propeller diameter; however, the diameter must be large enough such that operating speed at the required power is within the range of motors rated at this power.

The total power required by the vertical and horizontal propellers with respect to cruise velocity was calculated and plotted in Figure 29.

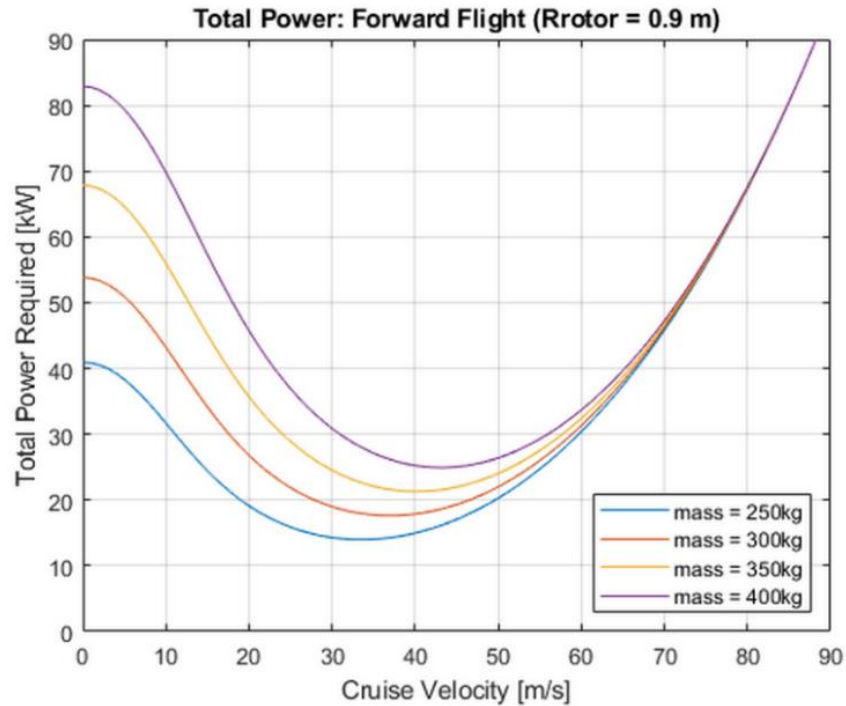


Figure 29. Total power required plotted against cruise velocity.

The total power calculations indicate that the best range speed, the speed at which the energy consumption to complete the mission is at a minimum, is approximately 50 m/s for masses near our expected UAV mass which is fast enough to complete the missions in the required time. The best range speed can be increased by reducing the drag on the UAV by streamlining the body and reducing the frontal area.

The main issues with our initial concept design was the low energy density of the battery and the high energy consumption required to complete the mission. By adding wings to the UAV and switching to fuel as the means of energy storage, we reduced the power and thus energy required to complete the mission as well as the weight of the energy storage medium due to the high energy density of fuel. The reduction in power required as the wings provide more and more lift is shown in Figure 30.

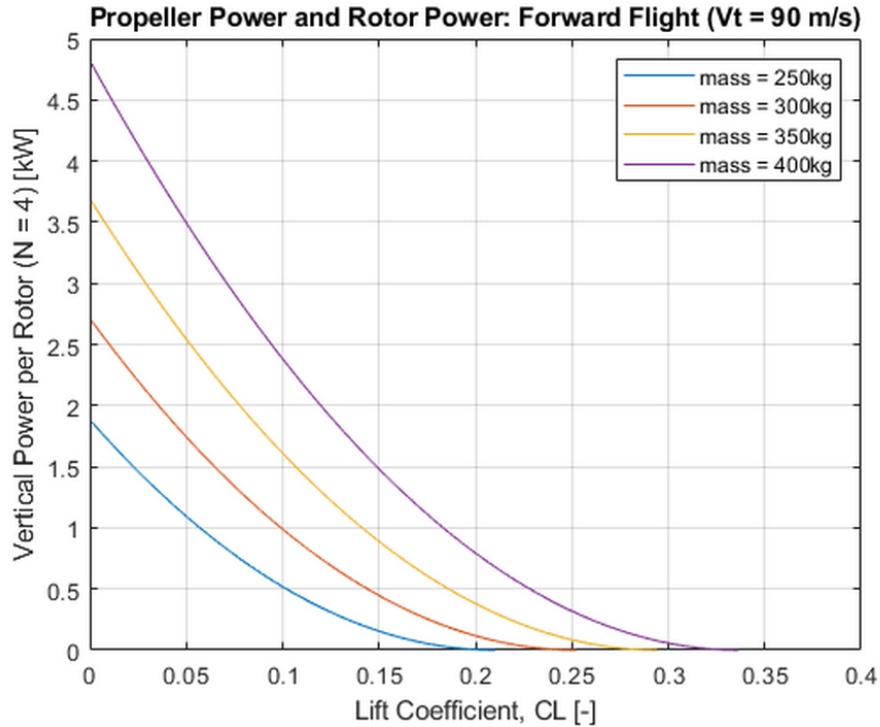


Figure 30. Vertical power required per rotor as wings provide more lift. Velocity is constant at 90 m/s.

Figure 30 illustrates how the power per rotor reduces significantly as wings provide more lift at higher velocities. As a result, the energy consumption required to complete the emission decreases and less stored energy is required. The MATLAB code used to compute these analyses is attached in Appendix G.

5.2.1 Propulsion System Analysis

Performance in forward flight relies on two parameters: the load distribution of the wing from lift and the drag of the aircraft. The size of the wing impacts how much stress the spars of the wing experience. To find the lift distribution across the wing, Prandtl’s Lifting Line Theory was applied using Schrenk’s approximation. Lifting Line Theory, when applied on its own, approximates the lift across the wing as an ellipse, which is the most ideal case. Schrenk’s approximation, however, takes the trapezoidal geometry of the wing into account and alters the lift distribution to be an average of the two, leading to a more accurate analysis. The loads on the wing end up not exceeding the loads cause from the weight and thrust of the rotors during climb, ensuring that the fixed-wing loads are not critical. This method was also used to calculate the induced drag and efficiency factor, e .

The parasitic drag of the aircraft was approximated using the component build-up method. Parasitic drag is comprised of two components: skin drag representing friction across the boundary layer, and form drag representing back pressure caused by the flow wake during boundary layer separation. Accurate determinations of both drag forms require aerodynamic flight or wind tunnel tests. However, skin friction drag can be reasonably approximated by analyzing the wetted surfaces



of the aircraft as a flat plate. Boundary-layer theory can be used to find the coefficient of friction of all exposed surfaces, which can be converted into a drag coefficient. Form drag was approximated using more statistical measures, in which the coefficient of drag was estimated using projected frontal areas and historical data from other aircraft. The coefficient of drag from each exposed aircraft component, including the fuselage, wings, empennages, rotors, rotor arms, and tires was found and added together, with corrections made for part wake interference. The coefficient of drag for this aircraft came to be around 0.02, close to the value typically seen in other homebuilt composite aircraft.

While the mission calls for a climb time of two minutes, our aircraft contains enough power and fuel to exceed this value if needed. Therefore, the main limiting factor on climb power and speed is rotor noise. Rotor noise can come from three main sources: rotational noise, blade vortex noise, and blade slap. Blade slap is a phenomenon specific to advancing tip velocities reaching transonic speeds in forward flight and will not occur at any point during the missions for this aircraft. Rotational noise is caused by resonance of the rotor blades vibrating at various harmonics at certain rotational speeds. The first few harmonics occur below the noise frequency heard by humans while the higher harmonics will not present concerning or annoying volume levels. Blade vortex noise is the critical noise source for our aircraft. It is caused by the interference of a rotor blade with the tip vortices caused by the blade in front. It's a phenomenon that increases in volume level as rotor RPM increases. Typical helicopters keep their noise level at or around 80dB for citizens 150m away, above which the noise begins to get annoying. During hover, our noise level stays at around 70dB. However, our climb RPM causes the rotor noise to reach a peak of close to 90dB. While this noise level is not damaging, further trade studies and analysis may allow this level to be reduced to acceptable levels.

5.2.2 Powerplant and Electronics Analysis

Much of the powerplant and electronic analysis comes down to making the correct selection of the components on our UAV. Starting with the turbogenerator, the goal was to find one that could provide enough power for our motors at a reasonable weight. Because there are not too many hybrid electric propelled aircraft out there, we were quite limited in our options. Table 8 below displays the three turbogenerators we found with a few of the most important engineering specifications.

Table 8: Turbogenerator options for hybrid-electric propulsion system

Turbogenerators	Manufacturer	Power Output (kW)	Weight (kg)	Power-to-weight ratio (kW/kg)
 TG-R90	TurboTech	90	64	1.406
 M250 Turboshaft + ETC-300 Generator	Bowman	70	113	0.619
 HTS900 Engine + 200 kW Honeywell Generator	Honeywell	200	181	1.105

Ultimately deciding on the turbogenerator to use was pretty straightforward. The M250 Turboshaft combined with the ETC 300 Generator was much less efficient than the TG-R90. The HTS900 Engine and 200 kW Honeywell Generator offered more power than necessary and with lots more weight. The TG-R90 clearly has the best power-to-weight ratio and provides 90 kW of power which was perfect to meet the vertical takeoff power required of 60-90 kW. Another upside of choosing the TG-R90 was the fact that it is all one component and acts as a true turbogenerator. The other two options were individual engines and generators that work well by themselves, but we were not sure if they would be compatible together to function as a turbogenerator.


The next step was to choose the best motors for our UAV, one for the horizontal propeller and four for the vertical rotors. This process involved finding the required thrust from each motor and selecting reliable motors that could meet these power demands. With a safety factor of 1.5 and determining the weight of the aircraft to be around 350 kg, we calculated the thrust required to be 131.25 kg from each motor. Finding motors to fit our needs was much easier than it was for the turbogenerator. Optimizing our design selection involved finding the highest power-to-weight ratio, minimizing the frontal area to reduce drag, and ensuring continuous power achieved the minimum desired values of 30 kW per motor. With all of this in mind, we ended up selecting 4 EMRAX 208 motors and 1 EMRAX 228 motor. These axial flux motors offer the perfect amount of power at a relatively small weight of 9 and 12 kg respectively. To further instill confidence in our design selection, we contacted EMRAX to verify if these motors would work for our application and if our desired rotor and propeller diameters were compatible. Once we provided all the power requirements of our project, EMRAX confirmed that we selected the correct motors. A few essential engineering specifications of the EMRAX 208 and EMRAX 228 are presented in Table 9.

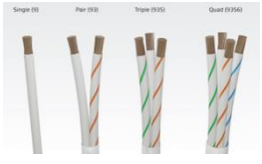

Table 9: Important specifications of the EMRAX 208 and EMRAX 228 axial flush motors

Specification	EMRAX 208	EMRAX 228
Continuous Power	41 kW	62 kW
Peak Power	68 kW	109 kW
Weight	9 kg	12 kg
Max RPM	6000 RPM	5500 RPM
Power-to-Weight Ratio	7.56 kW/kg	9.08 kW/kg
Continuous Torque	80 Nm	120 Nm

Along with the turbogenerator and motors, we needed to find a fuel tank, battery, voltage regulator, control system, inverter, and object detection system. We also had to identify wiring to be used to connect all these components. Not too much went into this selection process other than researching popular aircraft and finding reliable manufacturers for our components. Table 10 below displays the models and manufacturers for the rest of the electronic subsystem.

Table 10: Additional components within the electronics subsystem.

Component	Model	Manufacturer
Fuel Tank	 ATL-794-A	Aero Tec Laboratories
Battery	 24 V Lithium-Ion Battery	Eaglepicher Technologies
Voltage Regulator	 R15VOL	Zeftronics

Wiring	 <p>GWN3000</p>	GORE
Control System	 <p>AP10.1</p>	UAVOS
Inverter	 <p>PM100</p>	Cascadia Motion
Object Detectance System	 <p>Casia 360</p>	Iris Automation

Now that we understood what electrical components we needed onboard our UAV, we decided a fuel consumption analysis would help justify our decision to use hybrid-electric propulsion to complete our mission. For this analysis, we had to estimate at what percentage of maximum output the turbogenerator would operate at during different stages of the mission. For lift and descent, we assumed the turbogenerator operates at maximum power output, meaning the fuel consumption rate was also at its maximum of 25 L/hour of Jet A-1 fuel. During forward flight, the fuel consumption rate was 75% of the maximum rate, or 18.75 L/hour. Lastly, during hover mode, the rate was 50% of the maximum rate, so 12.5 L/hour. The velocity of our UAV was 2 m/s for lift and descent and 100 m/s for forward flight. Using all of this information, we were able to calculate the amount of time the UAV spent for each stage of the mission and thus find out how much fuel was consumed throughout. Figure 31 and Figure 32 below shows the altitude over time for missions 1 and 2 respectively, and it is clear to see when the UAV is in lift, descent, and either hover or cruise.

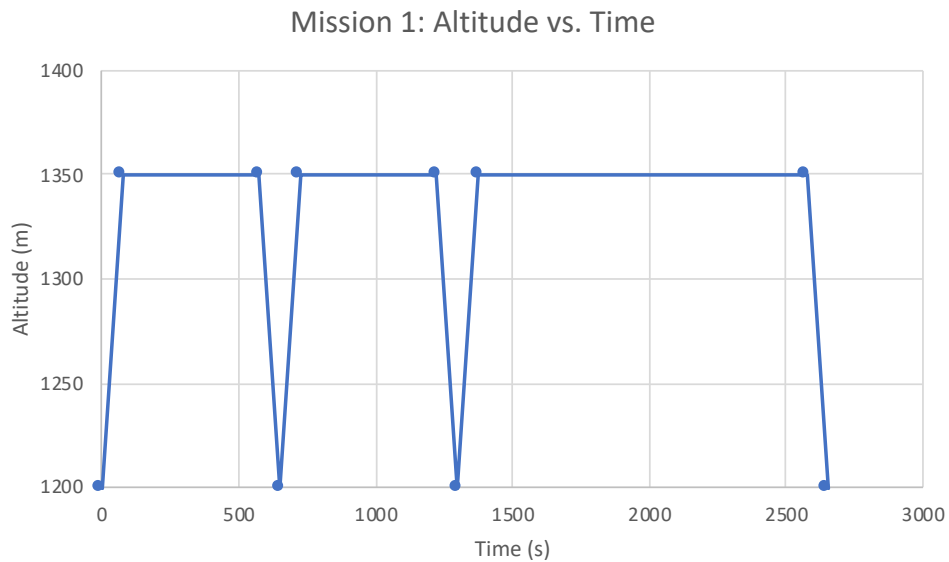


Figure 31. Altitude over time throughout mission 1.

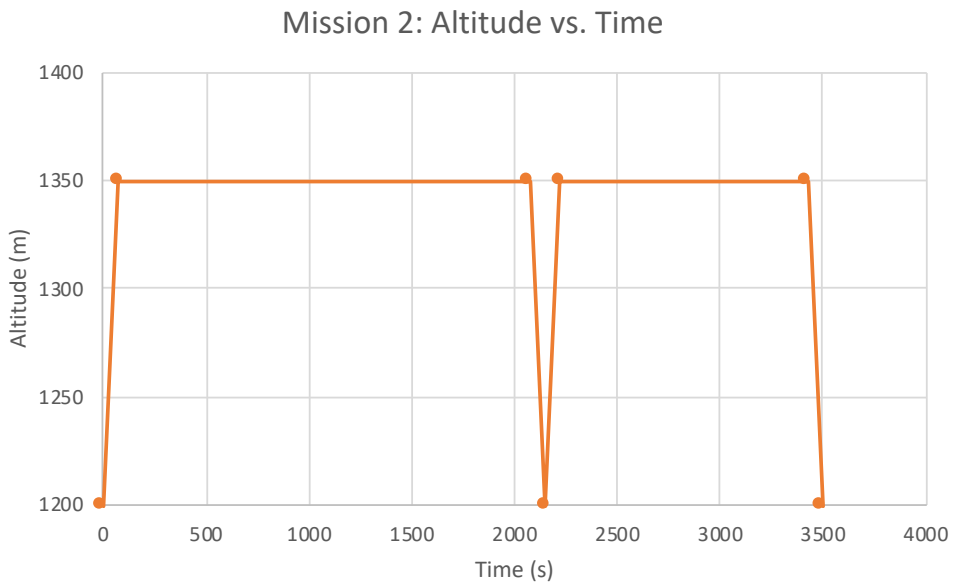


Figure 32. Altitude over time throughout mission 2.

After calculating the flight time for each mode of flight, we were able to determine based off the fuel consumption rates that mission 1 would use up a total of 13 liters of Jet A-1 and mission 2 would use up just under 17 liters. Because we want to have the two missions start with the same fuel capacity, we determined 17 liters to be the optimal amount of starting fuel that would allow both missions to be completed and prevent any additional weight from excess fuel. Figures 33 and 34 below show the decrease in percent fuel capacity throughout the mission.

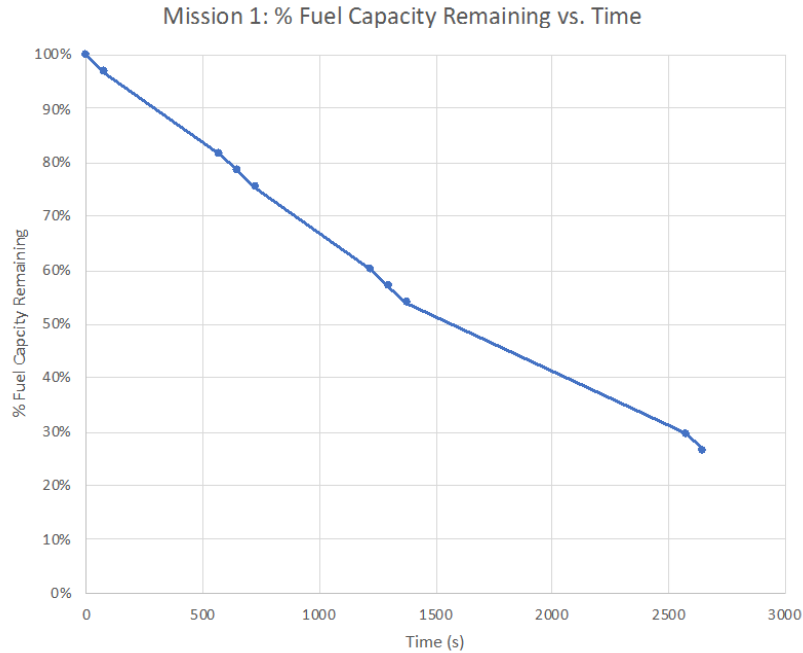


Figure 33. Fuel capacity percentage remaining over time throughout mission 1.

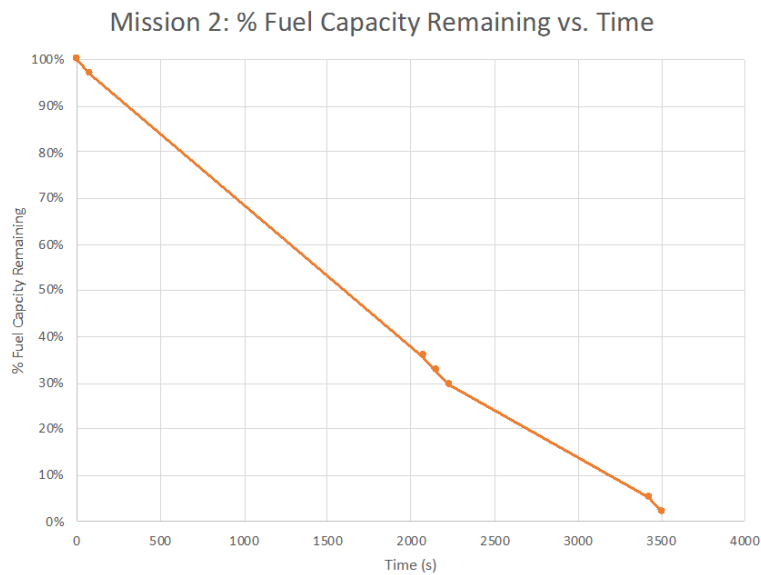


Figure 34. Fuel capacity percentage remaining over time throughout mission 2.

5.2.3 Payload Release Mechanism Analysis

The most critical part of the payload release mechanism are the two large linear actuators which are controlling the movement of the entire platform, cart and 50kg payload. Recall that the two linear actuators are each rated to move a force of 625N. By assuming they take the load symmetrically a model can be created to determine if the linear actuators will be able to handle the

loads required. Below you will see a figure describing the forces seen by the linear actuators and the maximum force they have available.

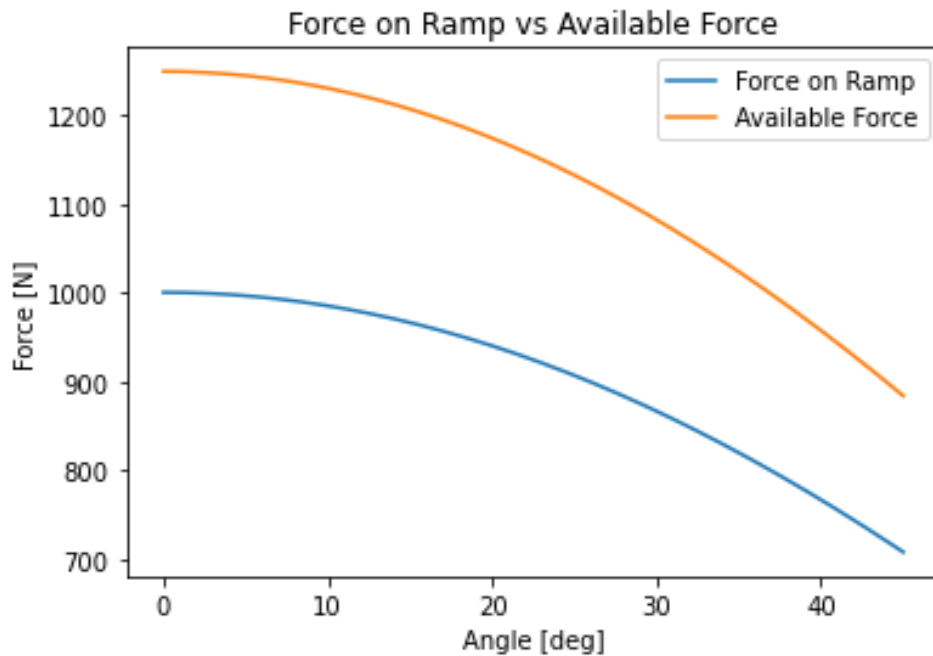
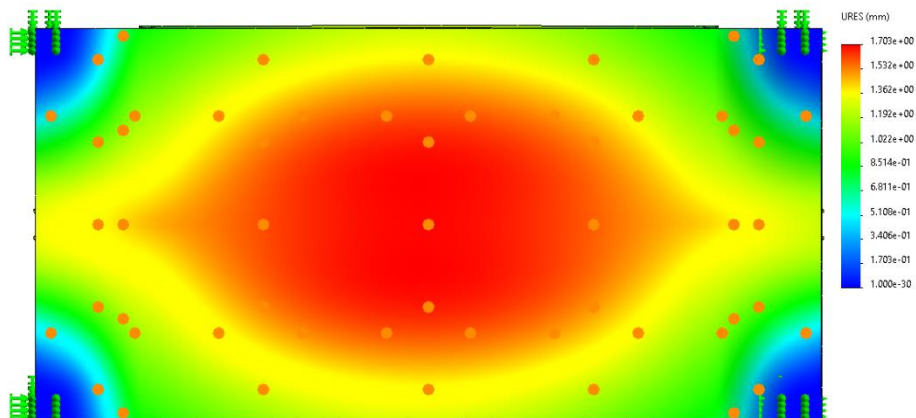


Figure 35. The force on the ramp represents the actual force seen by the linear actuators on the correct axis and the available force is the maximum force the linear actuators can see.

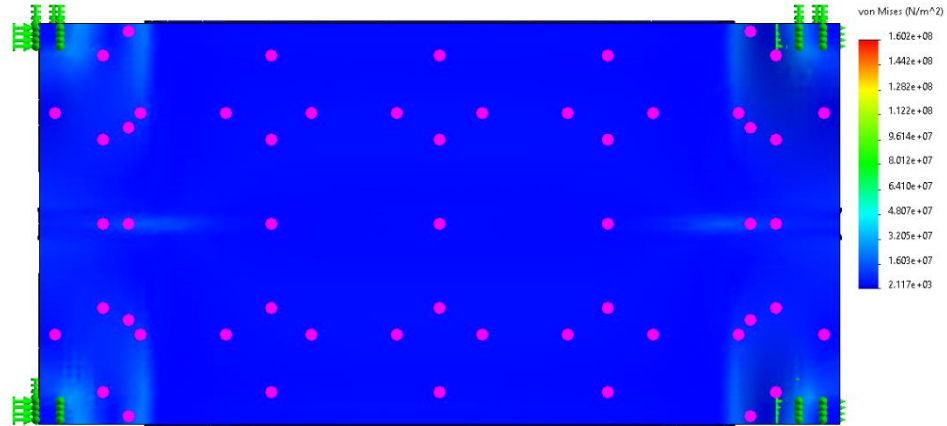
The ramp will never open more than 45 degrees, so as the figure above illustrates the linear actuator is rated well above the required loads and will not fail.



SOLIDWORKS Educational Product. For Instructional Use Only.

Figure 36. FEA of the payload release cart showing displacement due to payload loading

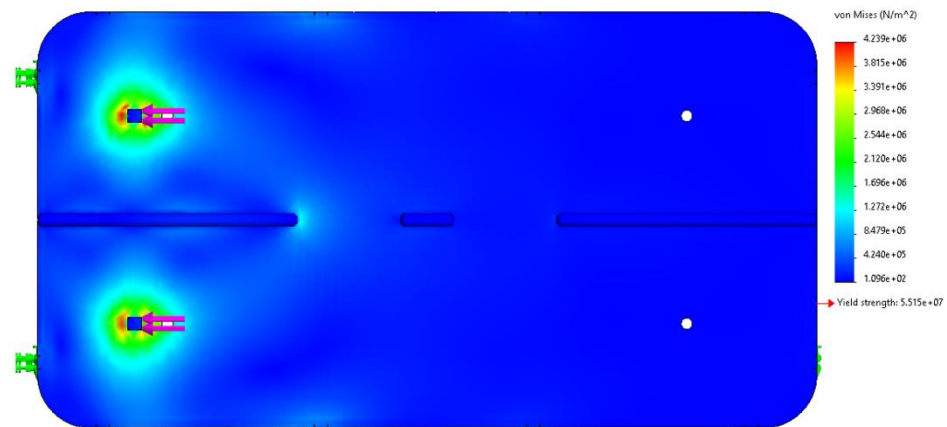
Above you can see the FEA model of the payload release cart. It is modeled with the wheels being fixed; this is not entirely accurate but can provide a reasonable estimation about the deflection. It shows a deflection in the center of the cart of about 1.7mm. This may seem like a large deflection, and is certainly not negligible, but we are not dealing with high-speed moving parts so a deflection of 1.7mm will not cause any critical failures.



SOLIDWORKS Educational Product. For Instructional Use Only.

Figure 37. FEA of the payload release cart showing stress due to payload loading

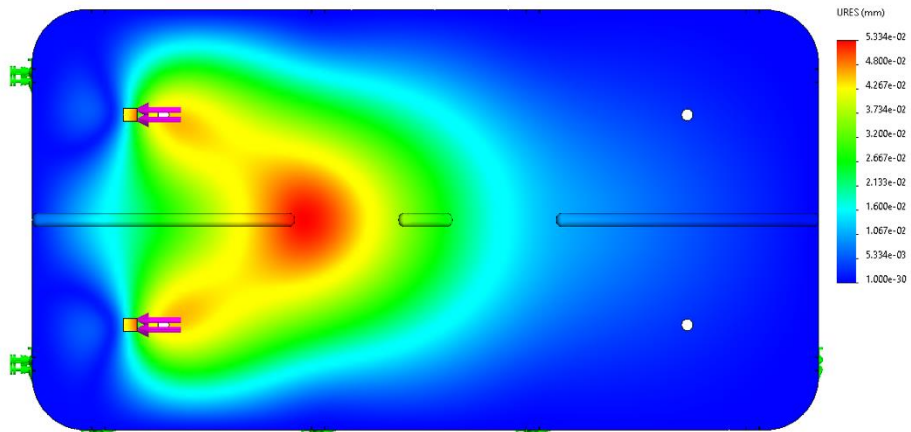
Above you can see the FEA model of the payload release cart showing the stress distribution when the payload is loaded onto the cart. This is to be expected because the payload has a relatively low weight when comparing it to the strength of aluminum.



SOLIDWORKS Educational Product. For Instructional Use Only.

Figure 38. FEA of the payload release ramp cart stoppers, stress

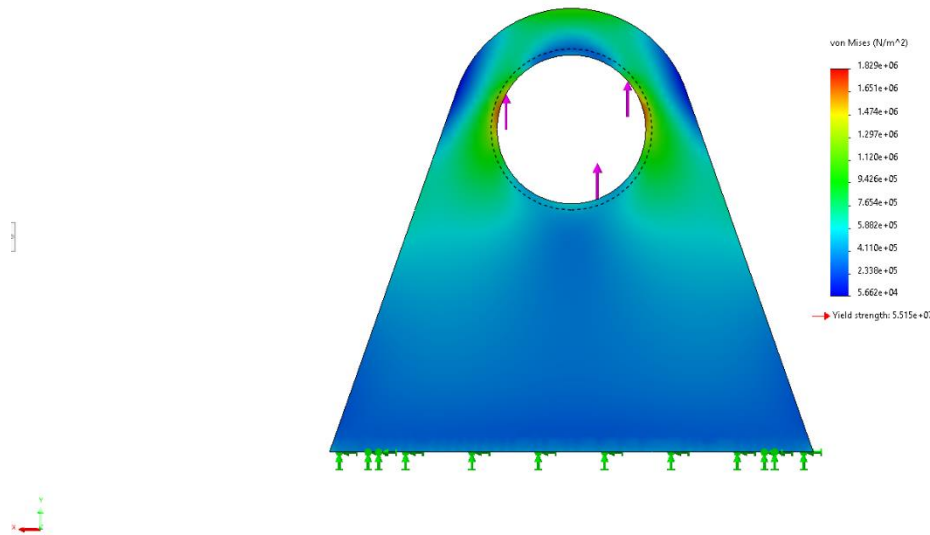
The FEA model shown above represents the maximum load seen by the cart stopper blocks. The maximum stress can be seen to be around $4.3 \times 10^6 \text{ N/m}^2$ which is around ten times lower than the yield stress of aluminum 6061.



SOLIDWORKS Educational Product. For Instructional Use Only.

Figure 39. FEA of the payload release ramp cart stoppers, displacement

The FEA model shown above shows the displacement to be 0.05mm which is quite small. This displacement is nothing to worry about.

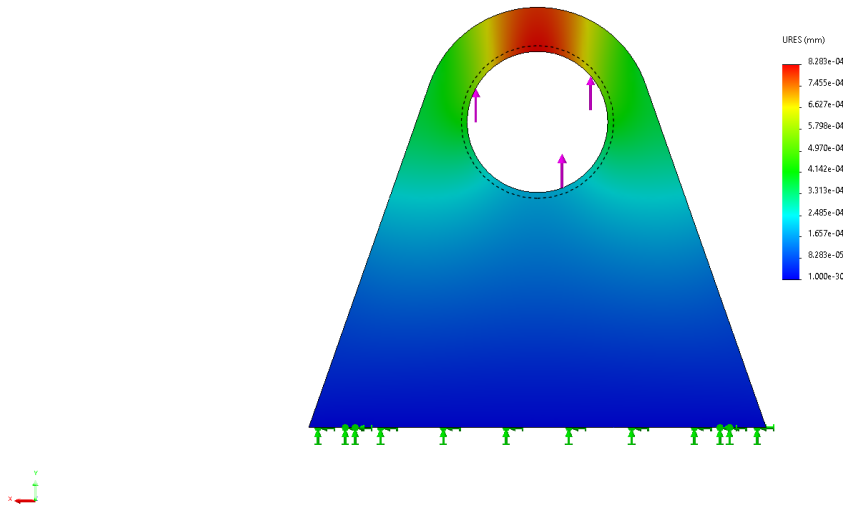


SOLIDWORKS Educational Product. For Instructional Use Only.

Figure 40. FEA of the attachment brackets, stress

The FEA model shows the stress at the maximum rated load for the large linear actuators evenly distributed to the 4 attachment brackets. This means that each bracket takes a load of 312.5 N.

These brackets will likely never see these loads since normal operating conditions will be significantly less rigorous.



SOLIDWORKS Educational Product. For Instructional Use Only.

Figure 41. FEA of the attachment brackets, deflection

The FEA model shows the deflection at the maximum rated load. This model shows that the deflection will be 0.0008 mm, which is negligible in this application.

5.2.4 Structural Analysis

The analysis on the structure was performed for the vertical takeoff segment of the missions which is the most critical load case for the UAV. During vertical takeoff, the rotors exert the greatest amount of thrust that they will need to provide to complete the mission. Therefore, the loads on the rotor beams, wing spars, and fuselage were calculated using the vertical takeoff load case shown in Figure 42.

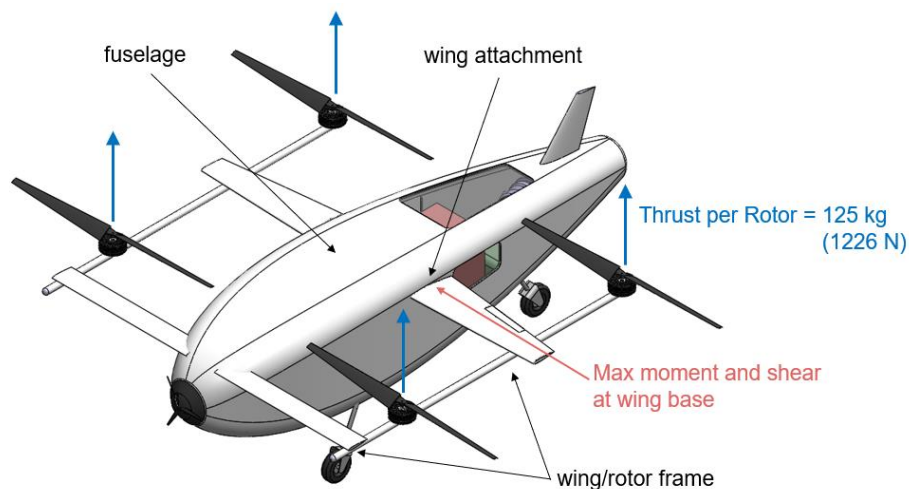


Figure 42. Vertical takeoff load case where thrust provided by the rotors is greatest and bending moments are greatest.

The shear and bending loads on the rotor and wing frame were determined by solving for the pin forces in each member and using the results to generate shear and moment diagrams. Hand calculations for the rotor and wing frame are attached in Appendix I. Calculations were performed for carbon fiber circular tubes and aluminum I-beams with selections made based on weight and packaging requirements. The yield strength of 2024 aluminum was used to determine the factor of safety for the carbon fiber tubes as a conservative estimate because the anisotropic properties of carbon fiber make the strength difficult to predict. The results of the analysis are tabulated in Table 11.

Table 11: Bending stress and FOS in rotor beam and wing spars for vertical takeoff load case.

Component	Material	Cross Section	Max Bending Stress [MPa]	FOS
rotor beam	CFRP	circular tube	179	1.81
wing spar	2024 Aluminum	I-beam	148	2.19

We constrained the factors of safety for both the rotor beams and wing spars to be at least 1.8 as failure of these components will cause catastrophic failure of the UAV because the rotors and wings will no longer be supported if these components fail. Two wing spars were required for the main wing in order to split the bending stress between the two spars and increase the factor of safety without having to increase the thickness of the wing to accommodate a thicker spar.

The maximum bending moment and shear force on the structure occurs at the base of the wing where the wing attaches to the fuselage. The spars run from wing-to-wing and will thus withstand the bending moments while the fuselage will withstand the shear force. We performed structural FEA simulations to verify the strength of the attachment bracket and fuselage skin at the wing attachment points as shown in Figure 43.

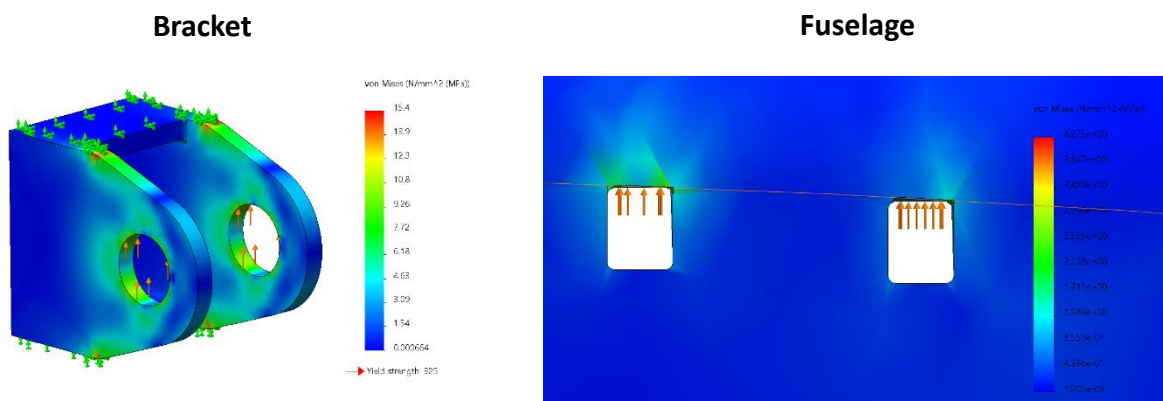


Figure 43. FEA structural simulations for force on attachment brackets and attachment points in the fuselage.

The stress is order of magnitude lesser than the material strength for both the attachment bracket and attachment holes in the fuselage indicating that both are over-designed and very unlikely to fail. Furthermore, the fuselage skin can be made thinner to reduce the weight of the structure and still have a large factor of safety.

5.3 Safety, Maintenance, and Repair Considerations

Because of the high risk involved in operating a delivery UAV, we will want to enforce plenty of safety procedures and maintenance. It is essential that inspections are done before and after the UAV operates, and that test flights are done routinely. We will ensure the UAV is manufactured with high-quality parts and inspected for any damaged parts throughout its lifetime. Any signs of damaged parts will be immediately replaced. During flight, there will be an emergency landing protocol in response to any threats to safety. If possible, the emergency landing will quickly be communicated via radio signals and we intend to incorporate an emergency parachute in case the UAV has lost flight control.

Protecting the users is critical safety requirement for the UAV. We will protect the user by including a kill switch for the rotors and propeller when the payload ramp is open as an open ramp indicates that an operator or customer is nearby. Furthermore, cautions signs will be added to the UAV near points where the user interacts with the UAV and near moving parts such as the rotors and propeller. Additionally, a caution sign will be added near the exhaust outlet of the UAV to warn user of hot temperatures.

To prevent fires and possible explosions, we put the turbogenerator and fuel tank at the rear of the UAV and the battery, propeller motor, and electronics at the front of the UAV with the payload in between to keep the gas turbine and electronics as far away as possible. We will add a firewall in front of the turbogenerator and behind the payload to reduce the likelihood of fires spreading from the rear to the front of the UAV.

5.4 Cost Analysis

Observing the total costs of the project, we see that electronics and structure of our UAV will be the most expensive. The payload mechanism will be relatively cheap, and we have yet to determine cost estimations for the propulsion system. Many of the costs for the electronics were very rough estimates since for many components we could not find any information online regarding prices. The total price of the electronics, payload, and structure subsystems came out to \$29,966. Tables 12-14 below show the cost estimates for each subsystem.

Table 12: Cost analysis of electronic subsystem

Electronics			
Component	Qty	Cost	Total Cost
Turbogenerator	1	\$4,000.00	\$4,000.00
Motor	5	\$700.00	\$3,500.00
Battery	1	\$500.00	\$500.00

Fuel Tank	1	\$600.00	\$600.00
Control System	1	\$1,000.00	\$1,000.00
Wiring	1	\$400.00	\$400.00
Voltage Regulator	1	\$500.00	\$500.00
Object Detection System	1	\$300.00	\$300.00
DC to AC Inverter	1	\$300.00	\$300.00
Total Cost: \$11,100			

Table 13: Cost analysis of payload mechanism subsystem

Payload Mechanism			
Component	Qty	Cost	Total Cost
36in Linear Actuator	2	\$269.99	\$539.98
2in Linear Actuator	4	\$56.99	\$227.96
1/8 Aluminum Plate, 28inx56in	1	\$365.52	\$365.52
1/2 Aluminum Plate, 31.5inx60in	1	\$78.66	\$78.66
1in Aluminum Bar stock, 12ft	1	\$56.59	\$56.59
1"x2" Aluminum Bar 36in	1	\$43.60	\$43.60
Caster Wheels	4	\$7.40	\$29.60
1/4in-20x1/2in Stainless Steel Hexbolt 5- pack	4	\$1.71	\$6.84
1/4in-20 Stainless Steel Hex Nut 4 pack	4	\$1.18	\$4.72
2"x2"x.125" Aluminum channel 60in	1	\$30.89	\$30.89
1/8in Aluminum Plate 27inx56in	1	\$365.52	\$365.52
Total Cost: \$1,750			

Table 14: Cost analysis of structure subsystem

Structure				
Component	Qty	Cost	Manufacturing	Total Cost
Prepreg 3K, 2x2 Twill Weave Carbon - 5yd roll	10	\$694.25	\$300.00	\$7,242.50
Nomex Honeycomb	2	\$2,445.72	\$-	\$4,891.44
Carbon fiber airfoil-shape legs	1	\$179.90	\$20.00	\$199.90
24n Linear Actuator	2	\$230.00	\$-	\$460.00
Actuator aluminum sheet metal straps	4	\$2.48	\$-	\$9.90
1/4in-20 Stainless Steel Hex Nut 4 pack	4	\$1.18	\$-	\$4.72

4" x 2" Polyolefin Wheel	2	\$9.94	\$-	\$19.88
3K 2x2 twill carbon fiber tube - 1.25 X 1.50	6	\$321.79	\$-	\$1,930.74
Rear generator brackets	2	\$297.75	\$20.00	\$635.50
Front generator brackets	2	\$297.75	\$20.00	\$635.50
Front generator struts	2	\$56.46	\$50.00	\$212.92
Motor mount	1	\$61.77	\$100.00	\$161.77
Battery box	1	\$91.26	\$20.00	\$111.26
Electronics enclosure	1	\$179.90	\$20.00	\$199.90
Fuel tank mount	2	\$179.90	\$20.00	\$399.80
Total Cost: \$17,116				

6. Final Design

6.1 Design Changes

We made several design changes to our UAV after critical design to reduce the drag and weight. Most notably, we changed the shape of the fuselage to one that is proven by research to minimize drag and maximize laminar flow near our operating Reynolds Number. The propeller and electronics were moved from the front to the back to reduce drag at the front of the UAV and as a result, the turbogenerator and fuel tank were moved from the back to the front. We modified the payload release mechanism and changed the cart and ramp material to carbon fiber for significant weight reduction. Our final UAV design is shown in Figure 44.



Figure 44. Final UAV design featuring propeller at the back and new fuselage shape designed to minimize drag.

6.1.1 Component Layout

The propeller, as well as the electronics and propeller motor, were moved to the back of the UAV to reduce the drag imposed by the propeller. As a result, we had to move the turbogenerator, fuel tank, and exhaust to the front.

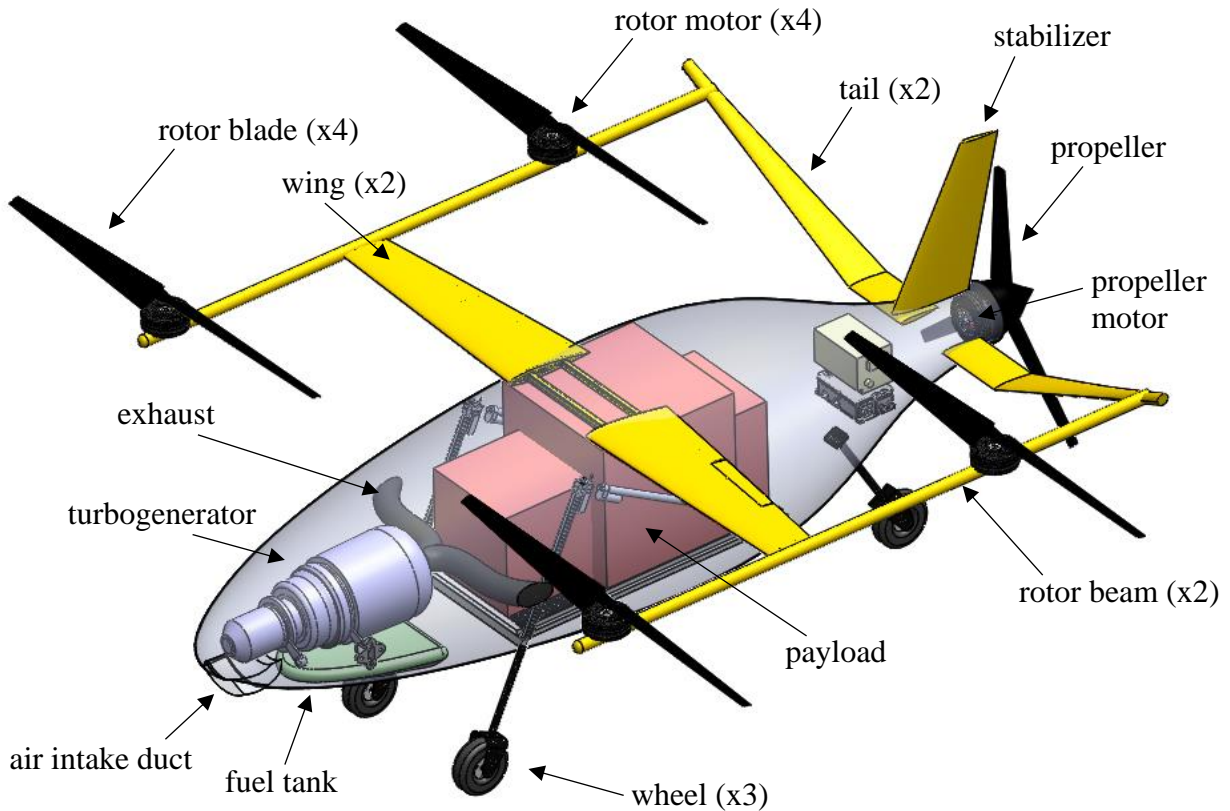


Figure 45. Overview of system layout.

We replaced the meshes from our design at CDR with an air intake duct at the front that will better direct air into the turbogenerator's compressor at a cost of increased drag. The tails were moved to the back to better integrate with the new shape of the fuselage.

6.1.2 Payload Release Mechanism Weight Reductions

The final design of the payload release mechanism reduced its weight significantly. This was achieved by changing the design of the ramp from a solid plate to a frame with two reinforced tracks for the cart to roll on. Additionally, the final frame and ramp plate are built from carbon fiber instead of aluminum 6061 with the exception of the tracks which are reinforced with aluminum 6061. The ramp will use the interior of the fuselage for support so the ramp does not need to be a standalone structure as it was in the critical design. An electric winch was added to hoist the cart up the ramp during the loading process and to slowly roll the ramp onto the group during the unloading process. This allowed for a net weight decrease of over 40%.

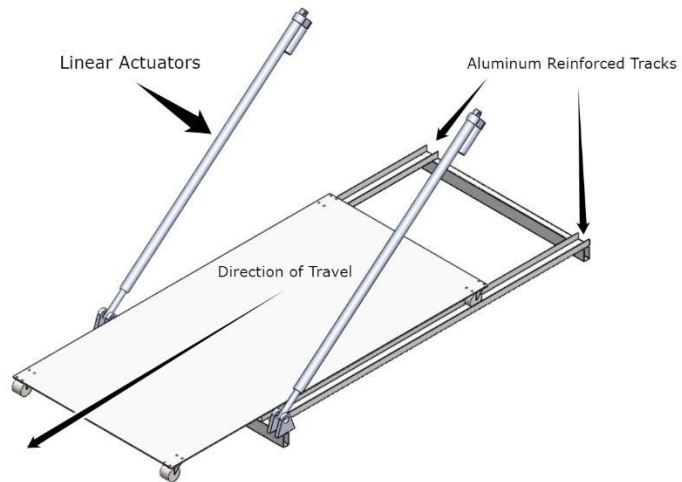


Figure 46. Payload Ramp and Cart

The cart will be autonomously released by utilizing the AP10.1 control system to lower the ramp until the limit switches signal that the ramp has touched the ground. Then it will unwind the winch slowly and letting gravity take the ramp down the cart. Next the clip will detach when the AP10.1 control system sends the release signal. This release signal can be preprogrammed into the flight plan by using the onboard ultrasonic sensor to determine when the cart is an appropriate distance away from the ramp. After the clip is detached the AP10.1 control system will wind up the winch and close the ramp.

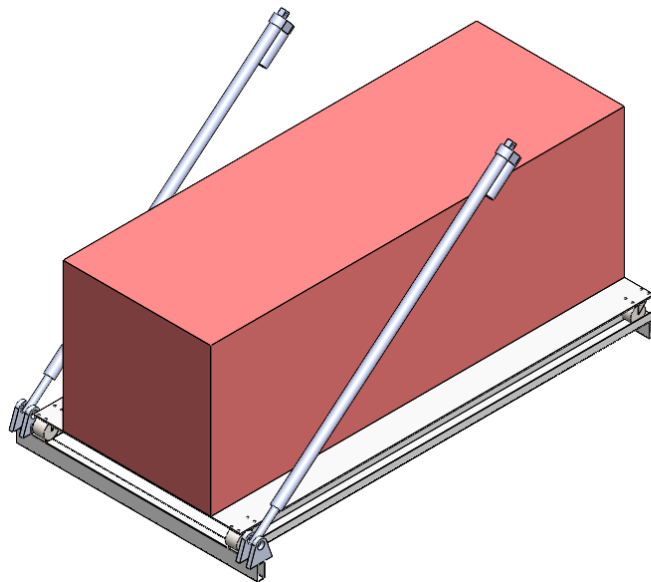


Figure 47. Ramp and Cart with Long Payload

Both payloads can be loaded onto the cart and attached using 2 winch straps located centrally on the payload and perpendicular to each other. These winch straps will be connected to the mounting points on the payload and the cart.

6.1.3 Fuselage Shape and Structure

The objective in modifying our fuselage was to adopt a body profile that could achieve low drag particularly at the order of magnitude of our estimated Reynolds number of 15 million (assuming a cruise velocity of 50 m/s). A study on the shaping of axisymmetric fuselages for minimum drag in incompressible flow presented a numerically generated body, shown in Figure 48 that exhibited low-drag, laminar behavior at a Reynolds numbers of 10^7 [27].

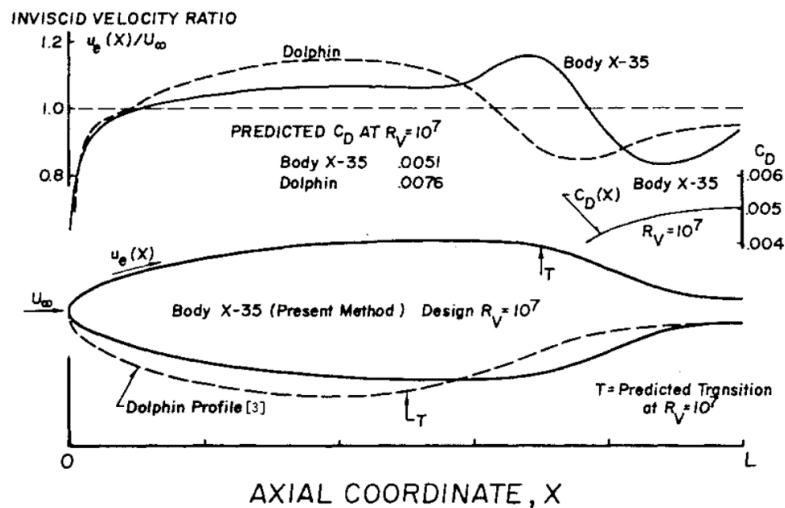


Figure 48. Low-drag, laminar body at Reynolds number of 10^7 [27].

This body, similar in shape to a dolphin, is relevant to our design because of its low drag performance near our estimated Reynolds number of 1.5×10^7 . An existing aircraft fuselage that is similar in shape to the body in Figure 49 is the axisymmetric fuselage of the Celera 500L by Otto Aviation which claims to maximize laminar flow and experience ~59% less drag than conventional aircraft of the same size [28].

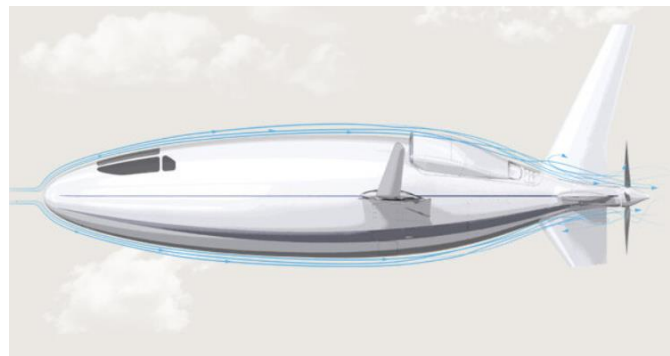


Figure 49. Celera 500L by Otto Aviation with fuselage shaped claimed to maximize laminar flow and reduce drag [28].

We aimed to base our new fuselage design on the low-drag, laminar body from the aforementioned study on shaping axisymmetric fuselages and on the fuselage shape of the Celeria 500L. The main challenge in sizing the fuselage was fitting the length within the objective geometric limits while accommodating the height of the payloads. As a result, we designed the alternative fuselage, shown in Figure 50, to have a lower aspect ratio than the two aforementioned bodies which is less advantageous for reducing drag but required to adequately package the internal components.

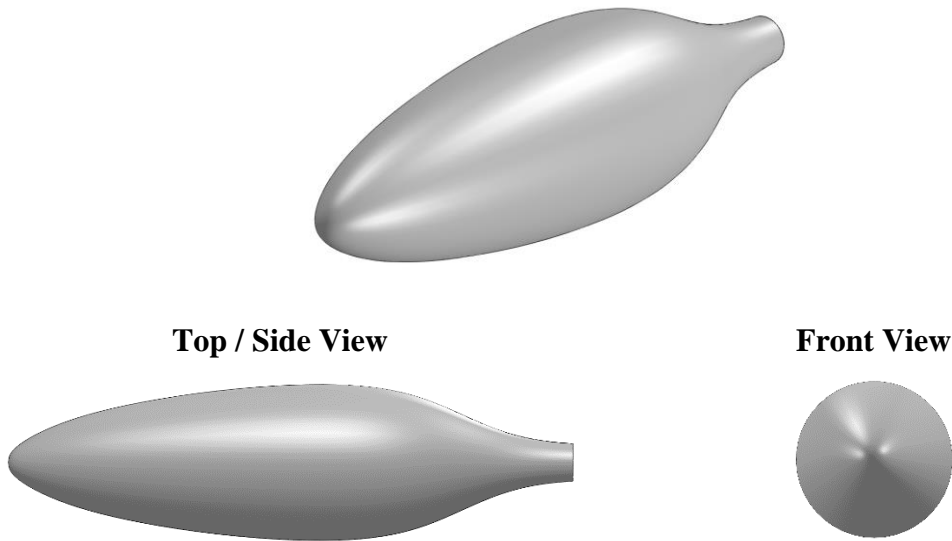


Figure 50. Axisymmetric fuselage model based on low-drag, laminar body at Reynolds numbers of 10^7 with reduced aspect ratio.

We analyzed the flight loads on the fuselage during cruise by using CFD simulation to predict the pressure distribution along the fuselage surface for a forward flight speed of 50 m/s.

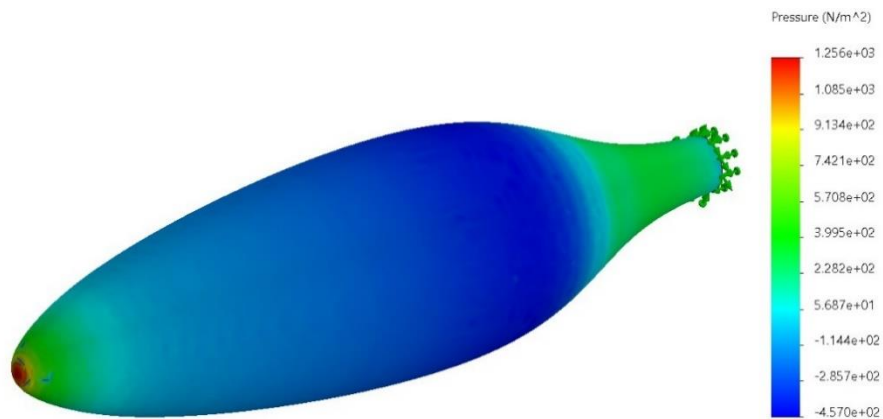


Figure 51. Pressure distribution along fuselage surface during forward flight at 50 m/s generated using CFD simulation.

Using the CFD simulation, we observed high pressure at the front and rear ends of the UAV which indicates low pressure drag and supported our adoption of this new fuselage shape.

We selected the axisymmetric laminar shape for the fuselage of our UAV because the general shape is corroborated by the referenced study on axisymmetric fuselages and offers the possibility for very low drag by maximizing laminar flow along the surface during cruise.

After selecting the fuselage shape, we re-evaluated various options for the fuselage structure and compared them in Table 15. Although we originally picked a monocoque shell, we wanted to ensure we were using the lightest structure required to meet our strength and manufacturing requirements.

Table 15: Comparison of structure types for fuselage. Assessments based on FAA Aircraft Construction handbook [29].

Criteria	Truss	Semi-monocoque	Monocoque
Weight			
Strength			
Safety			
Manufacturability			
Durability			
Geometric Freedom			

Although a truss structure is very strong, it would likely be very difficult to form into the shape of our desired fuselage and would be the heaviest option of the three structure types, so we ruled it out. The monocoque structure is an interesting option as it allows for the most geometric freedom and packaging volume of the three in a strong shell. However, the monocoque posed a challenge as the skin had to be thickened until achieving adequate strength which resulted in significant increases in weight. The semi-monocoque structure was an intriguing alternative as it likely allows for the best strength-to-weight ratio of the structure types. Although a semi-monocoque is more limited in its geometric freedom than a monocoque, we believe the axisymmetric geometry and smooth profiles of our fuselage design are compatible with the semi-monocoque structure.

We chose to pursue a semi-monocoque structure for our fuselage as was the lightest option that could meet our strength and manufacturing requirements. We selected carbon fiber reinforced plastic for the fuselage skin because it is stronger and lighter than an aluminum and relatively easy to cure into our desired fuselage shape.

7. Manufacturing

7.1 Full-System Manufacturing Plan

Although we are not building the UAV, section 6.1 will cover the manufacturing and assembly plan for the main UAV components with emphasis on material and part procurement, manufacturing processes, assembly story, and cost.

7.1.1 Material and Part Procurement

The main raw materials required to build the UAV is carbon fiber cloth, core material for the cured carbon fiber composite, and aluminum for machined brackets and struts. Prepreg 3K, 2x2 Twill Weave Carbon will be used as the cloth and Nomex Honeycomb will be used as the core, both of which will be purchased from FibreGlast. The stock aluminum for brackets and struts will be purchased from McMaster-Carr who sell bars, cubes, rods, and tube extrusions. Many components in the UAV will be purchased off-the-shelf and are discussed in more detail in the following sections.

7.1.2 Manufacturing Operations

Most components in the UAV will be purchased off-the-shelf including the turbogenerator, motors, and control system as will be further discussed in section 6.4. However, the structure, primarily the fuselage and wings, will need to be custom parts that require a particular manufacturing process. The fuselage is made of carbon fiber reinforced polymer which will be molded and cured into the desired shape using an out-of-autoclave curing process. In order to support the internal components of the UAV, it will have aluminum brackets and threaded spools inserted into the mold before curing at the appropriate mounting points. Furthermore, the wings and fuselage will be molded together to create one continuous body. As a result, the aluminum ribs and spars in the wings must be inserted in the carbon fiber mold before curing. Making the fuselage and wings will be the most expensive and challenging process in successfully manufacturing the UAV, so employing highly experienced carbon fiber molding vendors that specialize in out-of-autoclave curing is highly recommended.

Additional custom parts include the plastic fuel tank which will require an injection molding process to mold the fuel tank into the desired geometry. The mounting hardware in the UAV such as aluminum brackets and struts must be machined and may require some welding to join multiple pieces. The ramp and cart for the payload release mechanism will require a stamping process to form the aluminum sheet metal into the desired shape.

7.1.3 Assembly Story

The assembly story for the UAV was designed based on accessibility to the mounting points on the interior and exterior of the UAV. The order of major assembly steps is shown in Figure 44.

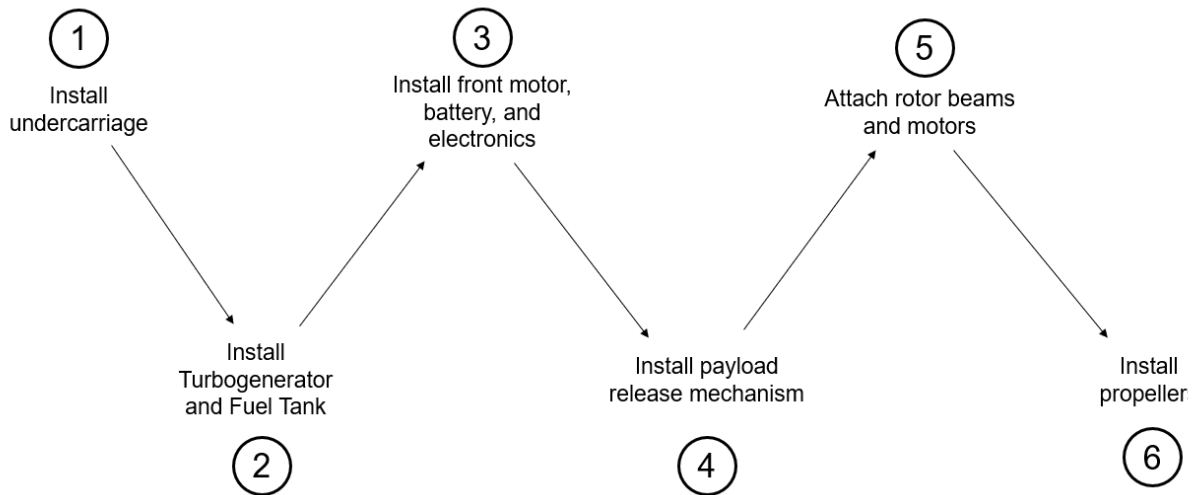


Figure 52. Assembly story for major components of the UAV.

First, the undercarriage, which includes the legs that support the UAV on the ground, is bolted to the fuselage. With the fuselage resting on its legs, the turbogenerator is bolted to the interior of the fuselage followed by the fuel tank which is mounted in front of the turbogenerator. The front legs must be bolted to the ground during this step, so the UAV does not tilt back due to the weight of the turbogenerator. Then, the propeller motor, battery, electronics, wiring, and coolant piping are installed inside the front nose of the fuselage. Then, the ramp and payload release mechanism is installed in the middle of the UAV which complete the assembly for the major components inside the fuselage. Next, the rotor beams are mounted on the front stabilizers and rear wings and the rotor motors are fastened to the rotor beams in their appropriate positions and connected to the electrical wiring and coolant tubes. Lastly, the four rotors and front propeller are attached to the motors and the assembly is complete.

7.1.4 Outsourcing

All the parts we will be outsourcing are summarized in Table 16 with the component name and where they will be manufactured or obtained. There are a few major custom parts and manufacturing processes where we will need additional assistance for. The carbon fiber fuselage with aluminum brackets and wing spars will be custom manufactured and assembled by MCM Composites. As for manufacturing brackets, struts, and the ramp, we will need the services of Planet Products Corporation for machining and Astro Machine Works for welding. The fuel tank will be custom designed by the reliable Aero Tec Laboratories and much of the electronics assembling will be outsourced to electrical engineers and manufacturers at Advanced Circuits.

Table 16: Outsourcing of aircraft parts

Subsystem	Component	Vendor
Propulsion	Propeller	Mejzlik
	Rotor Head Nuts	McMaster-Carr
	Rotor Spacers/Washers	McMaster-Carr
	Wing Stringers	McMaster-Carr

	Wing, Canard, and Tail Caps	McMaster-Carr
	Aileron, Elevator, and Rudder Linear Actuators	Progressive Automations
	Aileron, Elevator, and Rudder Ball Bearings	McMaster-Carr
	Aileron, Elevator, and Rudder Ball Set Screws	McMaster-Carr
	Variable Pitch Propeller	GT Propellers (custom design)
Structure	Carbon Fiber Fuselage	MCM Composites
	Threaded inserts	Applifast
	24-inch Linear Actuator	Progressive Automations
	M24x3x70 Hex Bolt	McMaster-Carr
	M24 Hex Nut	McMaster-Carr
	M16x2x30 Screw	McMaster-Carr
Power Plant	TG-R55 Turbogenerator	Turbotech
	24 V Lithium-Ion Battery	Eaglepicher Technologies
	ATL-794-A Fuel Tank	Aero Tec Laboratories
	EMRAX 208 Motors	EMRAX
	EMRAX 228 Motor	EMRAX
	PM100 Inverter	Cascadia Motion
	Casia 360 Object Detection System	Iris Automation
	AP 10.1 Control System	UAVOS
Payload Mechanism	36in Linear Actuator	Progressive Automations
	2in Linear Actuator	Amazon
	1/4in-20x1/2in Stainless Steel Hex Bolt 5-pack	Home Depot
	1/4in-20 Stainless Steel Hex Nut 4 pack	Home Depot

7.2 Prototype Manufacturing

Because we did not create a detailed design for the UAV or have the resources to manufacture and assemble a full-scale prototype, we instead 3D printed a simplified, scaled-down version for wind tunnel testing. We designed and 3D-printed simplified models of our UAV with two different fuselage shapes using a scaling factor of 1:8 for both. We used two different fuselage shapes to use our test results to evaluate and compare two potential design alternatives.

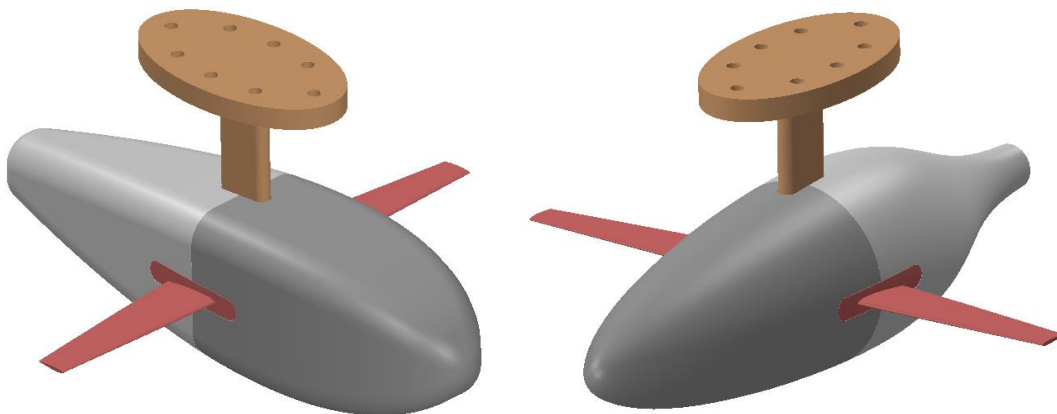


Figure 53. CAD models of prototypes with symmetrical airfoil fuselage (left) and axisymmetric fuselage (right).

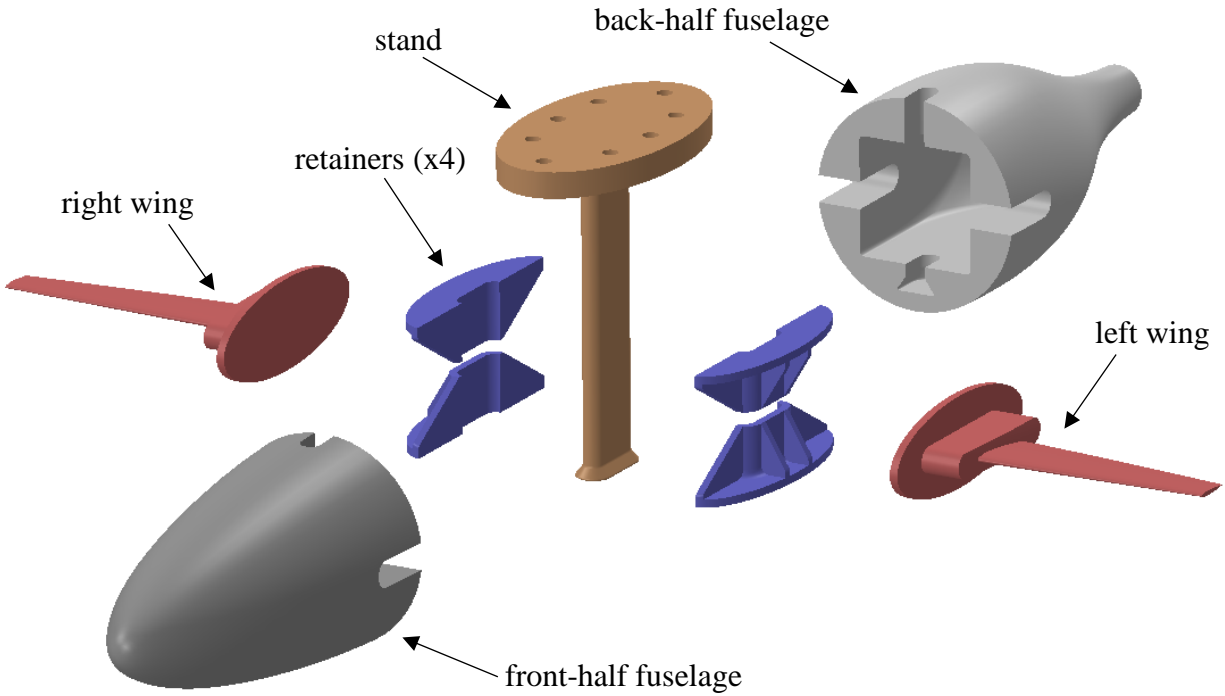


Figure 54. Exploded view of scaled-down UAV model with axisymmetric fuselage.

The UAV model features the fuselage and wings of the full-scale model and does not include the rotors, rotor arms, and stabilizers for simplicity. We designed the model so that none of the components required support material while ensuring that the model is constrained in all six degrees of freedom on the test stand. The components are fastened together using glue; the wings and retainers in Figure 54 provide mechanical retention in addition to adhesive shear retention provided by glue.

7.2.1 Manufacturing Operations

We 3D-printed that parts using our own 3D printer in addition to those at Mustang 60. We chose 1.75 mm diameter PLA filament because it is relatively cheap, the easiest to print, and provides enough durability to comfortably be used in a wind tunnel. For the joints, we used a combination of mechanical retention and adhesive bonding using glue that is compatible with plastic parts. The surface finish will be smoothed using sandpaper and filler to close seams and gaps in the models. We split up our design into the 4 parts shown below. We chose not to 3D print the rotors, support bars, or undercarriage since it would add lots of extra printing and might not sustain the forces in the wind tunnel. While designing the printable model, it was important to prevent drastic overhangs that could cause manufacturing defects. We ensured there were no vertical angles exceeding 45 degrees and frequently used chamfers and fillets to create more printable overhangs.

7.2.2 Part Procurement and Cost Analysis

We purchased 3D printing filament, glue, wood filler, and sandpaper from Amazon. We purchased two spools of 1.75 mm diameter PLA filament which are compatible with our personal 3D printers as well as the printers in the machine shop, two bottles of Gorilla Super Glue that are capable of bonding plastic surfaces, a tub of Elmers Wood Filler that works for filling seams plastic parts, and 120 to 3000 grit sandpaper for smoothing the part surfaces. Our purchases for the prototypes are summarized in Table 17.

Table 17: Purchased parts for verification prototype.

Item	Quantity	Unit Cost	Totals
 Gorilla Super Glue	2	\$6.84	\$13.68
 PLA Filament	6	\$22.53	\$135.18
 Sandpaper	1	\$8.99	\$8.99
 Wood Filler	1	\$14.92	\$14.92
Total (with Tax):			\$172.77

After our purchases, we had \$327.23 remaining in our senior project budget.

7.2.3 Prototype Assembly

The UAV models were comprised of six major 3D-printed components: the front half of the fuselage, rear half of the fuselage, right wing, left wing, stand, and retainers as shown in Figure 55.

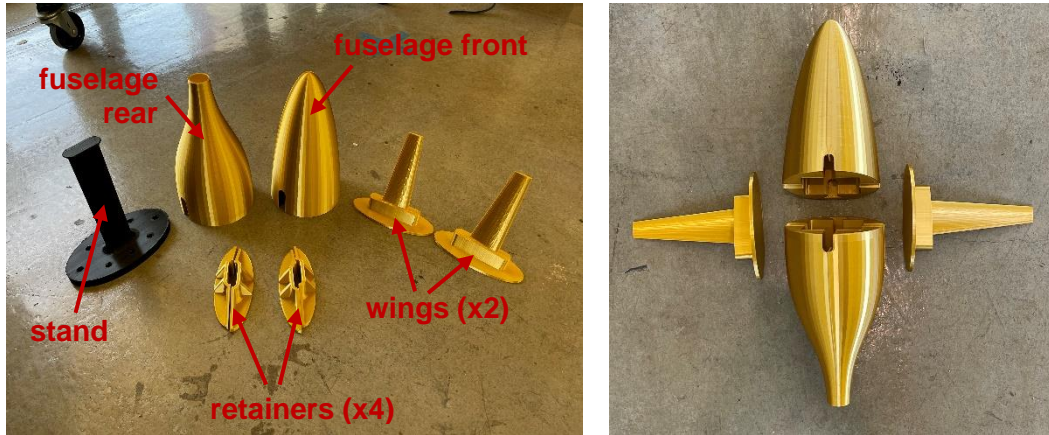


Figure 55. Major 3D-printed components of one of the scaled-down UAV models is shown on the left. The general layout of the aircraft components is shown on the right.

The model is assembled by inserting and gluing on the stand, axial retainers, and wings in one half of the fuselage, then sliding and gluing on the other half of the fuselage. We designed the models as that they would have self-aligning and self-securing features so that they would have enough static stability to not fall apart when fully assembled without any glue. We also aimed to design the glued joints to be loaded in shear and compression and tried to avoid loading the glue in tension. A redundant number of retainers were used to over constrain the assembly as we wanted to use friction between components to aid the glue in fastening the assembly. The front half of one of the models with the internal components installed is shown in Figure 56.



Figure 56. Front half of one of the scaled-down UAV models with stand, retainers, and wings installed in the internal cavity. The wings and stand are located using slots in the fuselage.

We created two models, one with the symmetrical airfoil fuselage shape from our critical design, and one with an axisymmetric shape used in our final design. The complete prototypes are shown in Figure 57.



Figure 57. Complete 3D-printed prototypes of UAV models with symmetrical airfoil fuselage (left) and axisymmetric fuselage (right). Both models are approximately 18 inches long, 16 inches wide, and 9 inches tall.

Once assembled, the prototypes were used for wind tunnel testing to measure the drag force on each model.

8. Design Verification

Instead of building a full-functional prototype of our UAV which would have been difficult to produce in our project timeframe, we performed wind tunnel tests on 3D-printed simplified versions of our UAV. We collected valuable and relevant data that informed and justified our design decisions and validated our numerical models.

8.1 Evaluation of Specifications

Due to the scale of our design in the allotted timeframe we were not able to physically evaluate each specification. This means that most of the evaluation of specifications were performed through inspection and analysis. We evaluated the specifications in Table 18 through either a visual inspection using CAD models, an analysis based on blade element momentum theory, or a physical test performed in the Cal Poly Aerospace wind tunnel.

However, through testing we were also able to determine a coefficient of drag. This allowed us to accurately evaluate a few of the specifications that were most essential to verifying our UAV would be able to meet the requirements of the competition. The table below shows the final specifications that were required for the competition.

Table 18: Final Design Specifications

#	Specification	Requirement	Tolerance	Risk	Compliance
1	Range	200 km (108 NM)	Min	M	A,S
2	Pay Load Dimensions	70 cm x 70cm x 70cm (27.6" x 27.6" x 27.6") 50cm x 50cm x140cm (19.7" x 19.7" x 55.1")	Min	L	A,I
3	Payload Mass	50 kg (110 lbf)	Min	L	A,I
4	System Dimensions	Objective: 4.6 m x 4.6 m (15' x 15') Threshold: 6.1 m x 6.1 m (20' x 20')	Max	L	A,I
5	Number of Collisions With Obstacles	0 collisions	Max	M	A
6	Delivery Site Area	15.2 m x 15.2 m (50' x 50')	Max	L	A,I
7	Vertical Lift Time	2 minutes	Max	H	A
8	Cruise Speed	160 km/h (86.4knots)	Min	H	A
9	System Weight	<500 lb.	Max	M	A,I
10	Time to Reach Destination	108 km/h or 160 km/h	Max	H	A

The payload dimensions, payload mass, system dimensions, and the delivery site area were all driving factors in the design. These specifications were evaluated visually by using the CAD model combined with the measuring tool in SolidWorks to verify that each of these specifications were met. The system weight was evaluated by compiling a part weights list made of the purchased parts weight and estimated weights based on the CAD models of each component we designed.

The number of collisions with obstacles was analyzed using a trade study of various control systems. Through this trade study we determined that the AP10.1 onboard control system would fit the specifications.

The range, vertical lift time, cruise speed and the time to reach destination were evaluated through an analysis method called blade element momentum theory. Blade element momentum theory was used to determine the optimum twist and taper ratio that would maximize the figure of merit. Through the use of blade element momentum theory each specification was met.

The final test performed was a wind tunnel test performed with two fuselage shapes, this test allowed us to find the fuselage with the best coefficient of drag to use in the final design. The test description can be seen in full in Appendix J.

8.2 Testing

Fuselage design often requires empirical wind tunnel testing to determine which shape will allow the aircraft to fly most efficiently while still holding all the necessary internal components. While thorough research was used to select the fuselage design to be used for the competition, we found it useful to conduct a wind tunnel test on our fuselage models to verify that our chosen design would behave as expected. Other forms of verification testing were proposed, such as testing propeller or rotor thrust outputs, aircraft sizing verification, aircraft power consumption, or even performing a flight test of the full or partial system. However, safety and manufacturing concerns regarding fabricating and testing high speed rotors, and concerns on constructing a full working prototype on our timeframe, let us to determine that a fuselage drag test using 3D printed models would be best.

The test was conducted in the back of the wind tunnel, as shown in Figure 58, due to last minute scheduling conflicts with the wind tunnel facility. The fuselage models were tied at the fairing mounting holes using string to a horizontal bar mounted across the walls of the wind tunnel so that the models could be analyzed as a physical pendulum. Each fuselage was then video recorded oscillating when the wind tunnel operated at a wind velocity of 10 m/s and 15 m/s across a backdrop of graph paper. This was so that the oscillation amplitude could be recorded from the video.



Figure 58: UAV model suspended behind outlet of wind tunnel during test.

During the test, it was noticed that both models had a noticeable amount of lateral instability and would yaw at large frequencies. In particular, the rectangular fuselage turned out to be more unstable. This instability could be fixed with the implementation of a tail in our model. However, this instability did not interfere with our data collection that much and could be ignored.

As we could not perform this test in the wind tunnel test section, there are many causes of uncertainty. The air in the diffuser of the wind tunnel experiences a large decrease in momentum that forces it to turbulent, non-uniform flow. Additionally, the exit of the wind tunnel is not closed off to the rest of the building so wind gusts from windows or air conditioning systems may affect the result. Also, the inability to use a calibrated sensor such as a load cell decreases the accuracy and precision of the data. The graph backdrop analysis will give us approximate numbers, but inconsistencies in the video recording and approximations in determining amplitude would also affect the results. The Reynold's number for our models is also different compared to that which would be found at cruise. For a scaled-down model, a higher windspeed than that of cruise would be needed to match Reynold's numbers to make a true fuselage comparison. However, this testing range would put our models in supersonic flow, which would introduce new forms of drag not normally experienced in our design's mission. Safety would also be a concern, because introducing supersonic drags and pressures to a 3D model may overwhelm the structural integrity of the PLA and damage the tunnel. Finally, the mass and moment of inertia of both models was approximated using the SolidWorks models. This does not take any of the 3D printing manufacturing techniques into consideration, such as infill and wall-thickness, so those values may also be inaccurate. While all these uncertainties would not allow us to compare an empirical coefficient of drag to the one found using the drag build-up method, it allows us to determine which fuselage shape is more ideal confidently.

8.3 Data Collection and Analysis

To analyze the test data, we treated the wind tunnel velocity as a ramp input. From there, we were able to perform a forced vibration analysis to find the force the wind put on the model as a function of the oscillation amplitude. The results are shown in Tables 19-22 below.

Table 19. Test Results for Circular Fuselage at 10 m/s Windspeed

Oscillation Amplitude (in.)	Time (s)	Coefficient of Drag
0.25	35.74	2.53
0.25	36.47	2.56
0.25	37.21	2.53
0.25	37.95	2.56
0.3	38.68	3.03
0.3	39.42	3.07
0.4	40.16	4.04
0.3	40.89	3.07
0.3	41.63	3.03
0.4	42.37	4.10
0.3	43.10	3.03
0.4	43.84	4.10
0.3	44.58	3.03
0.4	45.31	4.10

Table 20. Test Results for Circular Fuselage at 15 m/s

Oscillation Amplitude (in)	Time (s)	Coefficient of Drag
0.5	43.74	2.27
0.4	44.47	1.80
0.5	45.21	2.27
0.4	45.95	1.80
0.5	46.68	2.27
0.4	47.42	1.80
0.5	48.16	2.27
0.6	48.89	2.70
1	49.63	4.54
0.5	50.37	2.25
0.6	51.10	2.73
0.5	51.84	2.25
0.6	52.58	2.73
0.6	53.31	2.70
0.5	54.05	2.27
0.6	54.79	2.70
0.75	55.52	3.41

Table 21. Test Results for Rectangular Fuselage at 10 m/s.

Oscillation Amplitude (in)	Time (s)	Coefficient of Drag
0.25	35.70	1.87
0.4	36.40	2.98
0.4	37.10	2.99
0.1	37.79	0.75
0.4	38.49	2.99
0.5	39.19	3.73
0.4	39.89	2.99
0.1	40.59	0.75
0.4	41.29	2.99
0.1	41.99	0.75
0.5	42.69	3.74
0.5	43.38	3.73
0.25	44.08	1.87
0.5	44.78	3.73

Table 22. Test Results for Rectangular Fuselage at 15 m/s.

Oscillation Amplitude (in.)	Time (s)	Coefficient of Drag
0.5	43.70	1.34
0.5	44.40	1.36
0.5	45.10	1.34
0.75	45.79	2.04
0.6	46.49	1.61
1	47.19	2.71
0.5	47.89	1.34
1	48.59	2.71
1	49.29	2.69
0.5	49.99	1.36
1	50.69	2.69
0.5	51.38	1.36
0.5	52.08	1.34
0.5	52.78	1.36
0.5	53.48	1.34
0.5	54.18	1.36
0.5	54.88	1.34

Overall, the rectangular fuselage experiences a lower coefficient of drag at both wind speeds when compared to the circular fuselage. However, the weight and moment of inertia of the rectangular fuselage was found to be less than that of the circular one. Accounting for this correction, the rectangular fuselage experienced a greater amplitude and drag force than that of the circular one, aligning with our research and predictions.

An uncertainty analysis was conducted using the coefficient of drag equation to account for the uncertainty in force/amplitude, air density, reference wing area, and wind tunnel airspeed. An uncertainty of 0.5 was used for the amplitude to account for the resolution of the graph sheet, 0.01 for the air density to account for precision at the altitude of the wind tunnel facility, 0.02 for the wing reference area to account for 3D printing resolution, and 0.1 for the wind speed to account for wind tunnel error. The calculations are given in Appendix K and the total uncertainty was found to be ± 0.58 . While this uncertainty is large, it does not interfere with the distinction between empirical drag coefficients of the two fuselages.

8.4 Design Performance

We did not perform tests for the vertical lift angle, control system inputs, lift force or the thrust force. These specifications were not tested because they were very similar to the specifications already listed. We did not perform tests for the blade guard specification because we did not

include a blade guard in the final design. Instead of a blade guard we designed the UAV to have a hardware cutoff which will be used when the operators are near the UAV.

Table 23. Design Requirements and Performance

#	Specification	Requirement	Pass/Fail
1	Range	200 km (108 NM)	Pass
2	Payload Dimensions	70 cm x 70cm x 70cm (27.6" x 27.6" x 27.6") 50cm x 50cm x 140cm (19.7" x 19.7" x 55.1")	Pass
3	Payload Mass	50 kg (110 lbf)	Pass
4	System Dimensions	Objective: 4.6 m x 4.6 m (15' x 15') Threshold: 6.1 m x 6.1 m (20' x 20')	Pass
5	Number of Collisions with Obstacles	0 collisions	Pass
6	Delivery Site Area	15.2 m x 15.2 m (50' x 50')	Pass
7	Vertical Lift Time	2 minutes	Pass
8	Cruise Speed	160 km/h (86.4knots)	Pass
9	System Weight	< 227kg (500 lbf)	Fail
10	Time to Reach Destination	108 km/h (58.3 knots) or 160 km/h (86.4 knots)	Pass

The mass of our design is 349 kg which is significantly larger than the original mass target of 225 kg. This is okay for our design because the initial system weight specification was an arbitrary number used to give us a baseline estimate of how much the UAV should weigh. Our design weighs 349kg which is significantly larger than the system weight specification. Even with the added weight the UAV will be able to fly.

9. Project Management

The design process for this project will consist of six main milestones required to produce the deliverables: the Preliminary Design Review (PDR), Interim Design Review (IDR), Critical Design Review (CDR), Manufacturing and Test Review, Verification Prototype sign-off, and the Final Design Review (FDR).

For about 3 weeks, preliminary design and ideation was conducted. This process included steps such as functional decomposition, home ideation model building, and preliminary calculations. One concept was selected based on these results to be considered for detailed design during the PDR. After the PDR, about 5 weeks were spent modifying the initial conceptual design to account

for Failure Modes and Effects (FMEA) and Manufacturing and Assembly restrictions (DFMA). The IDR was conducted after this and led to another 4 weeks of identifying and modeling individual parts and drafting a manufacturing test plan. At this point, the CDR was conducted to determine whether our proposed design can meet the design and mission requirements to conclude the system design phase and the begin of manufacturing a prototype.

The CDR was modified to represent the deliverables outlined by the Vertical Flight Society for their competition. As a result, the design presented at CDR was primarily a system-level design featuring some analysis for critical features that greatly determine whether the design will work or not. As we drove the project closer to FDR, we performed a segment-to-segment analysis to analyze flight speed, energy consumed, power required, component performance, and emergency procedures. By the time we reached the FDR, we had improved and refined various aspects of the design to create a polished CAD model. Our last deliverable along with the FDR was to build a final prototype and perform experimental validation. Because of the complexity of our final CAD design, we opted to 3D print a very simplified model of it that we could test on instead.

Once the design, build, and testing were complete, we created our own website showcasing the results of the work we did the past three quarters. This website introduces our team, discusses the entire design process, shares our model and results, and includes a 5-minute video summarizing our whole project. Table 24 showcases the timeline of the project. Appendix B provides a Gantt chart with a more detailed schedule and responsibility delegation.

Table 24: Unmanned Vertical Lift Project Timeline

Task Name	Duration	Start	Date for Submittal
Scope of Work	16 days (~2 weeks)	Tue 9/22/20	Tue 10/13/20
Preliminary Design Review	21 days (3 weeks)	Wed 10/14/20	Thu 11/12/20
Critical Design Review	115 days (~16 weeks)	Tue 11/17/20	Thurs 3/11/21
Final Design Review and Website	90 days (~12 weeks)	Thurs 3/11/21	Fri 6/9/21

Overall, this design process was effective in producing the deliverables required for both our senior project and the student design competition we are participating in. Having a Gantt chart and weekly meetings as a team really helped keep our team on track and keep the goals we needed to accomplish each week listed out. The process for developing our design and refining it went really smoothly, and it helped to receive constant feedback from professors and our peers in senior project. There were times where our indecisiveness as a team for concept design and prototype testing set us back on deliverable submissions, but it was better to over-discuss things than to come to decision too quickly.

10. Conclusion

The goal of this project was to design a VTOL UAV that allows medical professionals to transport medical supplies quickly and precisely, in emergency situations, while avoiding the delays that come with ground transportation. We have provided background information, research findings, engineering specifications, ideation and design selection process, final system design justification, design analysis, experimental verification, and a prototype build within this document.

This project can be looked at as a success for a multitude of reasons. For one, we've created a UAV model that meets and exceeds the competition requirements. We can look back at our model and be proud and confident of the design decisions, justification, analysis, and testing we've completed. We have also completed all of the deliverables on time for our senior project class as well as the design competition we are participating in. However, the biggest achievement has to be the knowledge and experience we've gained over the past few months. As a team, we've come together and utilized our varying individual strengths to come up with great results. We are finishing this quarter with a much stronger understanding of the engineering design process and the aerospace industry than we had a few months ago. There was little to be said about goals we did not achieve or failures that we had. If any, it is that we had to complete most of this project through Zoom calls and we only really got to see one another in person towards the end of spring quarter. Being in-person to complete this project would have made communication much easier. Sharing design ideas could be easily drawn up for one another and concepts could be explained with visual aids. Being on campus also would have provided us easier access to engineering professors instead of communicating solely through email and Zoom office hours.

Because of the nature of being in both senior project and the design competition, there were times where it got hard to keep track of the content being asked for in both deliverables. Ideally, there would be one substantial report we would submit instead of having multiple documents to produce. On the next design project we do, it would also be good to have a final prototype we can actually manufacture and test on directly. Building our actual model of the UAV was simply not going to happen with our current experience, personnel, and resources, which is why we had to rely on a hugely simplified version of our model for testing.

Some advice for our sponsors would be to continue hosting these student design competitions because it provides an amazing opportunity to gain and apply aerospace knowledge in a fun and interactive manner. The engineering experiences we have had participating in this competition are not so far off from what real engineers do on a daily basis in industry. We hope our project will be looked at fondly by the competition judges and that this design can be considered for a top 3 finish. As well, it would be great to receive feedback from real Boeing engineers and members of the Vertical Flight Society to see what we could improve or things we could have done differently.

References

1. "2020-2021 Request for Proposal (RFP)." Vertical Flight Society, 2020. PDF. 8 October 2020. https://vtol.org/files/dmfile/boeing-rfp_-vfs-sdc-2020_final_1.2.pdf.
2. Baker, Aryn. "Zipline's Drones Are Delivering Blood to Hospitals in Rwanda." *Time*, 2017, time.com/rwanda-drones-zipline/.
3. Sotunde, Busayo. "Drones to the Rescue: Zipline's Blood Deliveries Save Lives in Rwanda." *Rural Reporters*, 8 Dec. 2018, ruralreporters.com/drones-to-the-rescue-ziplines-blood-deliveries-save-lives-in-rwanda/.
4. Zipline. "How It Works." Zipline, 2020, flyzipline.com/how-it-works/.
5. Deutsche Post DHL Group. "DHL Parcelcopter." *DPDHL*, 2020, www.dpdhl.com/en/media-relations/specials/dhl-parcelcopter.html.

6. GRIFF Aviation. "The Griff Fleet." *Griffaviation.com*, Griff Aviation AS, 11 May 2020, griffaviation.com/the-griff-fleet/.
7. VoloDrone. "VoloDrone." *Volocopter*, Volocopter GmbH, 2019, www.volocopter.com/en/volodrone/.
8. Lardinois, Frederic. "A First Look at Amazon's New Delivery Drone." *TechCrunch*, TechCrunch, 5 June 2019, techcrunch.com/2019/06/05/a-first-look-at-amazons-new-delivery-drone/.
9. Wisk. "Our Aircraft." Wisk, 16 Apr. 2021, wisk.aero/aircraft.
10. Schiebel. "CAMCOPTER S-100 System." *Schiebel*, 13 July 2015, schiebel.net/products/camcopter-s-100-system-2/.
11. "Aircraft." BETA, 9 June 2021, www.beta.team/aircraft.
12. "Joby Aviation" *Joby Aviation*, Joby Aviation, 2020, <https://www.jobyaviation.com/>.
13. Leon, Jacobs. "Aircraft Propulsion and Control." US1491954A. United States Patent and Trademark Office, 29 April 1924.
14. Horn, David. "Unmanned Aerial Vehicle (UAV) Having Vertical Takeoff and Landing (VTOL) Capability." CA2929254C. Canada Intellectual Property Office, 2016.
15. Price, Nathan. "Airplane for Vertical Take-off in Horizontal Attitude." US2780424A. United States Patent and Trademark Office, 5 Feb. 1957.
16. Chambers, Andrew, et al. "System and Method for Human Operator Intervention in Autonomous Vehicle Operations." US10365645B1. United States Patent and Trademark Office, 2016.
17. Chambers, Andrew, et al. "Unmanned Aerial Vehicle Management System." US10395543B2. United States Patent and Trademark Office, 2017.
18. Austin, Reg. *Unmanned Aircraft Systems UAVS Design, Development, and Deployment*. Wiley, 2010
19. Nise, Norman S. *Nise's Control Systems Engineering*. John Wiley & Sons, 2019.
20. Drake, Aaron. "Unmanned Aerial Vehicle." Private Interview. 1 Oct. 2020.
21. Anderson, John D. *Fundamentals of Aerodynamics*. McGraw Hill Education, 2017.
22. Leishman, J. Gordon. *Principles of Helicopter Aerodynamics*. Cambridge University Press, 2017.
23. United States Department of Transportation, Federal Aviation Administration. *Helicopter Flying Handbook*. Aviation Supplies & Academics, Inc., 2019.
24. P. Sanjana and M. Prathilothamai, "Drone Design for First Aid Kit Delivery in Emergency Situation," 2020 6th International Conference on Advanced Computing and Communication Systems (ICACCS), Coimbatore, India, 2020, pp. 215-220, doi: 10.1109/ICACCS48705.2020.9074487.
25. Raymer, Daniel P. *Aircraft Design: A Conceptual Approach*. American Institute of Aeronautics and Astronautics, 2006.
26. The NACA Airfoil Series. Stanford University, https://web.stanford.edu/~cantwell/AA200_Course_Material/The%20NACA%20airfoil%20series.pdf.
27. Parsons, J. S., Goodson, R. E. and Goldschmeid, F. R., Shaping of Axisymmetric Bodies for Minimum Drag in Incompressible Flow, *J. Hydronautics*, Vol 8 No. 3, 1974.
28. "TECHNOLOGY." OTTO AVIATION, 2021, www.ottoaviation.com/technology.
29. United States Department of Transportation, Federal Aviation Administration. *Pilot's Handbook of Aeronautical Knowledge*. Aircraft Construction, Inc., 2016.

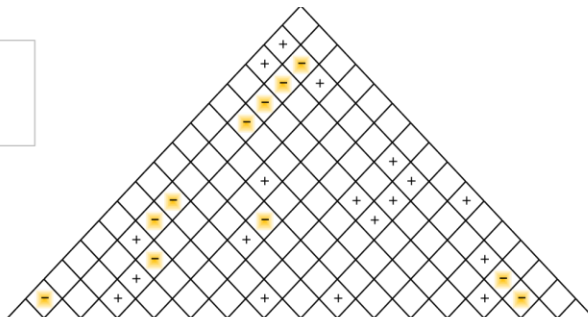
Appendix

- A. QFD House of Quality
- B. Gantt Chart
- C. Ideation
- D. Pugh Matrices
- E. Preliminary Analysis – Hand Calculations
- F. Design Hazard Checklist
- G. Power Calculations – MATLAB Code
- H. Drawing Package
- I. Rotor and Wing Frame Loads – Hand Calculations
- J. Design Verification Plan and Test Procedure
- K. Uncertainty Analysis

Appendix A: QFD House of Quality

Correlations	
Positive	+
Negative	-
No Correlation	
Relationships	
Strong	●
Moderate	○
Weak	▽
Direction of Improvement	
Maximize	▲
Target	◇
Minimize	▼

QFD House of Quality
 Project: F56 - UAV for Medical Supplies
 Revision Date: 10/7/20



Row #	WHO: Customers						WHAT: Customer Requirements (Needs/Wants)	HOW: Engineering Specifications (Means)	NOW: Curr. Products																										
	Weight Chart	Relative Weight	Medical professional	Medical dispatcher	Receiver of supplies	Manufacturer			Maximum Relationship	Range	Payload weight	System Dimensions	Number of collisions with obstacles	Required delivery site area	Pay Load Dimensions	Vertical Lift Time	Time to reach destination/Cruise	Vertical Lift Angle	Control System Inputs	Blade Guard/Protection	Max impact force	Lift Force	Thrust Force	System Weight	Number/Complexity of Subsystems	Griff 135	Zipline Drone	Volodrone	Flirtey Drones	DHL Parcelcopter	Row #				
1		5%	7	8	7	1	9	Able to reach far distances	●	▽	○	▽				▽						●		1	4	1	1	2	1						
2		7%	10	7	10	1	9	Fast enough to reach patients in n	▽	▽	○				○	●						●	●	2	4	1	4	4	2						
3		5%	8	4	8	1	9	Lift/deliver large/heavy medical su	▽	●	○			●			▽				○	○	▽	4	2	5	2	1	3						
4		5%	1	8	8	4	9	Vertical takeoff/landing	○	▽	○		●		○		○			●		○	▽	5	1	5	5	5	4						
5		7%	3	9	9	7	9	Vehicle not too big			●												▽	5	5	1	5	5	5						
6		6%	7	9	9	1	9	Obstacle detection/avoidance			●						●							2	3	3	4	3	6						
7		10%	8	10	9	10	9	Safety			●							●	○			▽		4	4	4	5	4	7						
8		4%	3	5	9	1	9	Limited delivery site area		▽			●			○	○								4	5	5	4	5	8					
9		6%	9	7	10	1	9	Able to deliver to a specific site		▽			○			▽	●								3	3	5	4	5	9					
10		6%	7	9	9	1	9	No damage to surroundings			●						○	○	○				○	3	4	5	5	4	10						
11		8%	10	7	9	4	9	No damage to payload			●		▽				▽		●	▽	▽			2	2	5	3	4	11						
12		7%	9	9	10	3	9	Efficient loading and unloading		●	▽			●				○							4	5	2	3	2	12					
13		8%	7	10	6	7	9	Controlled landing during failure		○							●		●			○	●	3	3	5		3	13						
14		6%	1	9	4	7	9	Easy to troubleshoot/repair			○	▽											○	●	3	5	3		3	14					
15		6%	1	8	1	10	9	Accessible, cost-efficient materials	▽						▽				●	○	○	●			4	4	5	3	3	15					
16		5%	1	8	1	7	9	Durable			○							▽	●	○	○	●	○		4	3	4	2	3	16					
HOW MUCH: Target Values								50 km / 200 km	50 kg	20' x 20'	0 collisions	50' x 50'	70 cm x 70 cm x 70 cm and 140 cm x 50	2 minutes	28 min to 50 km, 75 min to 200 km	+/- 5.5' off verticle	20 m object avoidance distance	Guard maximum gap of 1 cm	Max impact force of 100,000 Newtons	> Weight of payload and weight of UAV	> Drag force of air	< 500 lbs	≤ 10 subsystems												
Max Relationship								9	9	9	9	9	9	3	9	9	9	9	9	9	9	9	9	9	9	9	9	9	9	9	9				
Technical Importance Rating								80.5	152.6	164.5	287.9	100.9	119.8	40.7	64.5	63.89	249.9	133.3	279.8	99.6	118.7	279.1	156.9												
Relative Weight								3%	6%	7%	12%	4%	5%	2%	3%	3%	10%	6%	12%	4%	5%	12%	7%												
Griff 135								1	5	5	3	5	3	5	2	5	3	1	1	1	5	5	5	5											
Zipline Drone								3	2	5	4	5	2	5	3	1	4	1	1	5	5	5	5												
Volodrone								1	5	1	5	5	5	5	1	5	5	3	1	5	3	1	5	3	1										
Flirtey Drones								1	1	5	5	5	1	5	2	5	5	2	3	5	5	5	5	5											
DHL Parcelcopter								2	1	5	4	5	3	4	3	5	4	1	2	5	5	3	5												
Column #								1	2	3	4	5	6	7	8	9	10	11	12	13	14	15	16												

Appendix B: Gantt Chart

Part 1

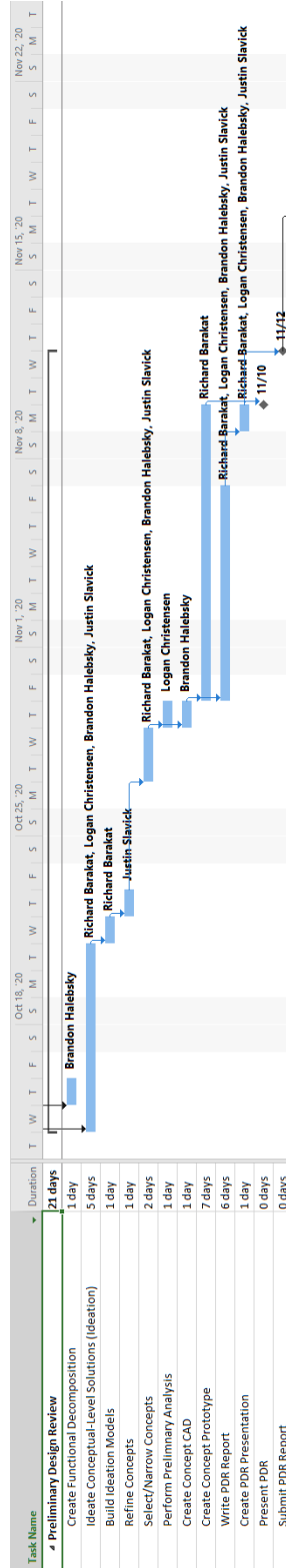


Figure B.1: Gantt chart up to Preliminary Design Review Milestone.

Part 2

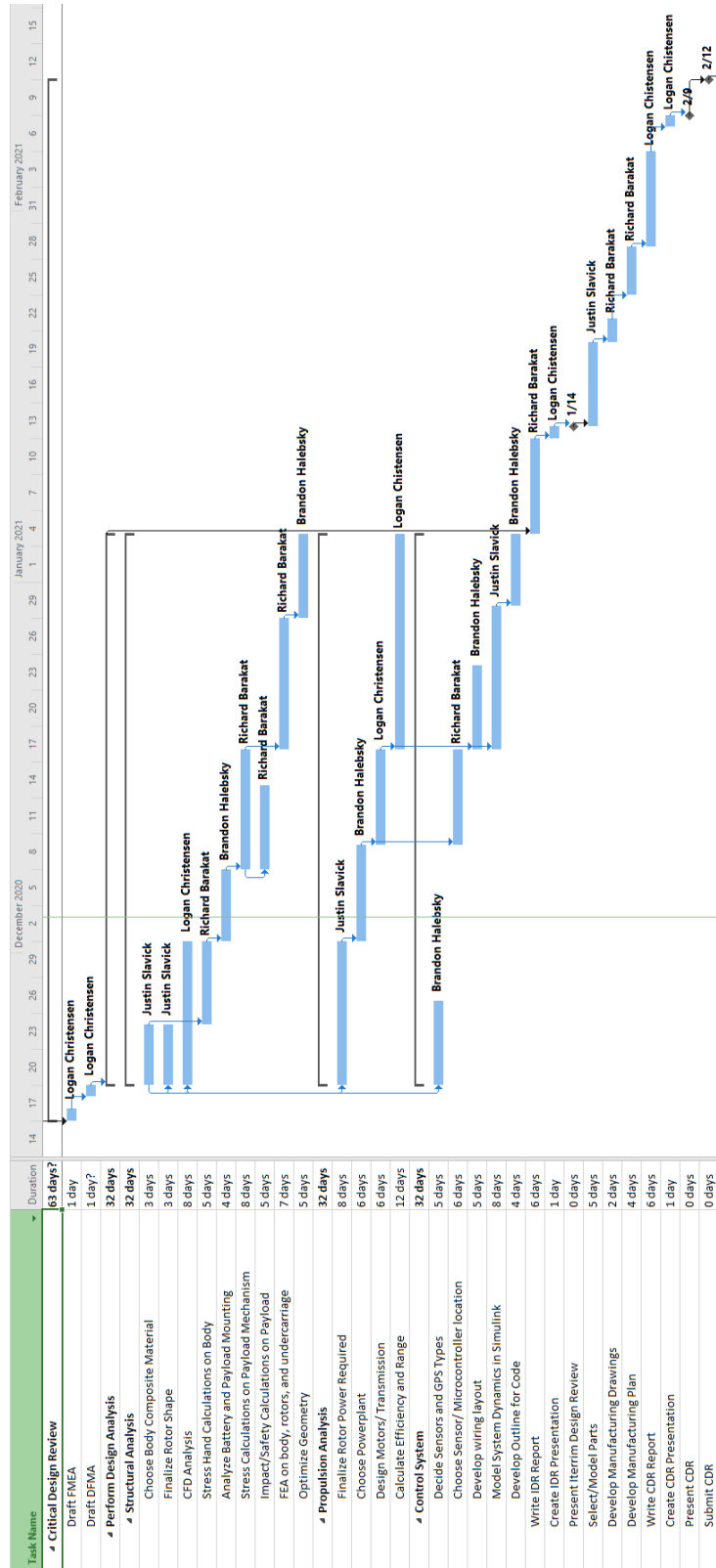


Figure B.2: Gantt chart up to Critical Design Review Milestone.

Appendix C: Ideation

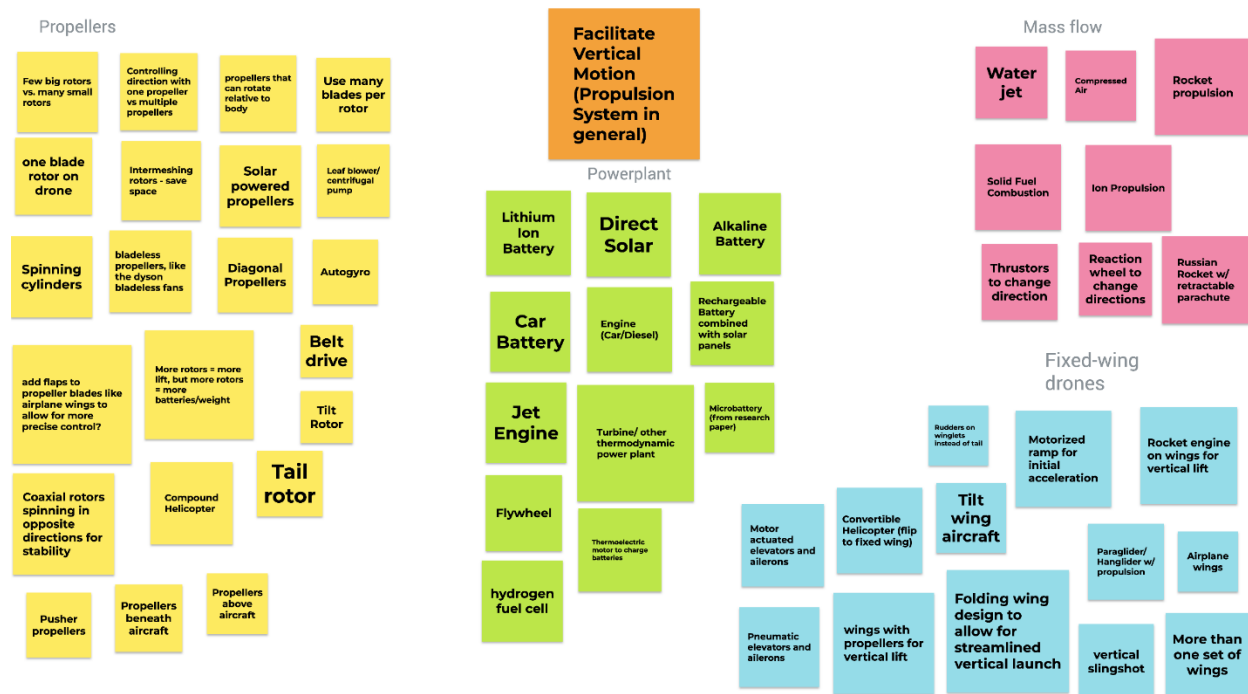


Figure C.1: Ideas for facilitating propulsion and providing power.

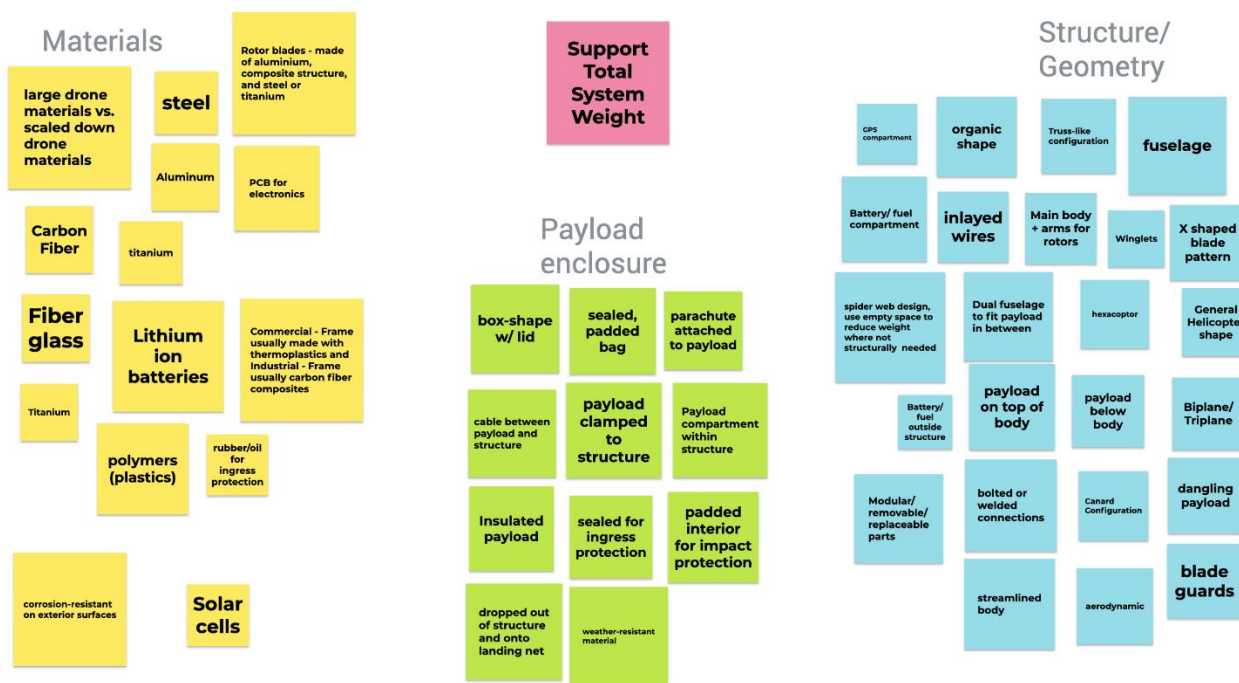


Figure C.2: Ideas for providing structural support, packaging components, and carrying and unloading payload.

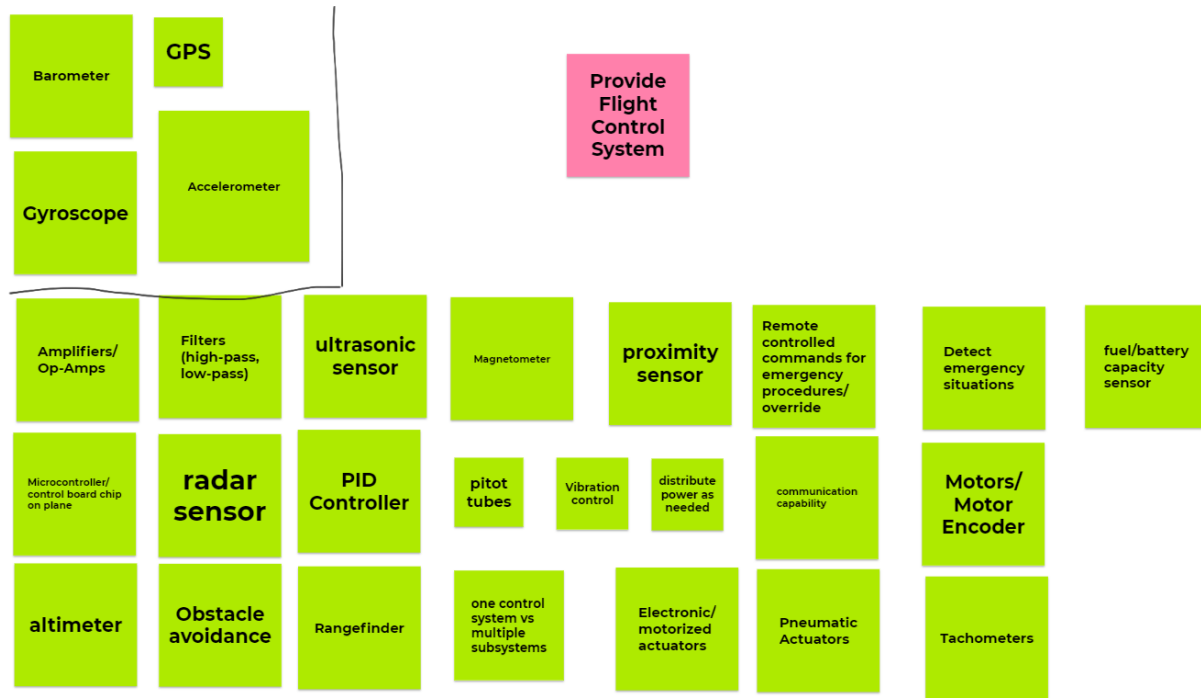


Figure C.3: Ideas for providing flight control.

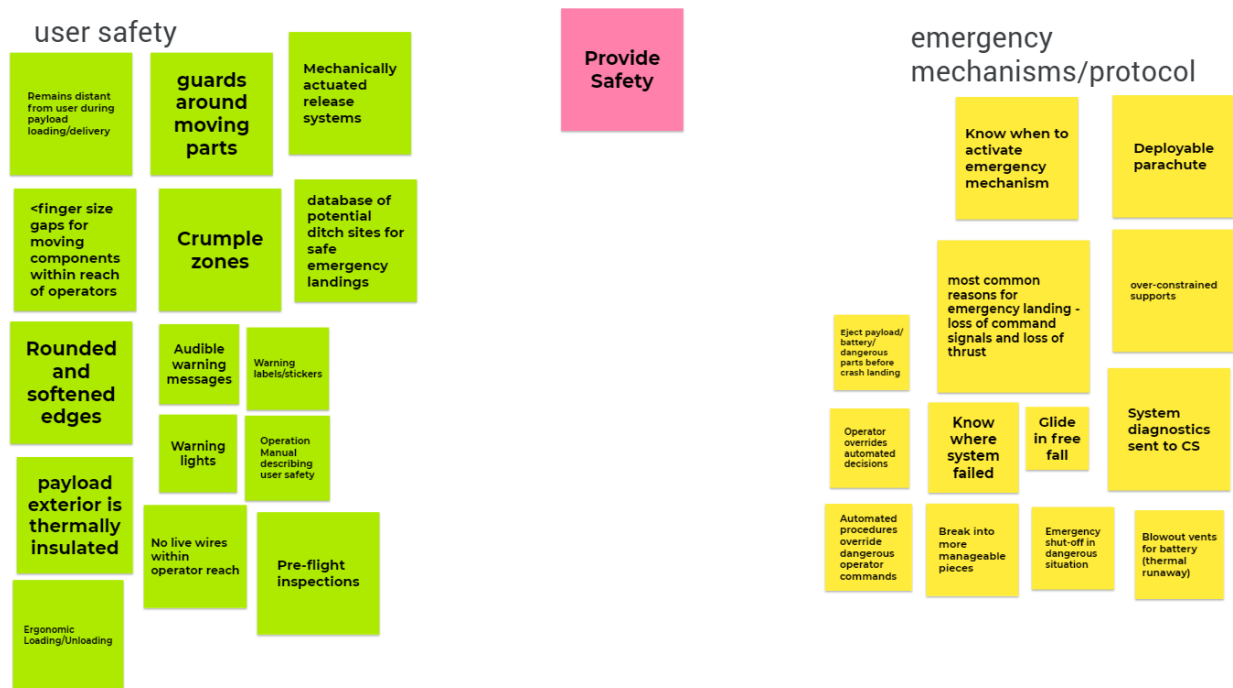


Figure C.4: Ideas for providing safety and emergency response capability.



(a) 4-rotor propulsion



(b) tilt-wing



(c) fixed-wing



(d) fixed-wing + rotors



(e) tilt-rotor



(f) tandem-rotor



(g) parachute payload drop



(h) unwinding payload drop



(i) flapping wing



(j) single-rotor

Figure C.5: Ideation models used to verify critical aspects of alternative designs.

Appendix D: Pugh Matrices

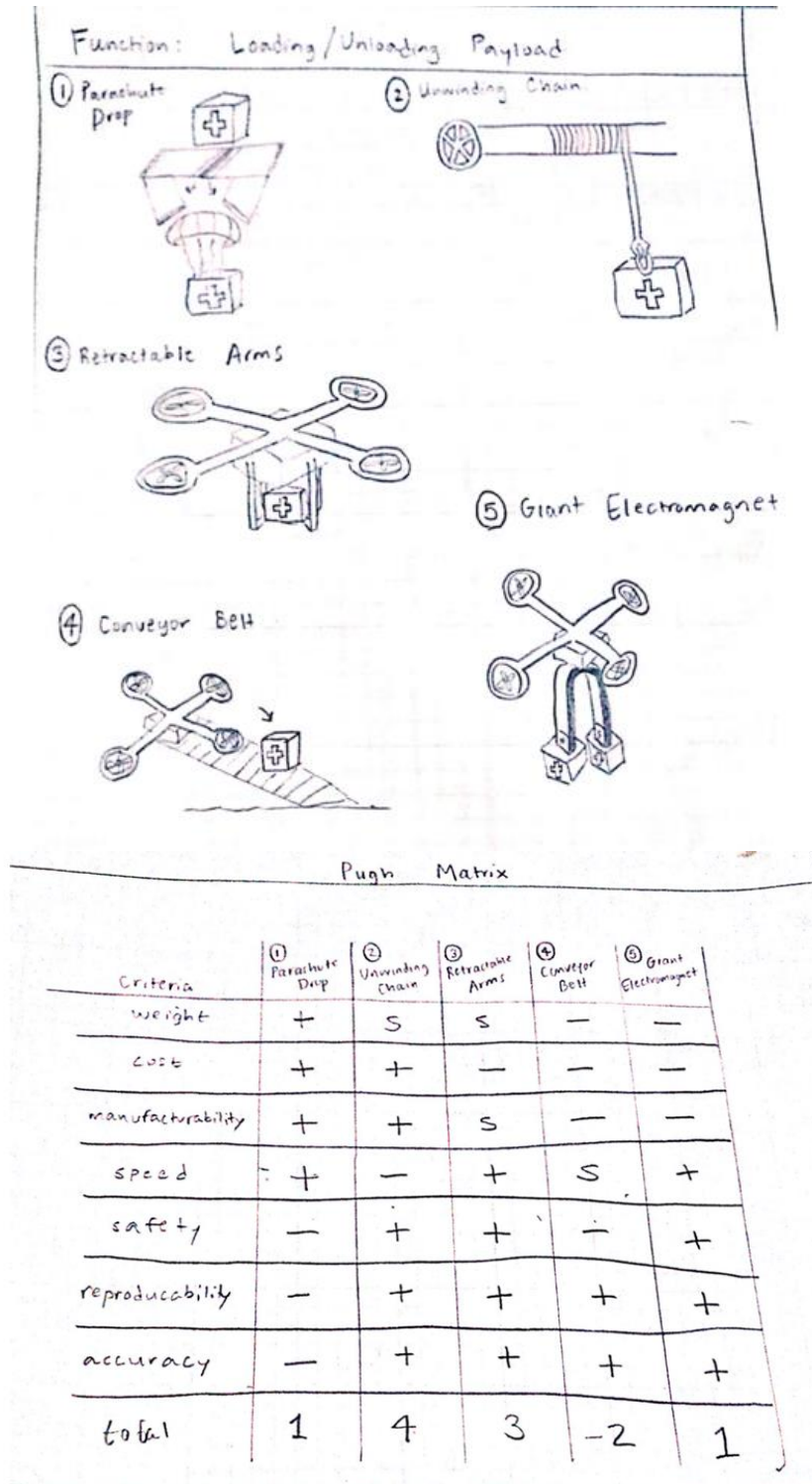
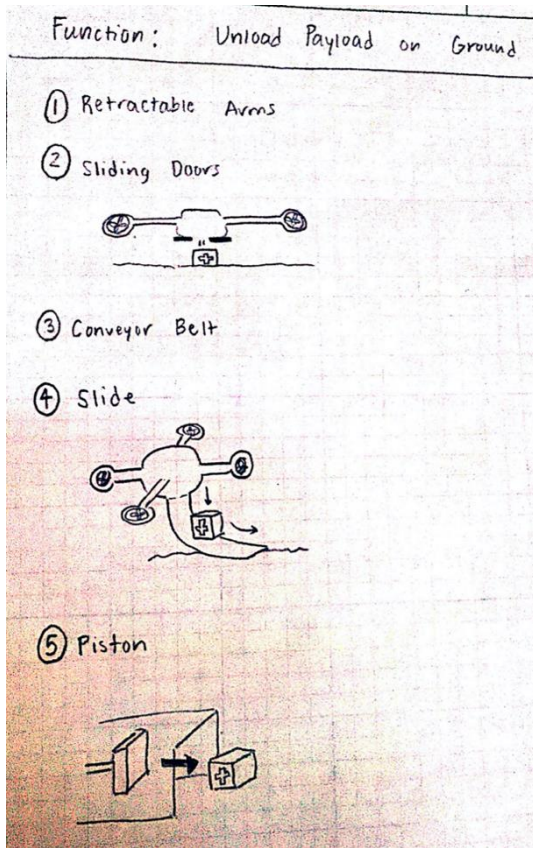


Figure D.1: Pugh Matrix for payload loading and unloading feature without competition design constraints (does not need to land on ground before payload unloading).



Criteria	① Retractable Arms	② Sliding Doors	③ Conveyor Belt	④ Slide	⑤ Piston
weight	S	+	-	-	S
cost	-	+	-	+	S
manufacturability	S	+	-	+	+
speed	+	+	S	+	+
safety	+	S	-	-	+
reproducibility	+	+	+	-	+
accuracy	+	+	+	+	+
total	3	6	-2	0	5

Figure D.2: Pugh Matrix for payload loading and unloading feature with competition design constraints (must land on ground before payload unloading)


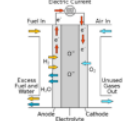
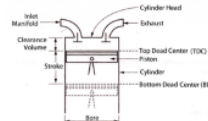


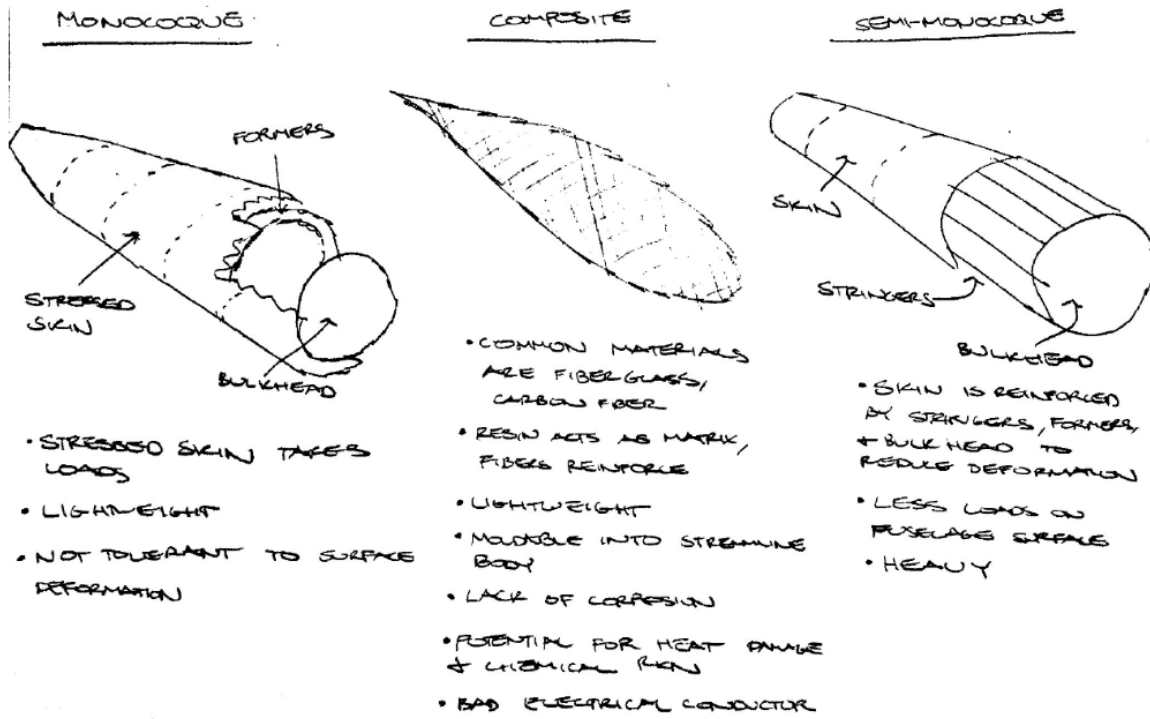
Pugh Matrix - Power System						
	Car Battery	Hydrogen fuel Cell	IC engine	Lithium Ion Battery	Direct Solar	
Criteria						
Able to Reach Far distances	S	S	+	+	-	
Fast enough	S	S	+	+	+	
Controlled landing during failure	S	+	-	S	-	
Accessible cost efficient materials	S	-	S	S	+	
Weight	S	+	-	+	+	
Total		0	1	0	3	1

Figure D.3: Pugh Matrix for power system



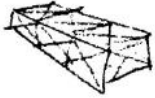




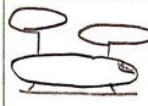
	1. TRUSS 	2. MONOCOQUE 	3. SEMI-MONOCOQUE 	4. COMPOSITE 	5. CHASSIS ONLY 
WEIGHT	-	+	-	+	+
STRENGTH	+	+	+	+	+
SAFETY	S	S	S	S	-
MANUFACTURABILITY	+	-	S	-	+
DURABILITY	+	S	S	+	-
AERODYNAMICS	-	+	S	+	-
TOTALS	1	2	1	3	0

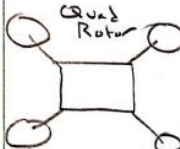
Figure D.4: Pugh Matrix for structure


Pugh Matrix


Attribute	Single Rotor	Tandem Rotor	Intermeshing Rotor	Cowtail Rotor	Quad Rotor	Multi-Rotor Helicopter	Tilt-Wing	Tilt-Rotor	Tilt-Body
Able to reach far distances	D	+	S	S	-	+	+	+	+
Fast enough to reach patients in need	D	S	S	S	S	S	+	+	+
Lift/Deliver large/heavy medical supplies	D	+	+	+	-	S	-	-	-
Vertical Take-Off/Landing	D	S	S	S	S	S	-	-	-
Safety	D	+	S	+	+	+	+	+	+
Vehicle not too big	D	-	S	=	+	-	S	S	+
Easy to troubleshoot/repair	D	-	-	-	+	-	S	S	S
Total		1	0	0	1	0	1	1	2

Top Idea Sketches and Descriptions

Tandem Rotor

 This is a helicopter that has two rotors that spin in opposite directions for balance. It is capable of carrying very large and heavy loads due to the large combined disc area. It's typically hard to implement in small UAVs.

Quad Rotor

 This is a drone that uses four fixed rotors to balance the aircraft in the air. It has the benefit of being very simple to build and repair. However, it requires a very complex control algorithm and typically does not carry large loads.

Tiltwing

 This is a fixed-wing airplane that can rotate its wings 90° in order to have Vtol and hover capabilities. It is very fast and efficient in horizontal flight compared to other Vtol aircraft. However, it has reduced efficiency and payload capacity to other fixed-wing aircraft.

Tiltrotor

 This is a tandem helicopter that can rotate its rotors 90° to provide horizontal propulsion. It is much faster in horizontal flight than a helicopter. It is also less efficient and can lift less mass than a helicopter.

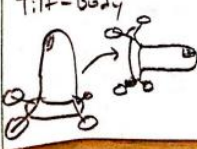
Tilt-Body

 This is an aircraft that can hover and take-off vertically, but can also rotate to cruise horizontally. It differs from a tiltrotor and a tiltwing in that it doesn't require motors to change flight orientation. However, it can very easily stall and is much less efficient than tiltrotors and tiltwings.

Figure D.5: Pugh Matrix for horizontal and vertical motion

Appendix E: Preliminary Analysis Hand Calculations

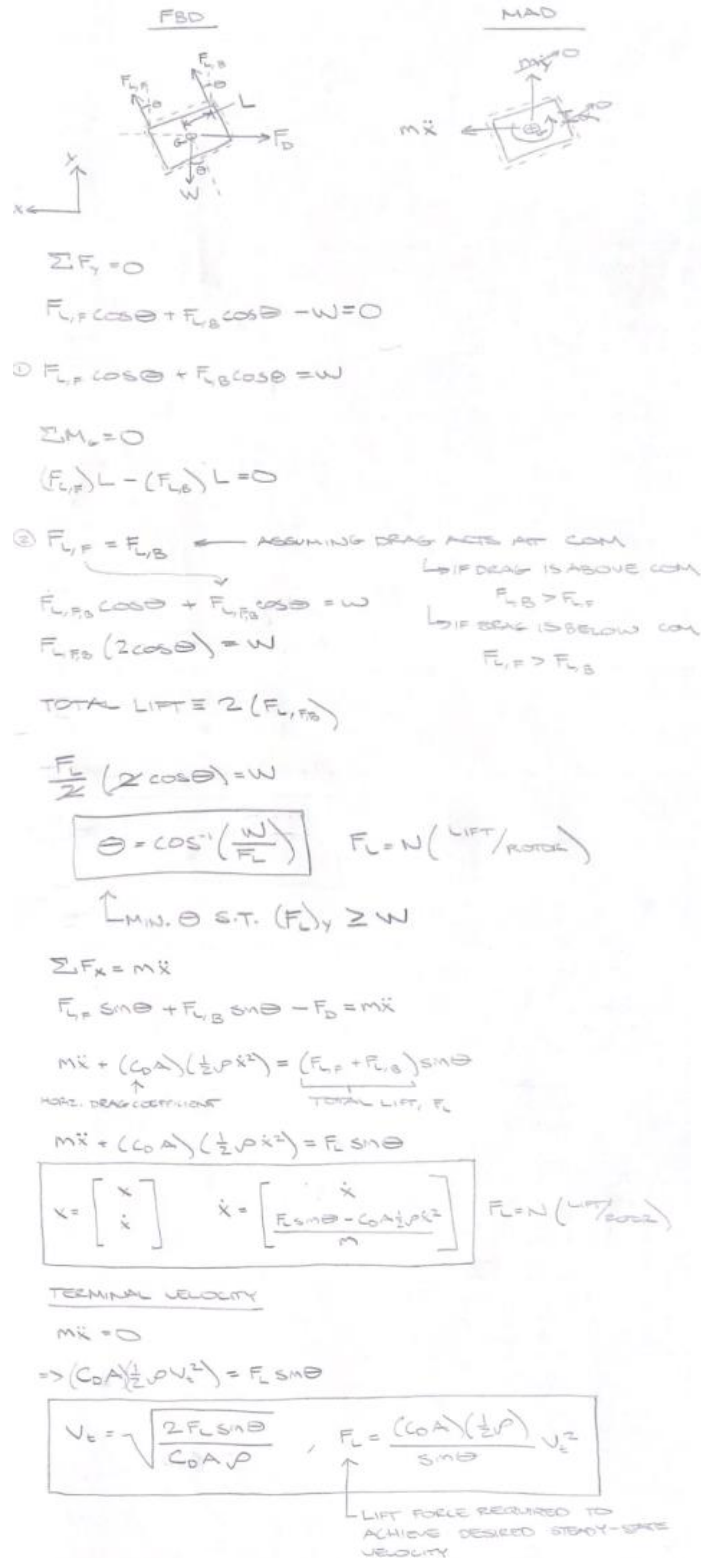


Figure E.1: Hand calculations for derivation of equations of motion UAV in forward flight.

- 1) CALCULATE V_t TO SATISFY SPEED REQUIREMENT
 ASSUME HORIZONTAL $C_D + A$ AND WEIGHT
 SOLVE FOR REQUIRED LIFT FORCE:

$$F_L = \frac{(C_D A) \left(\frac{1}{2} \rho\right) V_t^2}{\sin \theta}$$

$$\hookrightarrow \theta = \cos^{-1} \left(\frac{W}{F_L} \right)$$

$$F_L = \frac{(C_D A) \left(\frac{1}{2} \rho\right) V_t^2}{\sin \left(\cos^{-1} \left(\frac{W}{F_L} \right) \right)}$$

$$F_L = \frac{(C_D A) \left(\frac{1}{2} \rho\right) V_t^2}{\sqrt{1 - \left(\frac{W}{F_L} \right)^2}}$$

$$F_L^2 \left(1 - \left(\frac{W}{F_L} \right)^2 \right) = \left[(C_D A) \left(\frac{1}{2} \rho\right) V_t^2 \right]^2$$

$$F_L^2 - W^2 = \left[(C_D A) \left(\frac{1}{2} \rho\right) V_t^2 \right]^2$$

$$F_L = \sqrt{\left[(C_D A) \left(\frac{1}{2} \rho\right) V_t^2 \right]^2 + W^2}$$

- 2) SOLVE FOR MINIMUM PITCH ANGLE TO PREVENT
 FREE FALL

$$\theta = \cos^{-1} \left(\frac{W}{F_L} \right)$$

Figure E.2: Hand calculations for thrust force and pitch angle as a function of terminal velocity.

IDEAL POWER REQUIRED TO HOVER

MOMENTUM THEORY ANALYSIS

ASSUMPTIONS

- ① STEADY
- ② INCOMPRESSIBLE
- ③ 1D FLOW
- ④ FLUID IS QUIESCENT UPSTREAM OF ROTOR ($v_1 = 0$)

CONSERVATION OF LINEAR MOMENTUM

$$\Sigma F_i = \frac{d}{dt} \int_{CV} u \rho \, dV + \int_{CS_1} u \rho \vec{V}_i \cdot d\vec{A}_i + \int_{CS_2} u \rho \vec{V}_e \cdot d\vec{A}_e$$

$$T = \dot{m} v_2 = (\rho A v_1) v_2$$

CONSERVATION OF ENERGY

$$\frac{\partial E}{\partial t} \Big|_{sys} = \frac{d}{dt} \int_{CV} \left(\frac{v^2}{2} + gz + u \right) \rho \, dV + \int_{CS} \left(\frac{v^2}{2} + gz + u \right) \rho \vec{V} \cdot d\vec{A}$$

$$\dot{Q}_in - \dot{W} = \int_{CS} \frac{1}{2} v^2 \rho \vec{V} \cdot d\vec{A}$$

$$\Rightarrow |\dot{W}| = \frac{1}{2} v_2^2 (\dot{m})$$

$$\dot{W} = T v_1 = \dot{m} v_2 v_1$$

$$\dot{m} \frac{1}{2} v_2 v_1 = \frac{1}{2} v_2^2 \dot{m}$$

$$v_2 = 2 v_1$$

$$\Rightarrow T = \rho A v_1 (2 v_1)$$

$$T = 2 \rho A v_1^2 \Rightarrow v_1 = \sqrt{\frac{T}{2 \rho A}}$$

(CONST'D)

POWER REQ. PER PROPELLER

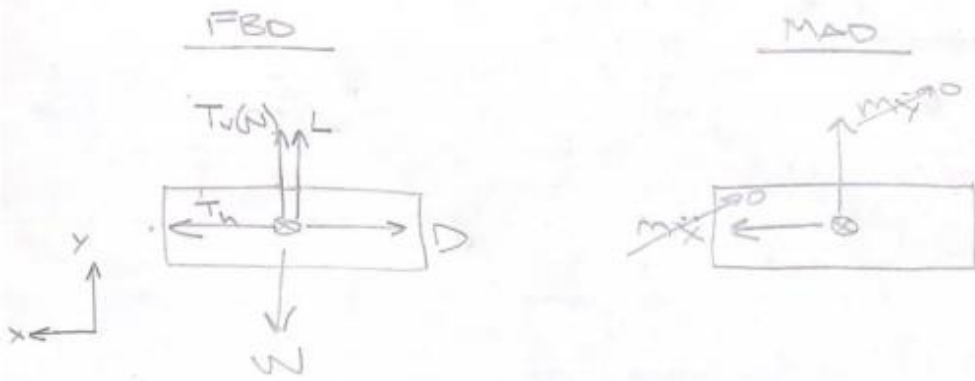
$$P = T v_1$$

$$P = T \left(\sqrt{\frac{T}{2 \rho A}} \right)$$

$$P = \frac{T^{3/2}}{\sqrt{2 \rho A}}$$

Figure E.3: Hand calculations for power required to hover.

HORIZONTAL FLIGHT: QUAD/FIXED-WING (STEADY)



$$\Sigma F_y = 0$$

$$T_v(N) + L - W = 0$$

$$T_v(N) = W - C_L A_S \left(\frac{1}{2} \rho V_t^2 \right)$$

$$T_v = \frac{W - C_L A_S \left(\frac{1}{2} \rho V_t^2 \right)}{N}$$

$$\Sigma F_x = 0$$

$$T_h - D = 0$$

$$T_h = C_D A \left(\frac{1}{2} \rho V_t^2 \right)$$

VERTICAL TO HORIZONTAL THRUST RATIO

$$T_v N = W - C_L A_S \left(\frac{T_h}{C_D A} \right)$$

$$T_v N + \frac{C_L A_S}{C_D A} T_h = W$$

Figure E.4: Hand calculations for horizontal and vertical thrust for quad configuration with wings and propeller.

Appendix F: Design Hazard Checklist

Y	N	
×		1. Will any part of the design create hazardous revolving, reciprocating, running, shearing, punching, pressing, squeezing, drawing, cutting, rolling, mixing or similar action, including pinch points and sheer points?
×		2. Can any part of the design undergo high accelerations/decelerations?
×		3. Will the system have any large moving masses or large forces?
	×	4. Will the system produce a projectile?
×		5. Would it be possible for the system to fall under gravity creating injury?
	×	6. Will a user be exposed to overhanging weights as part of the design?
×		7. Will the system have any sharp edges?
	×	8. Will any part of the electrical systems not be grounded?
	×	9. Will there be any large batteries or electrical voltage in the system above 40 V?
×		10. Will there be any stored energy in the system such as batteries, flywheels, hanging weights or pressurized fluids?
	×	11. Will there be any explosive or flammable liquids, gases, or dust fuel as part of the system?
	×	12. Will the user of the design be required to exert any abnormal effort or physical posture during the use of the design?
	×	13. Will there be any materials known to be hazardous to humans involved in either the design or the manufacturing of the design?
	×	14. Can the system generate high levels of noise?
	×	15. Will the device/system be exposed to extreme environmental conditions such as fog, humidity, cold, high temperatures, etc?
×		16. Is it possible for the system to be used in an unsafe manner?
	×	17. Will there be any other potential hazards not listed above? If yes, please explain on reverse.

Description of Hazard	Planned Corrective Action	Planned Date	Actual Date
Sharp rotor blades will be rotating at high speeds and can be dangerous to nearby users when on the ground. (1,3,7)	Design guards around the blades; select proximity sensors to be installed near the rotors that can detect nearby objects and signal an emergency stop if objects get within a specified range.	1/6/20	
The UAV can free fall if a system occurs mid-flight; this would result in a large impact force (large mass, high altitude, high velocity upon impact) that would be very dangerous to people nearby. (2,5)	Design redundant features (i.e. if one component fails, the rest of the system will not fail); determine if an emergency parachute can sufficiently slow down the free fall with basic hand calcs, design features that will enable gliding in event of power failure.	2/12/20	
Energy will be stored in a lithium-ion batteries which can explode at high temperatures (storage or short circuiting). (10)	Design a heat sink around the battery to conduct heat away in the case of over-heating. Will not over-charge batteries and not use the batteries if they suffer a major drop.	2/12/20	
If remote-controlled, the UAV may not operate as intended and an uncontrolled, dangerous response may occur. (16)	Program the UAV to only allow remote-controlled operations in emergency situations and allow limited actions when control is taken over by a human.	4/23/20	

Appendix G: Power Calculations – MATLAB code

Quadcopter Calculations:

Forward Flight: Required Lift Force & Pitch Angle

```
% Inputs
vt = 50; % Desired terminal velocity [m/s]
Cd = 1; % assumed drag coefficient
A = 0.8; % assumed frontal area [m^2]
p = 1.2; % density of air at 150m altitude [kg/m^3]
m = [100:1000]; % array of masses [kg]

g = 9.81; % gravitational acceleration [m/s^2]
w = g*m; % array of weights [N]

% solve for required lift and pitch angle

FL = sqrt((Cd*A*.5*p*vt^2)^2+w.^2);

th = acosd(w./FL);

% Plot Lift vs weight and Angle vs weight

figure(1)

yyaxis left
plot(m,FL);

yyaxis right
plot(m,th);

yyaxis left
title('Cruise Segment: Required Thrust and Pitch Angle (vt = 50 m/s)')
xlabel('system Mass [kg]')
ylabel('Required Thrust [N]')
ylim([0 12000])

yyaxis right
ylabel('Required Pitch Angle [deg]')
ylim([0 50])

% simplified rotor parameters
Rp = [0.5:0.5:2]; % radius of rotor disk area [m]
N = 4; % number of propellers

% calculate rotor disk area
Ap = pi*Rp.^2;

% calculate power required for forward flight

for i = 1:length(Rp)
    for j = 1:length(FL)
```

```

        % iteratively solve for induced velocity at each mass
        vi_t(i,j) = fzero(@(vi)FL(j)-
2*p*Ap(i)*vi*sqrt((Vt*cosd(th(j)))^2+(vt*sind(th(j))+vi)^2),0);
        % solve for total power
        Pt_forward(i,j) = FL(j)*(vt*sind(th(j))+vi_t(i,j))/1000;
        % iteratively solve for induced velocity (per rotor) at each mass
        vi_p(i,j) = fzero(@(vi)FL(j)/N-
2*p*Ap(i)*vi*sqrt((Vt*cosd(th(j)))^2+(vt*sind(th(j))+vi)^2),0);
        % solve for power per rotor
        Pp_forward(i,j) = FL(j)/N*(vt*sind(th(j))+vi_p(i,j))/1000;
    end
end

figure(2)
plot(m,Pt_forward(1,:))
hold on
plot(m,Pt_forward(2,:))
hold on
plot(m,Pt_forward(3,:))
hold on
plot(m,Pt_forward(4,:))
hold off
grid on
title('Ideal Power Required: Forward Flight (Vt = 50 m/s)')
xlabel('System Mass [kg]')
xlim([100 800])
ylabel('Ideal Total Power [kW]')
ylim([0 500])
legend('rotor radius = 0.5m','rotor radius = 1.0m','rotor radius = 1.5m','rotor radius = 2.0m')

figure(3)
plot(m,Pp_forward(1,:))
hold on
plot(m,Pp_forward(2,:))
hold on
plot(m,Pp_forward(3,:))
hold on
plot(m,Pp_forward(4,:))
hold off
grid on
title('Ideal Power per Rotor Required: Forward Flight (Vt = 50 m/s)')
xlabel('System Mass [kg]')
xlim([100 800])
ylabel('Ideal Power per Rotor [kW]')
ylim([0 60])
legend('rotor radius = 0.5m','rotor radius = 1.0m','rotor radius = 1.5m','rotor radius = 2.0m')

```

Hover - Momentum Theory Analysis

```
% Calculate power required

for i=1:length(Rp)
    % total power required
    Pt_hover(i,:) = w.^1.5/sqrt(2*p*Ap(i))/1000;
    vh_t(i,:) = sqrt(w/(2*p*Ap(i))); % induced hover velocity
    % power required per rotor
    Pp_hover(i,:) = (w/N).^1.5/sqrt(2*p*Ap(i))/1000; % assume weight distributed equally
    vh_p(i,:) = sqrt((w/N)/(2*p*Ap(i))); % induced hover velocity
end

% plot total power required to hover
figure(4)
plot(m,Pt_hover(1,:))
hold on
plot(m,Pt_hover(2,:))
hold on
plot(m,Pt_hover(3,:))
hold on
plot(m,Pt_hover(4,:))
hold off
grid on
title('Ideal Power Required: Hover')
xlabel('System Mass [kg]')
xlim([100 800])
ylabel('Ideal Total Power [kW]')
legend('rotor radius = 0.5m','rotor radius = 1.0m','rotor radius = 1.5m','rotor radius = 2.0m')

% plot power per rotor required to hover
figure(5)
plot(m,Pp_hover(1,:))
hold on
plot(m,Pp_hover(2,:))
hold on
plot(m,Pp_hover(3,:))
hold on
plot(m,Pp_hover(4,:))
hold off
grid on
title('Ideal Power Required Per Rotor: Hover')
xlabel('System Mass [kg]')
xlim([100 800])
ylabel('Ideal Power per Rotor [kW]')
legend('rotor radius = 0.5m','rotor radius = 1.0m','rotor radius = 1.5m','rotor radius = 2.0m')
```

Climb - Momentum Theory Analysis

```
% climb velocity
vc = 2.5; % [m/s]

% calculate required power
for i = 1:length(Rp)
    for j=1:length(vh_t)
        Pt_climb(i,j) = Pt_hover(i,j)*(vc/(2*vh_t(i,j))+sqrt((vc/(2*vh_t(i,j)))^2+1));
        Pp_climb(i,j) = Pp_hover(i,j)*(vc/(2*vh_p(i,j))+sqrt((vc/(2*vh_p(i,j)))^2+1));
    end
end

% plot total power required to hover
figure(6)
plot(m,Pt_climb(1,:))
hold on
plot(m,Pt_climb(2,:))
hold on
plot(m,Pt_climb(3,:))
hold on
plot(m,Pt_climb(4,:))
hold off
grid on
title('Ideal Power Required: Climb (vc = 2.5 m/s)')
xlabel('System Mass [kg]')
xlim([100 800])
ylabel('Ideal Total Power [kW]')
legend('rotor radius = 0.5m','rotor radius = 1.0m','rotor radius = 1.5m','rotor radius = 2.0m')

% plot power per rotor required to hover
figure(7)
plot(m,Pp_climb(1,:))
hold on
plot(m,Pp_climb(2,:))
hold on
plot(m,Pp_climb(3,:))
hold on
plot(m,Pp_climb(4,:))
hold off
grid on
title('Ideal Power Required Per Rotor: Climb (vc = 2.5 m/s)')
xlabel('System Mass [kg]')
xlim([100 800])
ylabel('Ideal Power per Rotor [kW]')
legend('rotor radius = 0.5m','rotor radius = 1.0m','rotor radius = 1.5m','rotor radius = 2.0m')
```

Quadcopter/Fixed-Wing/Propeller Calculations:

Forward Flight: Required Thrust

```
% Inputs
vt_ss = 90; % Desired terminal velocity [m/s]
vt = [0:vt_ss]; % Range of terminal velocities [m/s]
vc = 2.5; % Desired climb velocity [m/s]
vd = -2.5; % Desired descent velocity [m/s]

% simplified rotor parameters
Rp_v = [0.6:0.1:1]; % radius of vertical rotors [m]
Rp_h = [0.4:0.1:0.8]; % radius of horizontal propeller [m]
N = 4; % number of vertical rotors [m]
% calculate rotor disk area
Ap_v = pi*Rp_v.^2;
Ap_h = pi*Rp_h.^2;

% Drag
Cd = 0.2; % assumed drag coefficient
A = 1; % assumed frontal area [m^2]

% air density
p = 1.2; % density of air at 150m altitude [kg/m^3]

% weight
m = [250:50:400]; % array of masses [kg]
g = 9.81; % gravitational acceleration [m/s^2]
w = g*m; % array of weights [N]
m_h = [100:500]; % larger array [kg]
w_h = m_h*g; % larger array [N]

% Lift
As = 2*1.2; % assumed wing surface area [m^2]

% solve for required lift coefficient and horizontal propeller thrust
for i = 1:length(w);
    for j = 1:length(vt);
        Cl(i,j) = w(i)./(As*(.5*p*vt(j).^2));
        Th(j) = Cd*A*.5*p*vt(j).^2;
    end
end

Cl_ss = Cl(:,vt==vt_ss); % predicted Cl at each mass

% solve for required vertical thrust per rotor
for i = 1:length(w);
    for j = 1:length(vt);
        Tv(i,j) = (w(i)-Cl_ss(i)*As*.5*p*vt(j).^2)/N;
    end
end
```

```

% plot Thrust vs Velocity and Lift Coeff. vs Velocity
figure(1)

yyaxis left
plot(vt,T_h/g);

yyaxis right
plot(vt,c_l);

yyaxis left
title('Propeller Thrust and Lift Coefficient: Forward Flight')
legend('Thrust','mass = 250kg','mass = 300kg','mass = 350kg','mass = 400kg','Location','southwest')
xlabel('Steady State Velocity [m/s]')
xlim([0 vt_ss])
ylabel('Required Propellor Thrust [kg]')

yyaxis right
ylabel('Required Lift Coefficient [-]')
ylim([0 1.5])
yticks(0:0.25:1.5)

% plot thrust vs velocity
figure(2)

yyaxis left
plot(vt,T_v/g);

yyaxis right
plot(vt,T_h/g);

yyaxis left
title('Propeller Thrust and Rotor Thrust: Forward Flight')
legend('Vert. Rotor, mass = 250kg','Vert. Rotor, mass = 300kg','Vert. Rotor, mass = 350kg','Vert. Rotor, mass = 400kg','Horiz. Prop','Location','southwest')
xlabel('Steady State Velocity [m/s]')
xlim([0 vt_ss])
ylabel(['Vertical Thrust per Rotor (N = ' num2str(N) ') [kg]'])

yyaxis right
ylabel('Horizontal Propellor Thrust [kg]')

```

Forward Flight - Momentum Theory Analysis

```

% Hover efficiency
nh = 0.6; % [-]

% rotor and propeller angles
th_v = 0; % rotor angle relative to z axis [deg]
th_h = 90; % propeller angle relative to z axis [deg]

for i = 1:length(w)

```



```

for j = 1:length(Vt)
    for k = 1:length(Rp_h)
        % vertical rotors
        % iteratively solve for induced velocity (per rotor) at each mass (Leishman, eq 2.121
pg 95)
        vi_p_v(i,j) = fzero(@(vi) T_v(i,j)-
2*p*Ap_v(4)*vi*sqrt((Vt(j)*cosd(th_v))^2+(Vt(j)*sind(th_v)+vi)^2),0);
        % solve for power per rotor (Leishman, eq 2.139 pg 99)
        Pp_forward_v(i,j) = (T_v(i,j)*(Vt(j)*sind(th_v)+vi_p_v(i,j))/1000)/nh;

        % horiozntal propeller
        % iteratively solve for induced velocity (per rotor) at each mass (Leishman, eq 2.121
pg 95)
        vi_p_h(k,j) = fzero(@(vi)T_h(j)-
2*p*Ap_h(k)*vi*sqrt((Vt(j)*cosd(th_h))^2+(Vt(j)*sind(th_h)+vi)^2),0);
        % solve for power per rotor (Leishman, eq 2.139 pg 99)
        Pp_forward_h(k,j) = T_h(j)*(Vt(j)*sind(th_h)+vi_p_h(k,j))/1000;
    end
end
end

% plot power required vs velocity
figure(3)

yyaxis left
plot(Vt,Pp_forward_v);

yyaxis right
plot(Vt,Pp_forward_h);

yyaxis left
title(['Propeller Power and Rotor Power: Forward Flight (Rrotor = ' num2str(Rp_v(4)) ' m)'])
legend('Vert. Rotor, mass = 250kg','Vert. Rotor, mass = 300kg','Vert. Rotor, mass = 350kg','Vert.
Rotor, mass = 400kg','Horiz. Prop, Rp = 0.4 m','Horiz. Prop, Rp = 0.5 m','Horiz. Prop, Rp = 0.6
m','Horiz. Prop, Rp = 0.7 m','Horiz. Prop, Rp = 0.8 m','Location','northwest')
xlabel('Cruise velocity [m/s]')
xlim([0 vt_ss])
ylabel(['Vertical Power per Rotor (N = ' num2str(N) ') [kw]'])
ylim([0 50])

yyaxis right
ylabel('Horizontal Propellor Power [kw]')
ylim([0 90])

% plot total power required per velocity
P_total = N*Pp_forward_v+Pp_forward_h(1,:);

figure(6)
plot(Vt,P_total);
title(['Total Power: Forward Flight (Rrotor = ' num2str(Rp_v(4)) ' m)'])
legend('mass = 250kg','mass = 300kg','mass = 350kg','mass = 400kg','Location','southeast')
xlabel('Cruise velocity [m/s]')
xlim([0 vt_ss])
ylabel(['Total Power Required [kw]'])

```

```

ylim([0 90])
grid on

% calculate power required to fly at desired terminal velocity for range of lift coefficients
Cl_ang = [linspace(0.001,Cl_ss(1),50); linspace(0.001,Cl_ss(2),50); linspace(0.001,Cl_ss(3),50);
linspace(0.001,Cl_ss(4),50)];

for i=1:length(w)
    for j=1:length(Cl_ang(1,:))
        T_v_ang(i,j) = (w(i)-Cl_ang(i,j)*As*.5*p*Vt_ss^2)/N;

        vi_p_v_ang(i,j) = fzero(@(vi)T_v_ang(i,j)-
2*p*Ap_v(2)*vi*sqrt((Vt_ss*cosd(th_v))^2+(Vt_ss*sind(th_v)+vi)^2),0);
        % solve for power per rotor (Leishman, eq 2.139 pg 99)
        Pp_v_ang(i,j) = (T_v_ang(i,j)*(Vt_ss*sind(th_v)+vi_p_v_ang(i,j))/1000)/nh;
    end
end

% plot vertical rotor power required vs lift coefficient
figure(4)

plot(Cl_ang(1,:),Pp_v_ang(1,:))
hold on
plot(Cl_ang(2,:),Pp_v_ang(2,:))
hold on
plot(Cl_ang(3,:),Pp_v_ang(3,:))
hold on
plot(Cl_ang(4,:),Pp_v_ang(4,:))
hold off

grid on
title(['Propeller Power and Rotor Power: Forward Flight (Vt = ' num2str(Vt_ss) ' m/s)'])
legend('mass = 250kg','mass = 300kg','mass = 350kg','mass = 400kg','Location','northeast')
xlabel('Lift Coefficient, CL [-]')
xlim([0 0.4])
ylabel(['Vertical Power per Rotor (N = ' num2str(N) ') [kw]'])

```

Hover - Momentum Theory Analysis

```

% Calculate power required

for i=1:length(Rp_v)
    % total power required
    Pt_hover(i,:) = w_h.^1.5/sqrt(2*p*Ap_v(i))/1000;
    Pt_hover_actual(i,:) = Pt_hover(i,+)/nh; % account for hover efficiency
    vh_t(i,:) = sqrt(w_h/(2*p*Ap_v(i))); % induced hover velocity
    % power required per rotor
    Pp_hover(i,:) = (w_h/N).^1.5/sqrt(2*p*Ap_v(i))/1000; % assume weight distributed equally
    Pp_hover_actual(i,:) = Pp_hover(i,+)/nh; % account for hover efficiency
    vh_p(i,:) = sqrt((w_h/N)/(2*p*Ap_v(i))); % induced hover velocity
end

```

```

%% plot total power required to hover
figure(4)
plot(m_h,Pt_hover_actual)
grid on
title('Actual Power Required: Hover')
xlabel('System Mass [kg]')
xlim([100 300])
ylabel('Actual Total Power [kW]')
legend('rotor radius = 0.4m','rotor radius = 0.5m','rotor radius = 0.6m','rotor radius = 0.7m','rotor radius = 0.8m','Location','northwest')

%% plot power per rotor required to hover
figure(5)
plot(m_h,Pp_hover_actual)
grid on
title('Actual Power Required Per Rotor: Hover (eff = 60%)')
xlabel('System Mass [kg]')
xlim([200 400])
ylim([0 40])
xticks(200:25:400)
ylabel('Actual Power per Rotor [kW]')
legend('rotor radius = 0.6m','rotor radius = 0.7m','rotor radius = 0.8m','rotor radius = 0.9m','rotor radius = 1.0m','Location','northwest')

```

Climb - Momentum Theory Analysis

```

%% calculate required power
for i = 1:length(Rp_v)
    for j=1:length(vh_t)
        Pt_climb(i,j) = Pt_hover(i,j)*(Vc/(2*vh_t(i,j))+sqrt((Vc/(2*vh_t(i,j)))^2+1));
        Pt_climb_actual(i,j) = Pt_climb(i,j)/nh; % account for hover efficiency
        Pp_climb(i,j) = Pp_hover(i,j)*(Vc/(2*vh_p(i,j))+sqrt((Vc/(2*vh_p(i,j)))^2+1));
        Pp_climb_actual(i,j) = Pp_climb(i,j)/nh; % account for hover efficiency
    end
end

%% plot total power required to hover
figure(6)
plot(m_h,Pt_climb_actual)
grid on
title('Actual Power Required: Climb (Vc = 2.5 m/s)')
xlabel('System Mass [kg]')
xlim([100 300])
ylabel('Actual Total Power [kW]')
legend('rotor radius = 0.4m','rotor radius = 0.5m','rotor radius = 0.6m','rotor radius = 0.7m','rotor radius = 0.8m','Location','northwest')

%% plot power per rotor required to hover
figure(7)
plot(m_h,Pp_climb_actual)
grid on
title('Actual Power Required Per Rotor: Climb (Vc = 2.5 m/s, eff = 60%)')

```

```

xlabel('System Mass [kg]')
xlim([200 400])
ylim([0 40])
xticks(200:25:400)
ylabel('Actual Power per Rotor [kW]')
legend('rotor radius = 0.6m','rotor radius = 0.7m','rotor radius = 0.8m','rotor radius = 0.9m','rotor radius = 1.0m','Location','northwest')

```

Descent - Momentum Theory Analysis

```

% calculate required power
for i = 1:length(Rp_v)
    for j=1:length(vh_t)
        Pt_des(i,j) = Pt_hover(i,j)*(Vd/(2*vh_t(i,j))+sqrt((Vd/(2*vh_t(i,j)))^2+1));
        Pt_des_actual(i,j) = Pt_des(i,j)/nh; % account for hover efficiency
        Pp_des(i,j) = Pp_hover(i,j)*(Vd/(2*vh_p(i,j))+sqrt((Vd/(2*vh_p(i,j)))^2+1));
        Pp_des_actual(i,j) = Pp_des(i,j)/nh; % account for hover efficiency
        vcvh(i,j) = Vd/vh_p(i,j);
    end
end

% plot total power required to hover
% figure(8)
% plot(m_h,Pt_des)
% grid on
% title('Actual Power Required: Descent (Vd = -2.5 m/s)')
% xlabel('System Mass [kg]')
% xlim([100 300])
% ylabel('Actual Total Power [kW]')
% legend('rotor radius = 0.4m','rotor radius = 0.5m','rotor radius = 0.6m','rotor radius = 0.7m','rotor radius = 0.8m','Location','northwest')

% plot power per rotor required to hover
figure(9)
plot(m_h,Pp_des_actual)
grid on
title('Actual Power Required Per Rotor: Descent (Vd = 2.5 m/s, eff = 60%)')
xlabel('System Mass [kg]')
xlim([200 400])
ylim([0 40])
xticks(200:25:400)
ylabel('Actual Power per Rotor [kW]')
legend('rotor radius = 0.6m','rotor radius = 0.7m','rotor radius = 0.8m','rotor radius = 0.9m','rotor radius = 1.0m','Location','northwest')

```

Energy Consumption: Mission 1

```

% mechanical efficiency (aerodynamic efficiency of rotors)
nm = 0.98; % [-]

% flight height

```

```

h = 150; % [m]

% forward flight distance
d1 = 50; % [km]

% calculate time and energy consumed during climb
t_climb_1 = (h/vc)/3600; % [hours]
E_climb_1 = N*(Pp_climb_actual*(1/nh)*t_climb_1); % [kWh]

% calculate time and energy consumed during forward flight
t_forward_1 = ((d1*1000)/vt_ss)/3600; % [hours]
% power at vt_ss at propeller radius of 0.5 m
P_h_ss = Pp_forward_h(Rp_h==Rp_h(2),vt==vt_ss); % [kw]
E_forward_1 = (P_h_ss*(1/nm)*t_forward_1); % [kWh]

% calculate time and energy consumed during descent
t_des_1 = (h/-vd)/3600; % [hours]
E_des_1 = N*(Pp_des_actual*(1/nh)*t_des_1); % [kWh]

% calculate power required to hover
t_res_1 = 20; % [minutes]
E_res_1 = N*(Pp_hover_actual*(1/nh)*(t_res_1/60)); % [kWh]

% total energy consumption
E_1 = 2*E_climb_1 + 2*E_forward_1 + 2*E_des_1 + E_res_1; % [kWh]

% total mission time excluding 20 minute hover at end
t_1 = (t_climb_1+t_forward_1+t_des_1)*60 % [minutes]

% plot energy consumption required
figure(10)
plot(m_h,E_1)
grid on
title(['Mission 1: Required Energy Consumption (vc = ' num2str(vc) ' m/s, vt = ' num2str(vt_ss) '
m/s)'])
xlabel('System Mass [kg]')
xlim([200 400])
xticks(200:25:400)
ylim([0 160])
ylabel('Energy Consumption [kWh]')
legend('rotor radius = 0.6m','rotor radius = 0.7m','rotor radius = 0.8m','rotor radius =
0.9m','rotor radius = 1.0m','Location','northwest')

```

Energy Consumption: Mission 2

```

% mechanical efficiency (aerodynamic efficiency of rotors)
nm = 0.98; % [-]

% flight height
h = 150; % [m]

% forward flight distance

```

```

d2 = 200; % [km]

% calculate time and energy consumed during climb
t_climb_2 = (h/vc)/3600; % [hours]
E_climb_2 = N*(Pp_climb_actual*(1/nh)*t_climb_2); % [kWh]

% calculate time and energy consumed during forward flight (Rp = 0.5m)
t_forward_2 = ((d2*1000)/vt_ss)/3600; % [hours]
E_forward_2 = (P_h_ss*(1/nm)*t_forward_2); % [kWh]
% calculate time and energy consumed during descent
t_des_2 = (h/-vd)/3600; % [hours]
E_des_2 = N*(Pp_des_actual*(1/nh)*t_des_2); % [kWh]
% calculate power required to hover
t_res_2 = 20; % [minutes]
E_res_2 = N*(Pp_hover_actual*(1/nh)*(t_res_2/60)); % [kWh]

% total energy consumption
E_2 = E_climb_2 + E_forward_2 + E_des_2 + E_res_2; % [kWh]

% total mission time excluding 20 minute hover at end
t_2 = (t_climb_2+t_forward_2+t_des_2)*60 % [minutes]

% plot energy consumption required
figure(11)
plot(m_h,E_2)
grid on
title(['Mission 2: Required Energy Consumption (vc = ' num2str(vc) ' m/s, vt = ' num2str(vt_ss) '
m/s)'])
xlabel('System Mass [kg]')
xlim([200 400])
xticks(200:25:400)
ylim([0 160])
ylabel('Energy Consumption [kWh]')
legend('rotor radius = 0.6m','rotor radius = 0.7m','rotor radius = 0.8m','rotor radius =
0.9m','rotor radius = 1.0m','Location','northwest')

```

Energy Consumption: Mission 2 Forward Flight

```

t_2_v = (d2*1000/3600)./vt; % [hours]
E_forward_2_v = (P_total.*t_2_v); % [kWh]
% plot energy consumption required
figure(12)
plot(vt,E_forward_2_v)
grid on
title(['Mission 2: Energy Consumption during Forward Flight (Rrotor = ' num2str(Rp_v(4)) ' m)'])
legend('mass = 250kg','mass = 300kg','mass = 350kg','mass = 400kg','Location','northeast')
xlabel('Cruise Velocity [m/s]')
xlim([0 vt_ss])
ylabel('Energy Consumption [kWh]')
ylim([0 160])
grid on

```

Appendix H: Drawing Package

100 – Top Level Assembly

101 – UAV Assembly

200 – Electronics

201 – EMRAX 208 Motor

202 – EMRAX 228 Motor

203 – TG-R90 Turbogenerator

300 – Structure

301 – Fuselage

400 – Payload Mechanism

401 – Exploded Payload Mechanism

410 – Exploded Payload Ramp

411 – Large Linear Actuator

412 – Small Linear Actuator

413 – Ramp Base

414 – Brackets

415 – Cart Stopper

416 – Guide Small

417 – Guide Large

420 – Exploded Payload Cart

421 – Caster Wheels

422 – Long Support

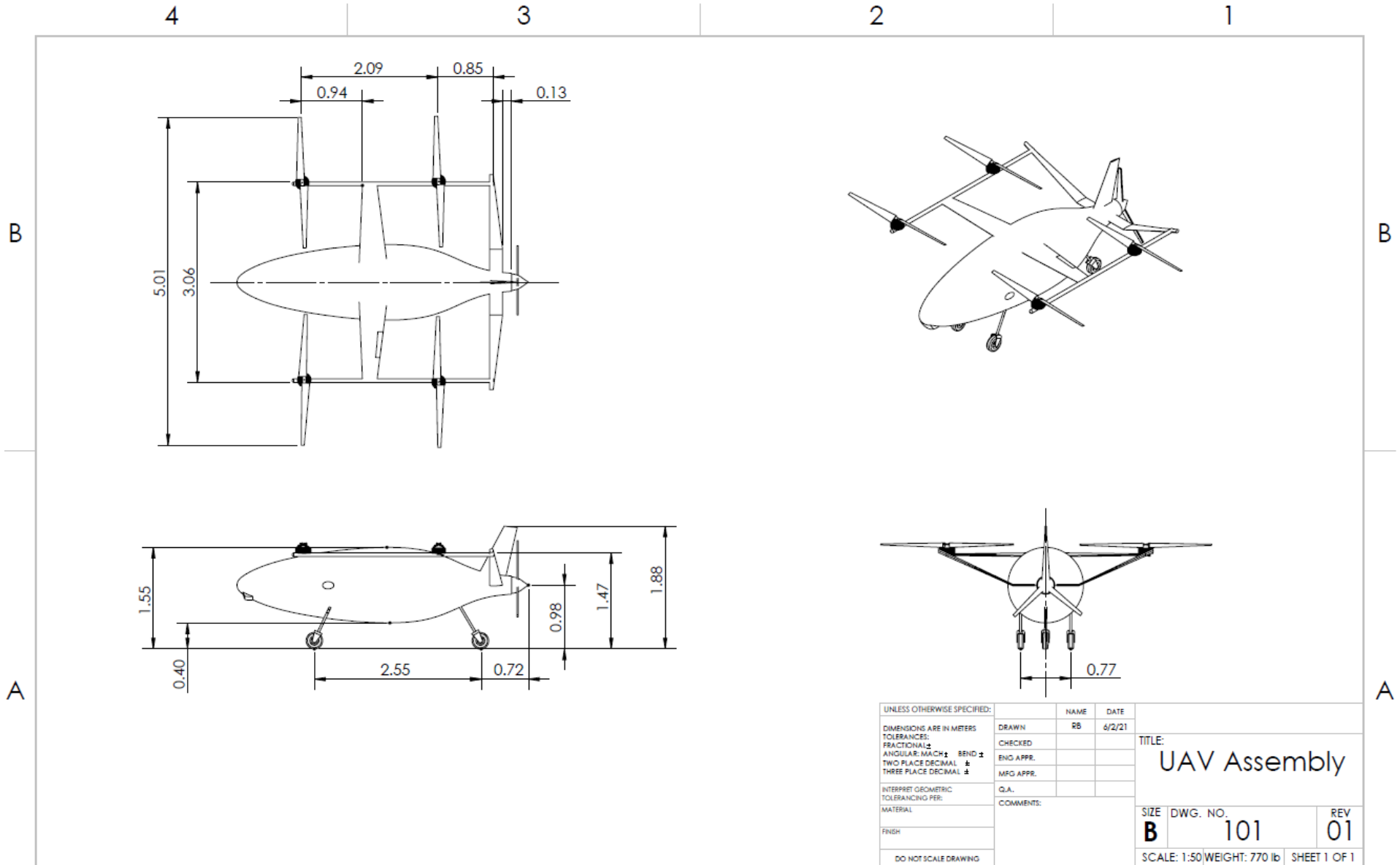
423 – Short Support

424 – 2" x 2" x 0.125" Aluminum Channel 60in

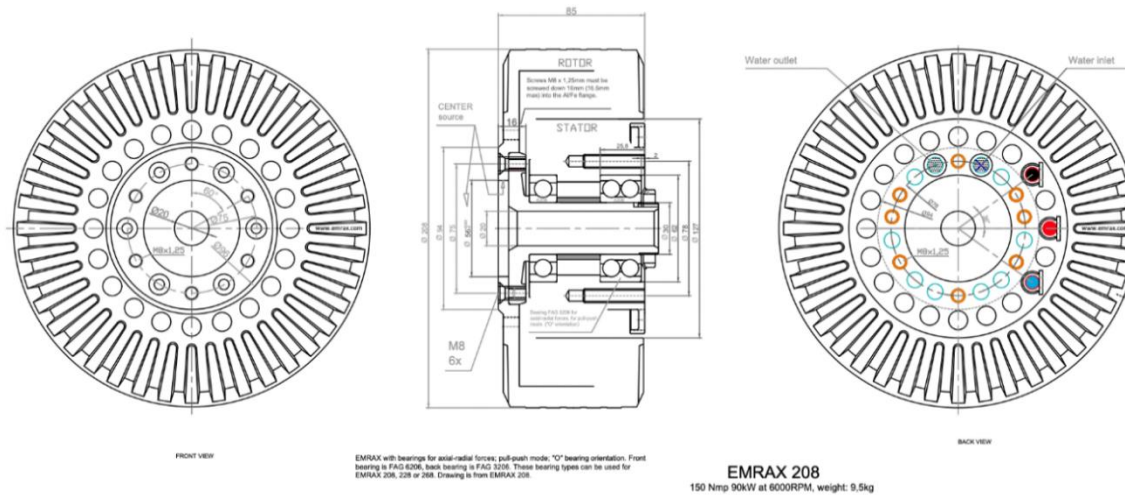
425 – Aluminum Plate, 1/8"

426 – Cart Assembly

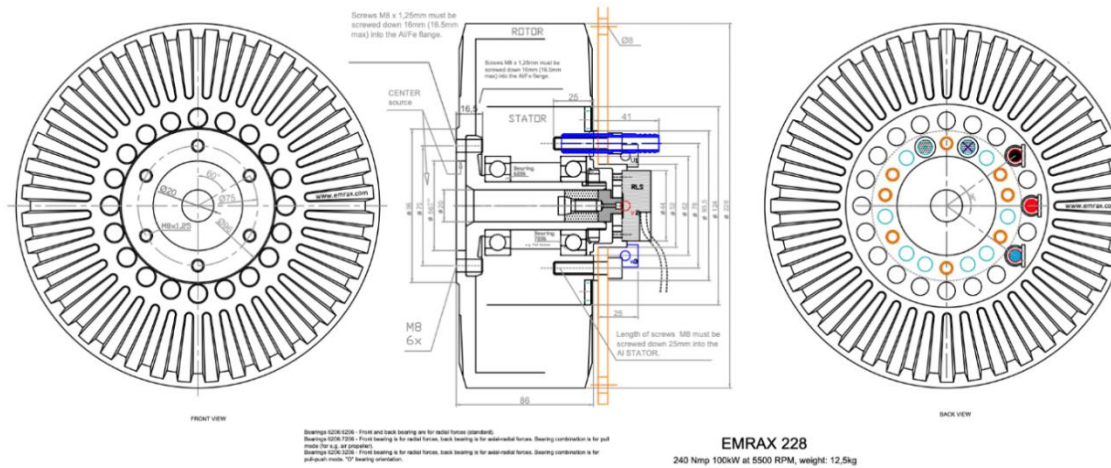
500 – Propulsion



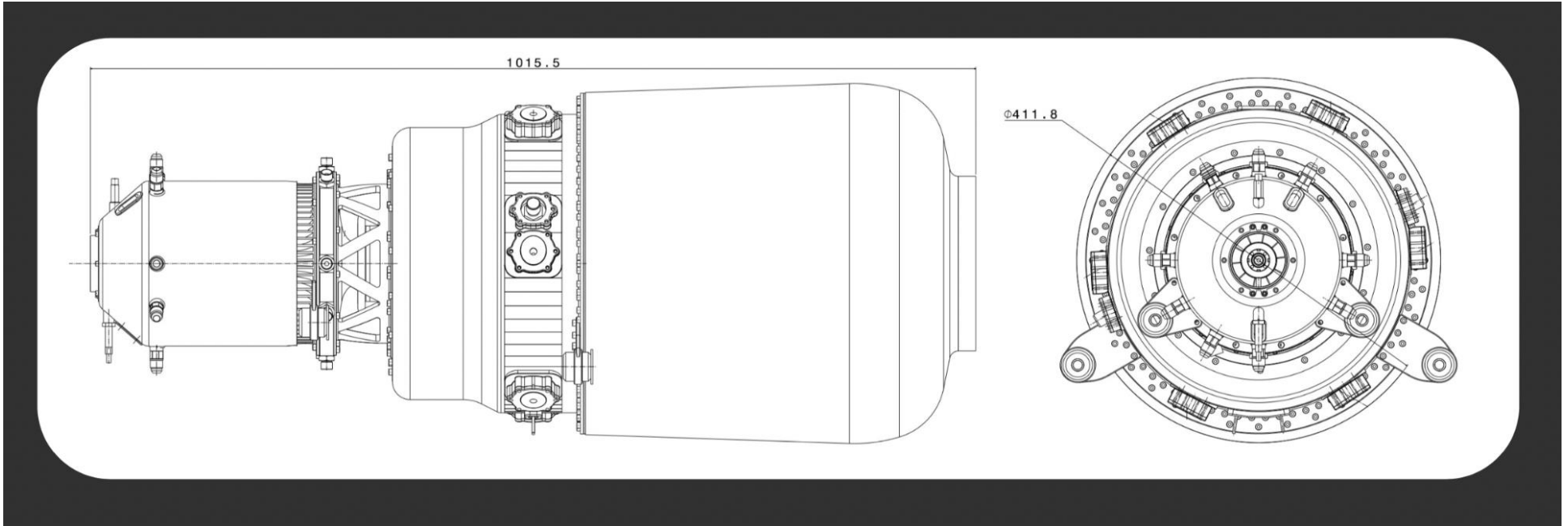
201 – Emrax 208 Motor

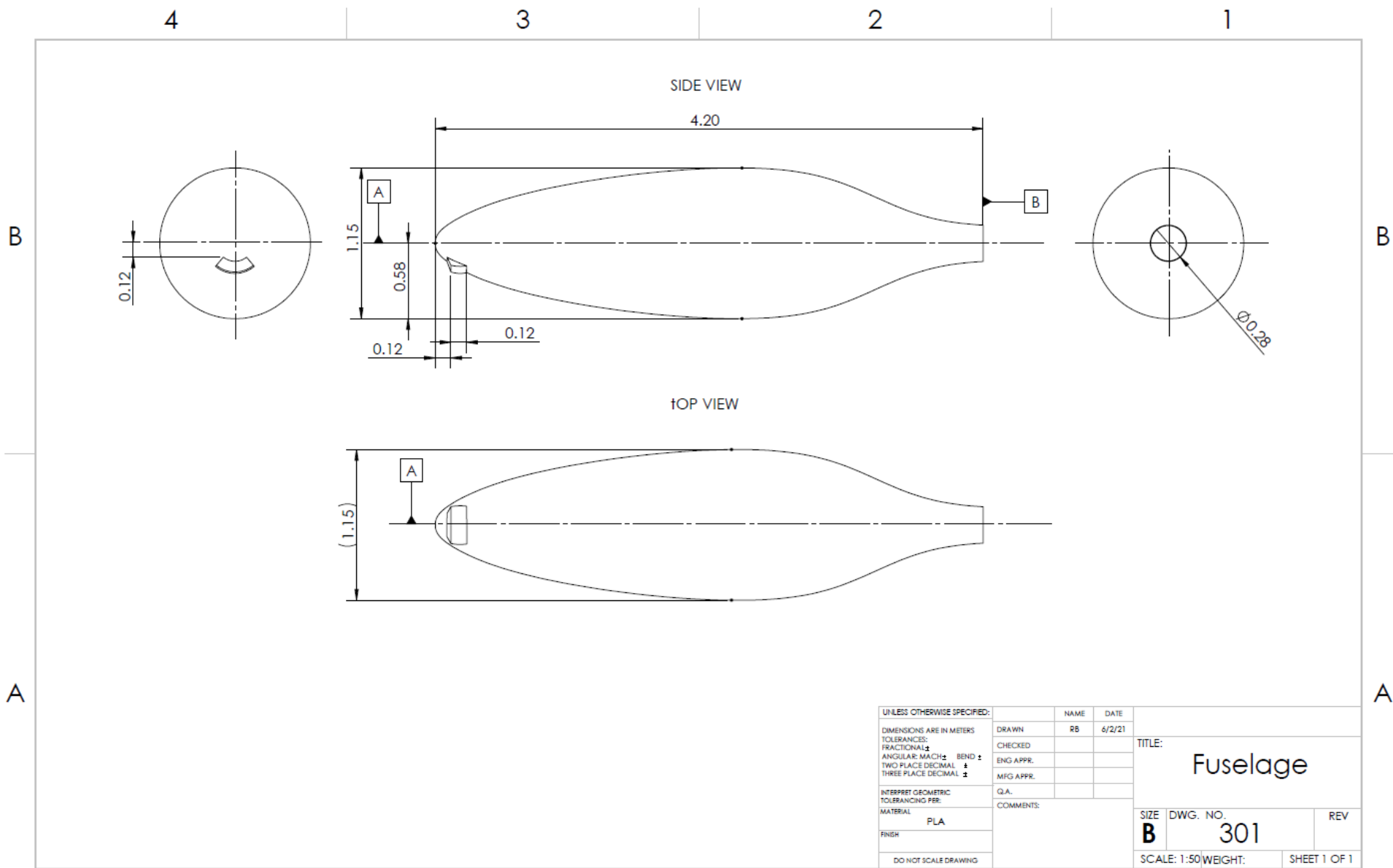


202 – Emrax 228 Motor

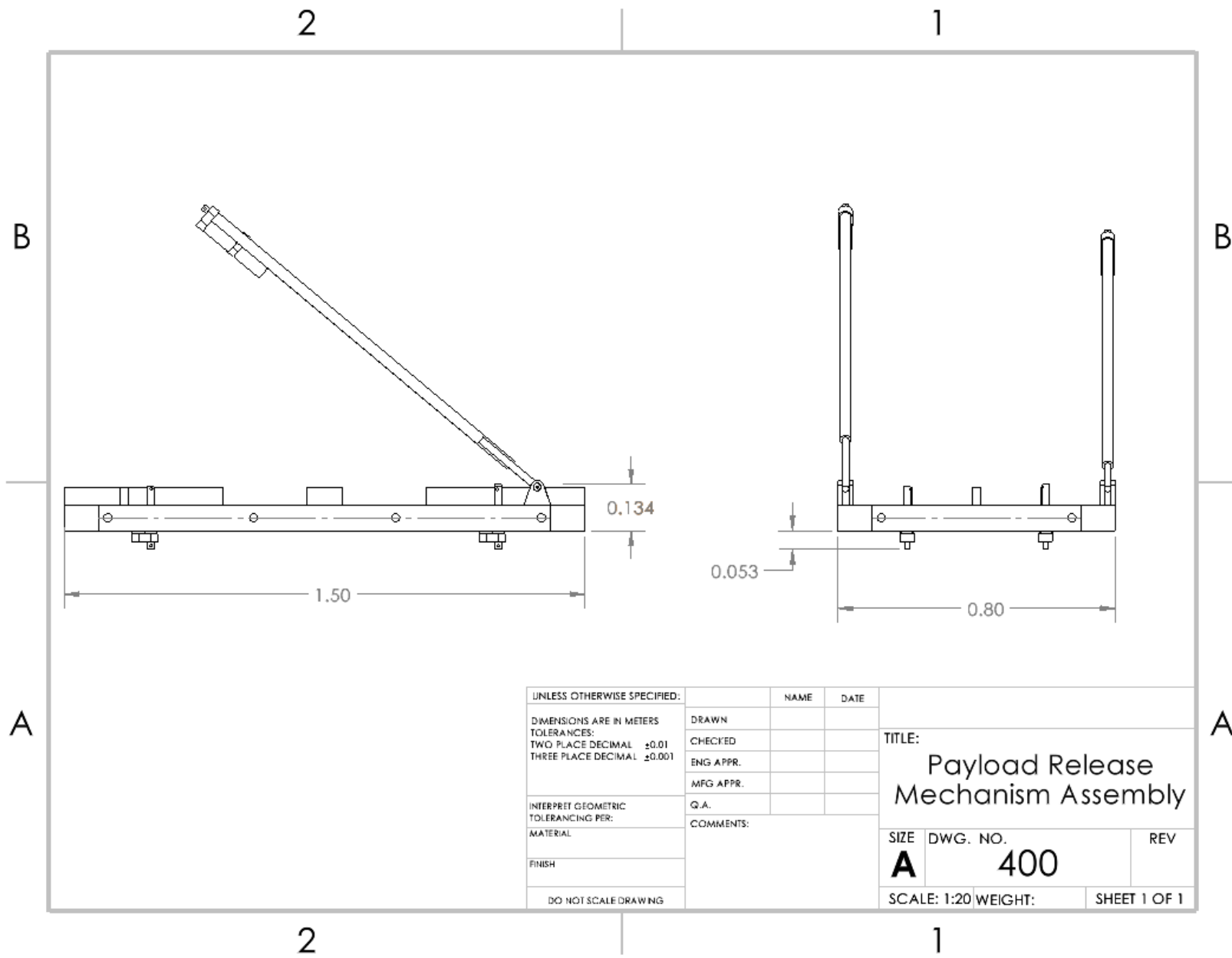


203 – TG-R90 Turbogenerator

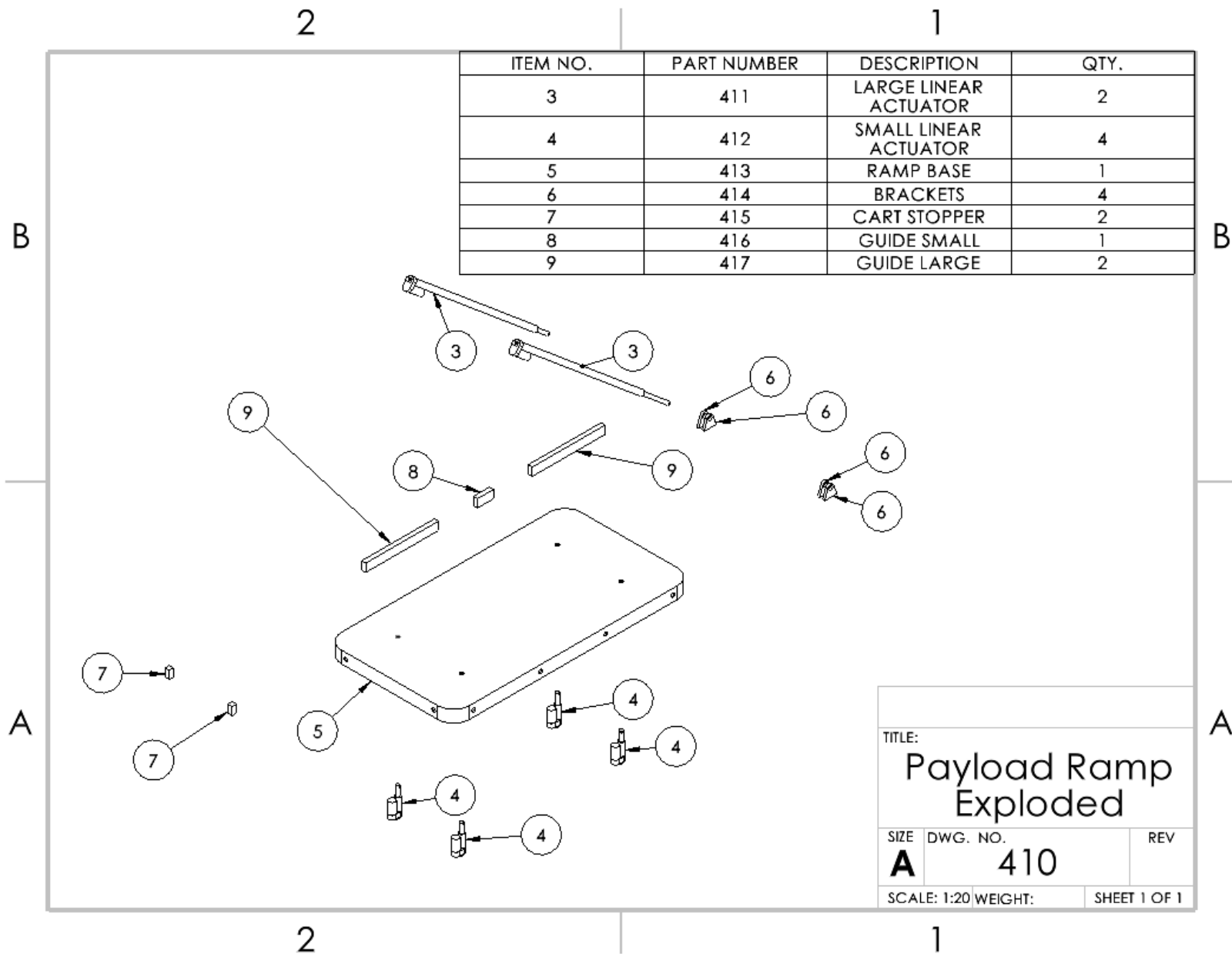




UNLESS OTHERWISE SPECIFIED:		NAME	DATE		
DIMENSIONS ARE IN METERS		DRAWN	RB	6/2/21	
TOLERANCES:		CHECKED			TITLE:
FRACTIONAL: \pm		ENG APPR.			Fuselage
ANGULAR: MATCH BEND \pm		MFG APPR.			SIZE
TWO PLACE DECIMAL: \pm		Q.A.			DWG. NO.
THREE PLACE DECIMAL: \pm		COMMENTS:			301
INTERPRET GEOMETRIC TOLERANCING PER:					REV
MATERIAL: PLA					
FINISH:					
DO NOT SCALE DRAWING					SCALE: 1:50
				WEIGHT:	SHEET 1 OF 1



UNLESS OTHERWISE SPECIFIED:		NAME	DATE			
DIMENSIONS ARE IN METERS		DRAWN		TITLE: Payload Release Mechanism Assembly		
TOLERANCES:		CHECKED				
TWO PLACE DECIMAL ±0.01		ENG APPR.				
THREE PLACE DECIMAL ±0.001		MFG APPR.				
INTERPRET GEOMETRIC TOLERANCING PER:		Q.A.		SIZE DWG. NO. REV A 400		
MATERIAL		COMMENTS:				
FINISH						
DO NOT SCALE DRAWING				SCALE: 1:20	WEIGHT:	SHEET 1 OF 1



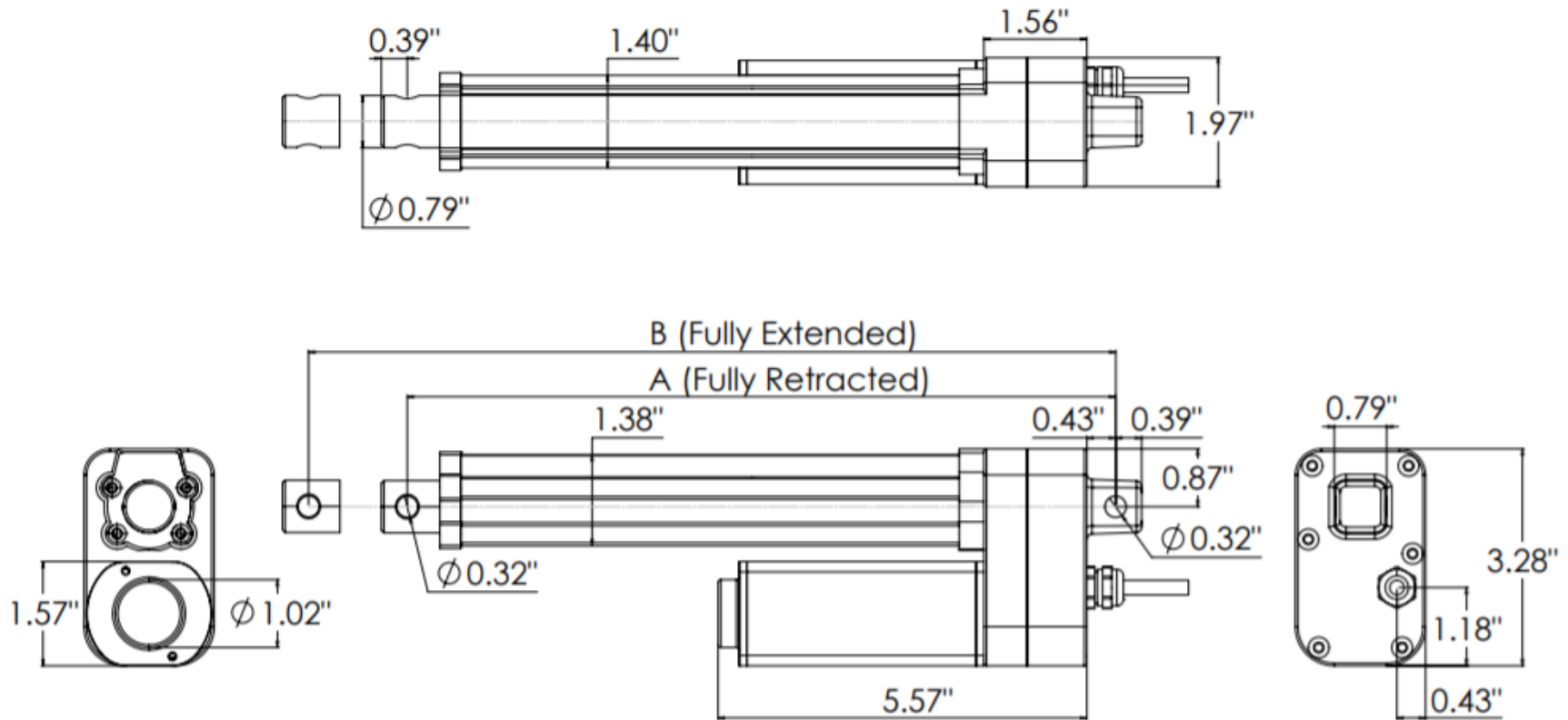
ITEM NO.	PART NUMBER	DESCRIPTION	QTY.
3	411	LARGE LINEAR ACTUATOR	2
4	412	SMALL LINEAR ACTUATOR	4
5	413	RAMP BASE	1
6	414	BRACKETS	4
7	415	CART STOPPER	2
8	416	GUIDE SMALL	1
9	417	GUIDE LARGE	2

TITLE:		
Payload Ramp Exploded		
SIZE	DWG. NO.	REV
A	410	
SCALE: 1:20 WEIGHT:		SHEET 1 OF 1



Dimensions

(Dimensions in inches)



Hole to Hole

PA-10	Stroke	1	2	4	6	8	10	12	14	16	20	22	24	30	36
	A	6.7	6.7	8.7	10.7	12.7	14.7	16.7	18.7	20.7	25.1	27.1	29.9	35.9	41.9
	B	7.7	6.7	12.7	16.7	20.7	24.7	28.7	32.7	36.7	45.1	49.1	53.9	65.9	77.9

For stroke length less than 2.0"

$$A = 6.7"$$

$$B = \text{Stroke} + 6.7"$$

For stroke length greater than 16" and less than 23.5"

$$A = \text{Stroke} + 5.1"$$

$$B = \text{Stroke} + \text{Stroke} + 5.1"$$

For stroke length 2.0" to 16"

$$A = \text{Stroke} + 4.7"$$

$$B = \text{Stroke} + \text{Stroke} + 4.7"$$

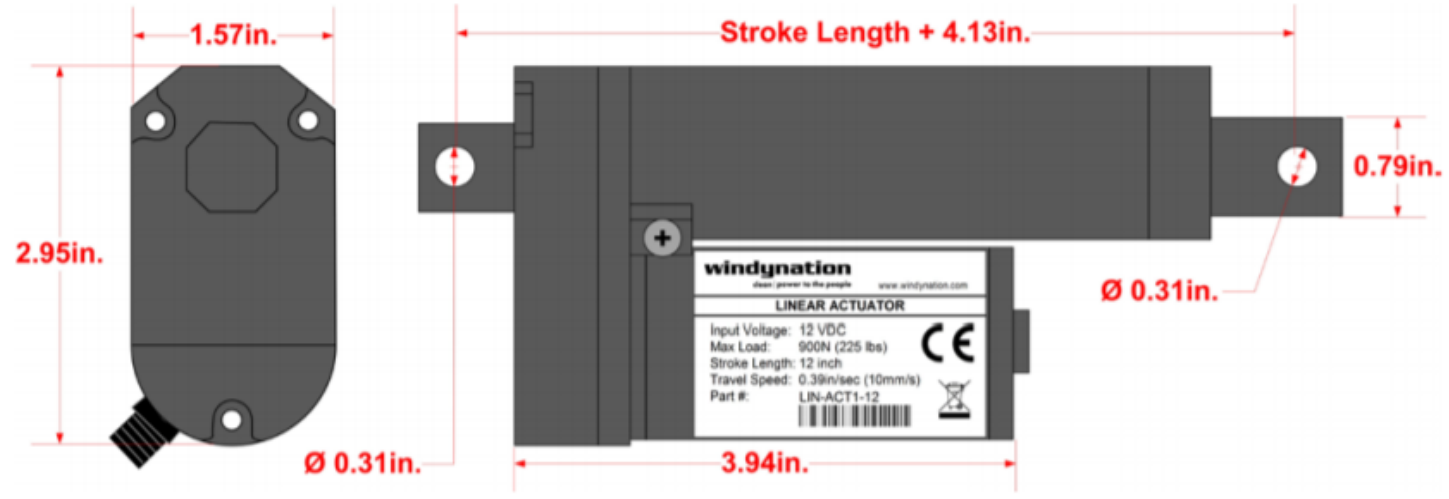
For Stroke Length 23.5" to 36.0"

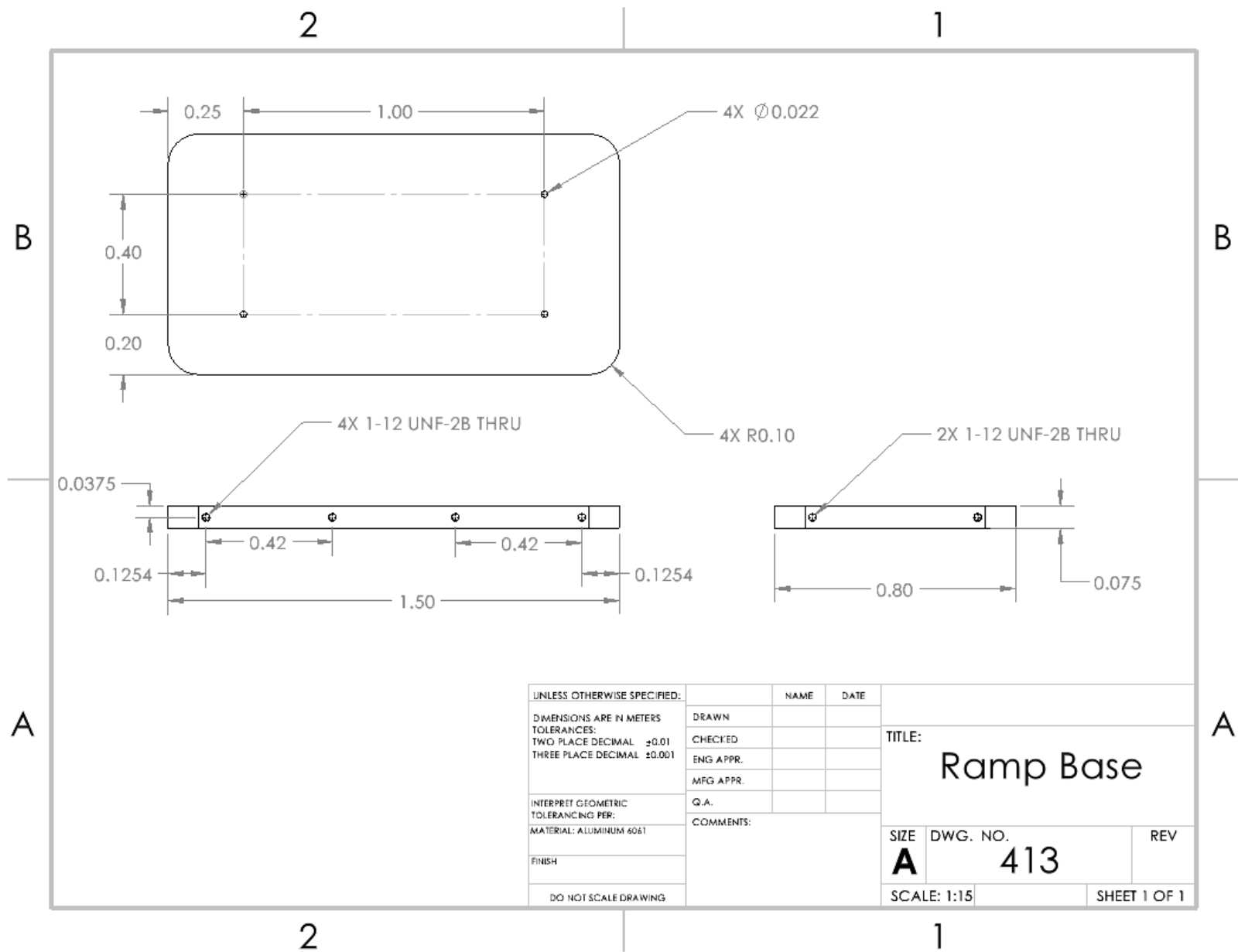
$$A = \text{Stroke} + 5.9"$$

$$B = \text{Stroke} + \text{Stroke} + 5.9"$$

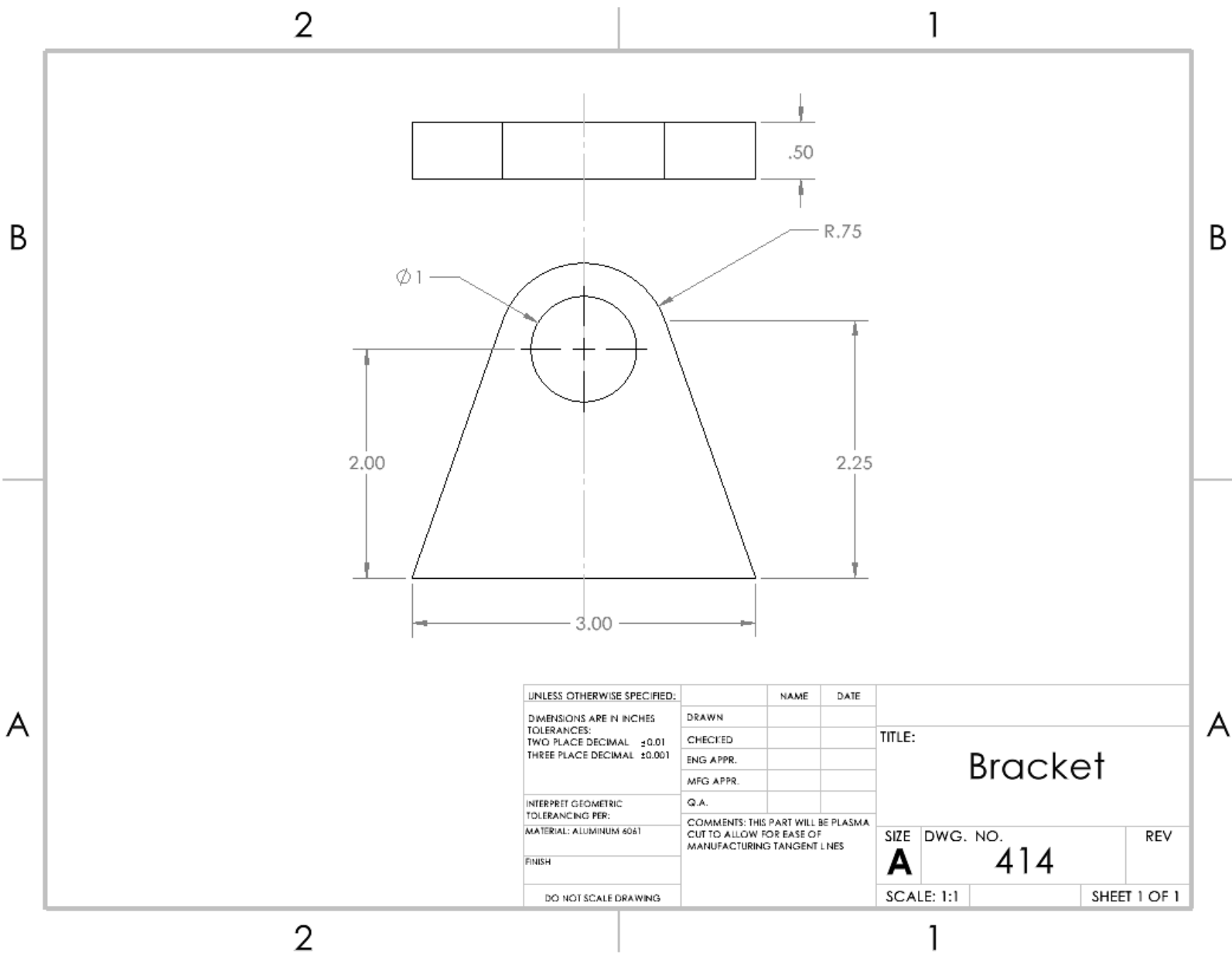
Part Number 412

SPECIFICATION	LIN-ACT1-02	LIN-ACT1-04	LIN-ACT1-06	LIN-ACT1-08	LIN-ACT1-12	LIN-ACT1-16	LIN-ACT1-20	LIN-ACT1-30
Stroke Length	2" (51mm)	4" (102mm)	6" (152mm)	8" (203mm)	12" (305mm)	16" (406mm)	20" (508mm)	30" (762mm)
Rated Load	225 lbs (900N)							
Travel Speed (Max)	0.39 in/sec (10 mm/sec)							
Rated Voltage	12 VDC							
Current Draw (Max)	≤ 2.5 A							
Install Dimension (Min)	Stroke Length + 4.33" (110mm)							
Mounting Holes	0.31" (8mm)							
Limit Switches	Fixed Inner (not adjustable)							
Operating Temp	-14.8°F to +149°F (-26°C to +65°C)							
Protection Class	IP65							
Duty Cycle	25%							
Noise Level	≤ 50dB							

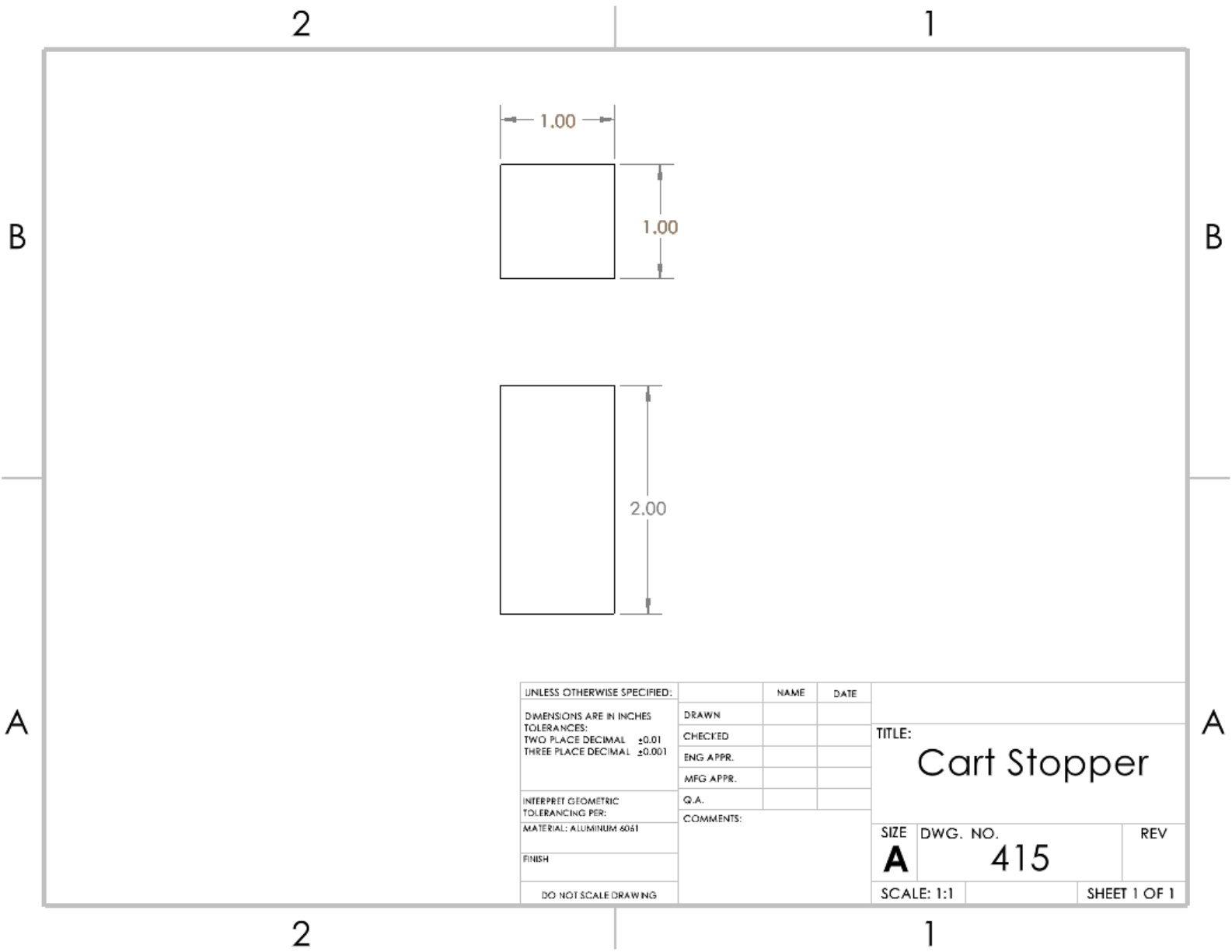




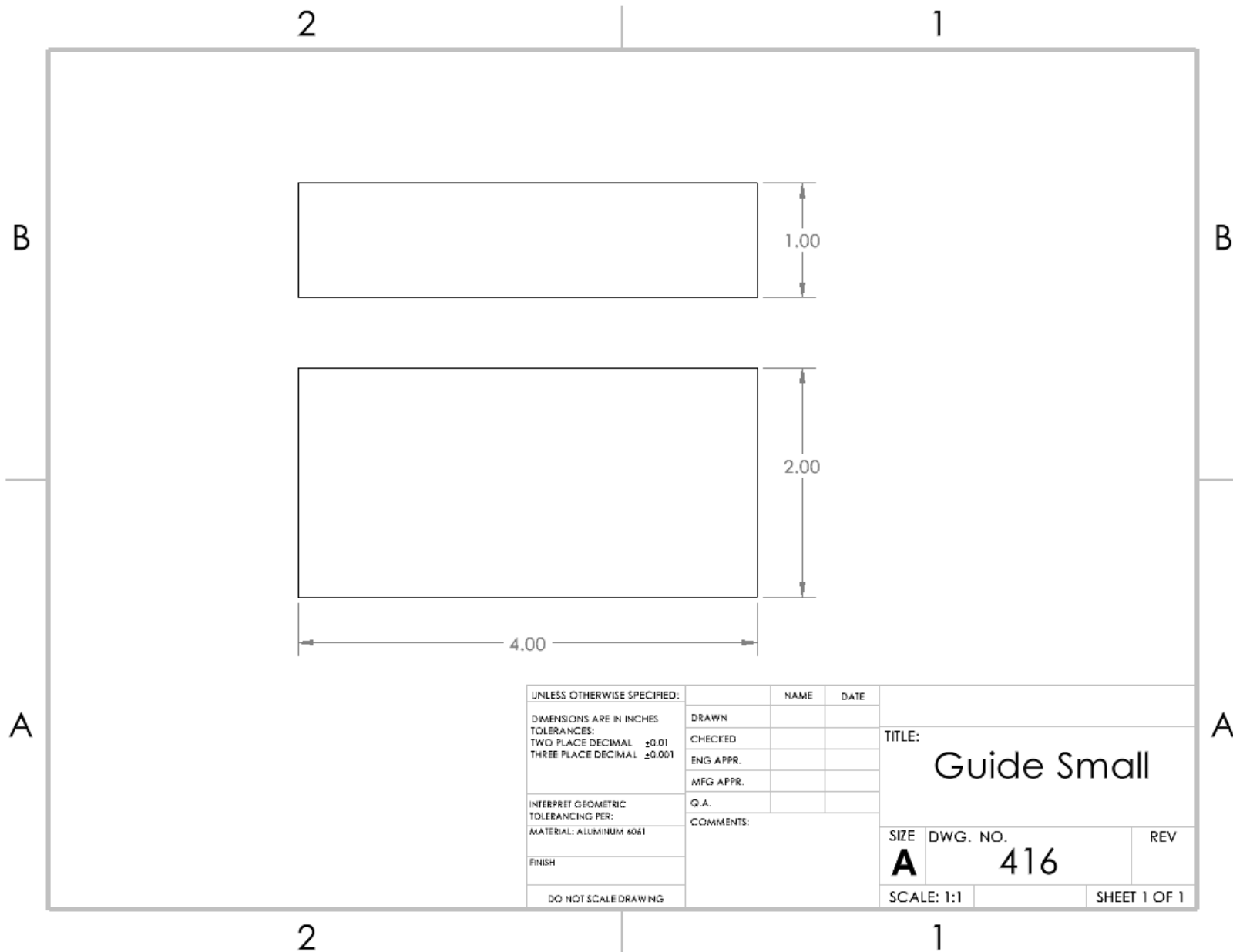
UNLESS OTHERWISE SPECIFIED:	NAME	DATE	TITLE: Ramp Base
DIMENSIONS ARE IN METERS	DRAWN		
TOLERANCES:	CHECKED		
TWO PLACE DECIMAL ± 0.01	ENG APPR.		
THREE PLACE DECIMAL ± 0.001	MFG APPR.		
INTERPRET GEOMETRIC TOLERANCING PER:	Q.A.		SIZE DWG. NO. REV
MATERIAL: ALUMINUM 6061	COMMENTS:		A 413
FINISH			SCALE: 1:15 SHEET 1 OF 1
DO NOT SCALE DRAWING			



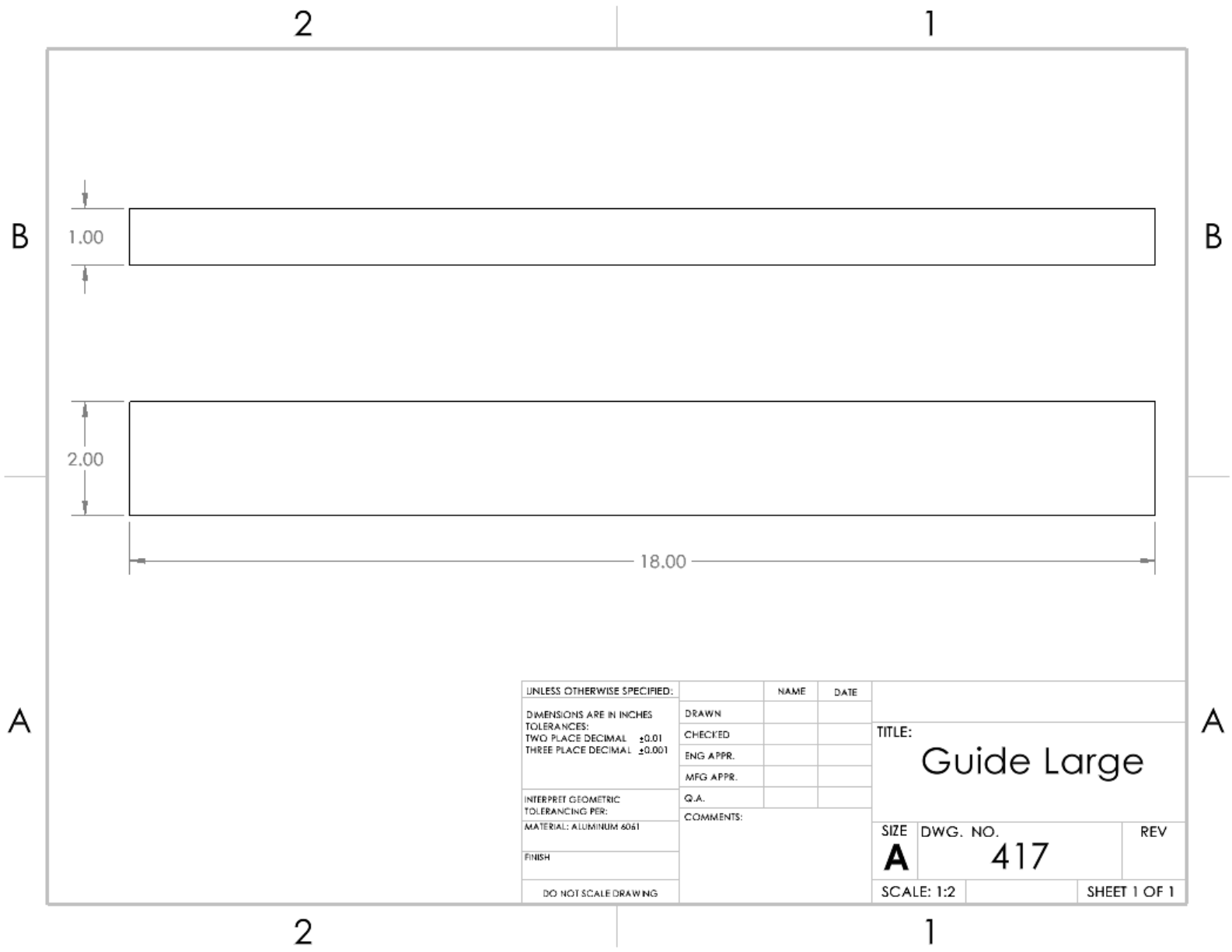
UNLESS OTHERWISE SPECIFIED:		NAME	DATE	TITLE: Bracket
DIMENSIONS ARE IN INCHES		DRAWN		
TOLERANCES:		CHECKED		
TWO PLACE DECIMAL ± 0.01		ENG APPR.		
THREE PLACE DECIMAL ± 0.001		MFG APPR.		
INTERPRET GEOMETRIC TOLERANCING PER:		Q.A.		REV
MATERIAL: ALUMINUM 6061		COMMENTS: THIS PART WILL BE PLASMA CUT TO ALLOW FOR EASE OF MANUFACTURING TANGENT LINES		
FINISH		SIZE	DWG. NO.	
DO NOT SCALE DRAWING		A	414	
		SCALE: 1:1		SHEET 1 OF 1



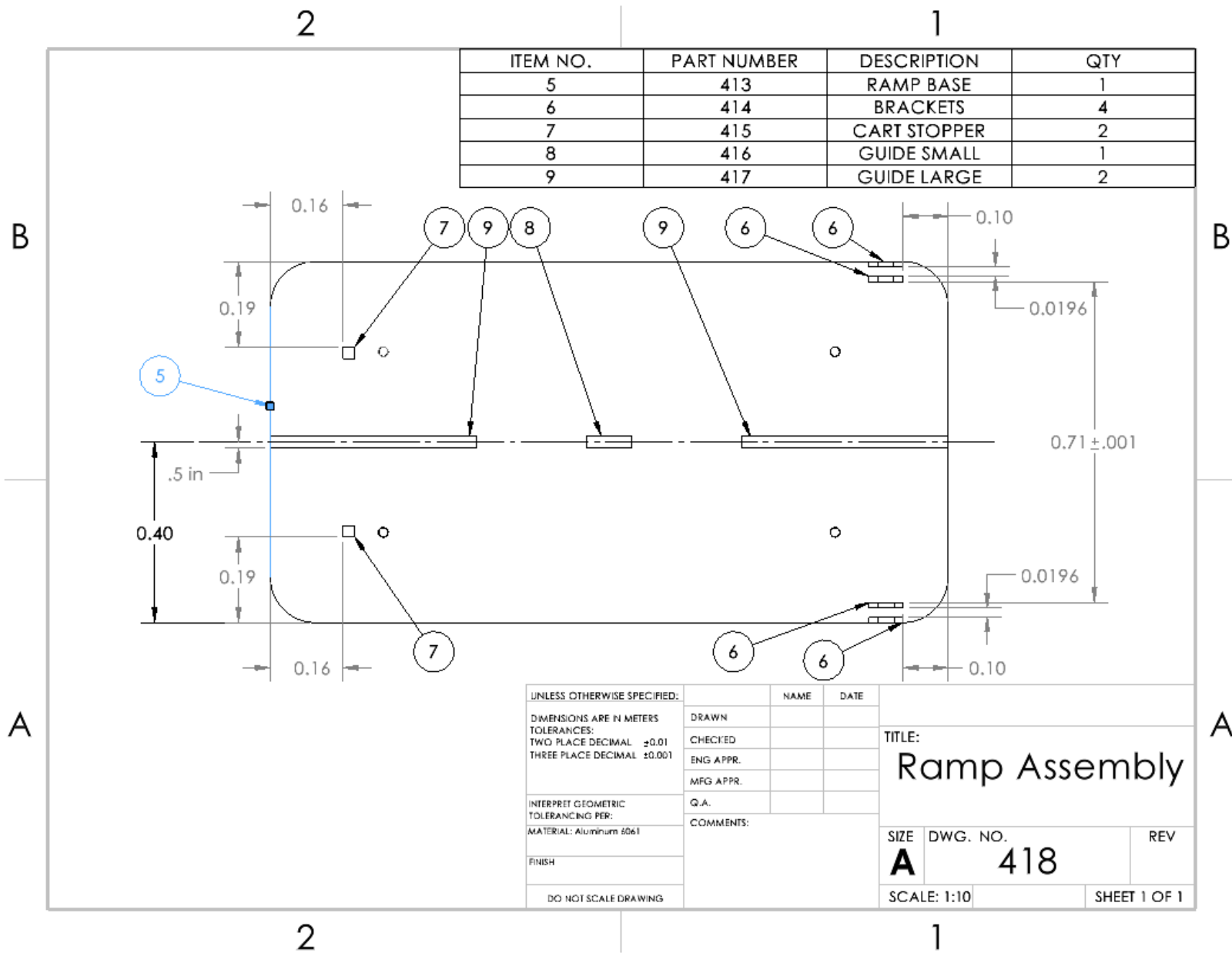
LINLESS OTHERWISE SPECIFIED:		NAME	DATE	
DIMENSIONS ARE IN INCHES	DRAWN			TITLE: Cart Stopper
TOLERANCES:	CHECKED			
TWO PLACE DECIMAL ≤ 0.01	ENG APPR.			
THREE PLACE DECIMAL ≤ 0.001	MFG APPR.			
INTERPRET GEOMETRIC TOLERANCING PER:	Q.A.			
MATERIAL: ALUMINUM 6061	COMMENTS:			
FINISH				SIZE A DWG. NO. 415 REV
DO NOT SCALE DRAWING				SCALE: 1:1 SHEET 1 OF 1



UNLESS OTHERWISE SPECIFIED:		NAME	DATE		
DIMENSIONS ARE IN INCHES	DRAWN			TITLE: Guide Small	
TOLERANCES:	CHECKED				
TWO PLACE DECIMAL ±0.01	ENG APPR.				
THREE PLACE DECIMAL ±0.001	MFG APPR.				
INTERPRET GEOMETRIC TOLERANCING PER:	Q.A.			SIZE DWG. NO. REV A 416	
MATERIAL: ALUMINUM 6061	COMMENTS:				
FINISH				SCALE: 1:1	SHEET 1 OF 1
DO NOT SCALE DRAWING					

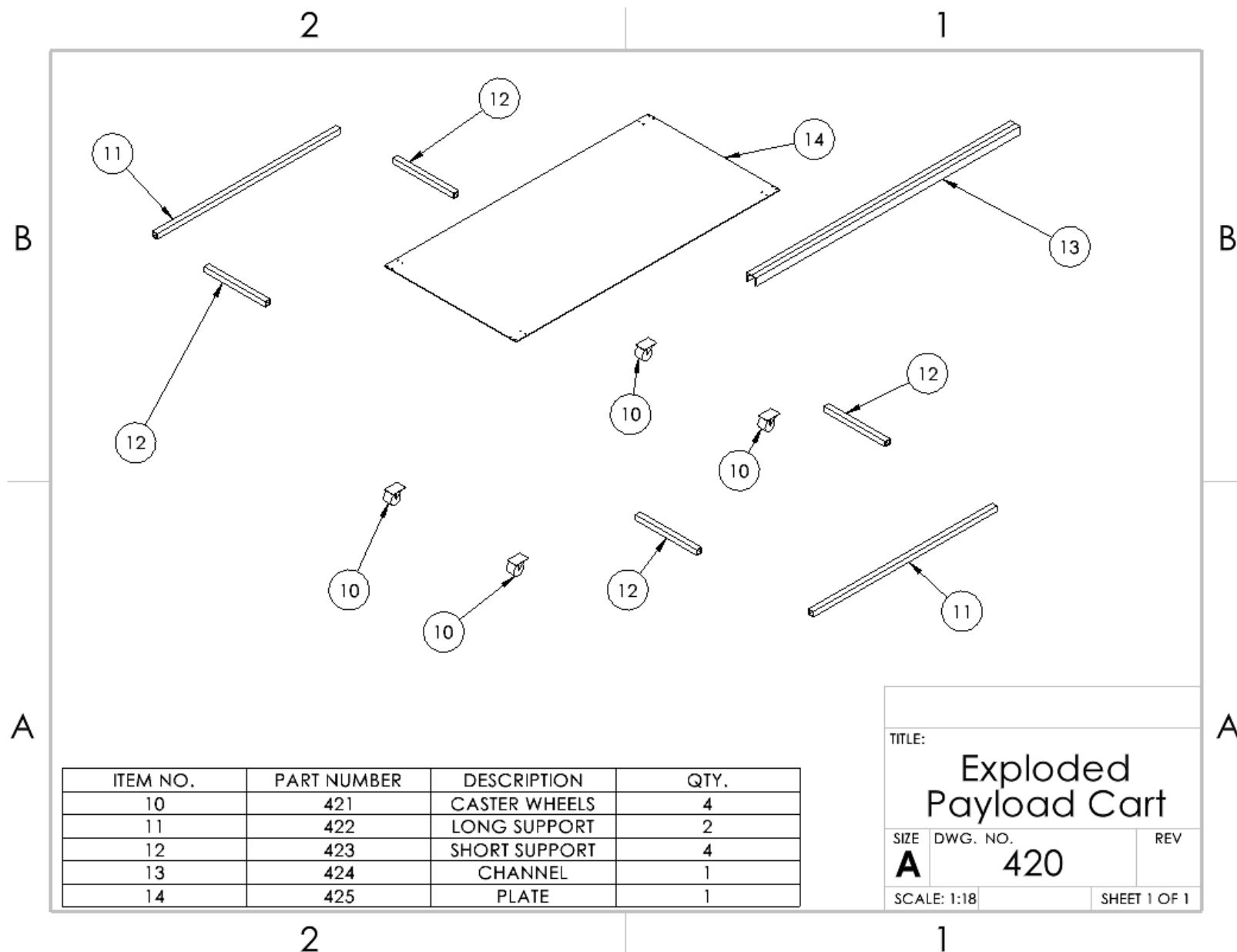


UNLESS OTHERWISE SPECIFIED:		NAME	DATE	
DIMENSIONS ARE IN INCHES	DRAWN			
TOLERANCES:	CHECKED			TITLE:
TWO PLACE DECIMAL ±0.01	ENG APPR.			Guide Large
THREE PLACE DECIMAL ±0.001	MFG APPR.			
	Q.A.			
INTERPRET GEOMETRIC TOLERANCING PER:	COMMENTS:			
MATERIAL: ALUMINUM 6061		SIZE	DWG. NO.	REV
FINISH		A	417	
DO NOT SCALE DRAWING		SCALE: 1:2		SHEET 1 OF 1



UNLESS OTHERWISE SPECIFIED:	NAME	DATE
DIMENSIONS ARE IN METERS	DRAWN	
TOLERANCES:	CHECKED	
TWO PLACE DECIMAL ±0.01	ENG APPR.	
THREE PLACE DECIMAL ±0.001	MFG APPR.	
INTERPRET GEOMETRIC TOLERANCING PER:	Q.A.	
MATERIAL: Aluminum 6061	COMMENTS:	
FINISH		
DO NOT SCALE DRAWING		

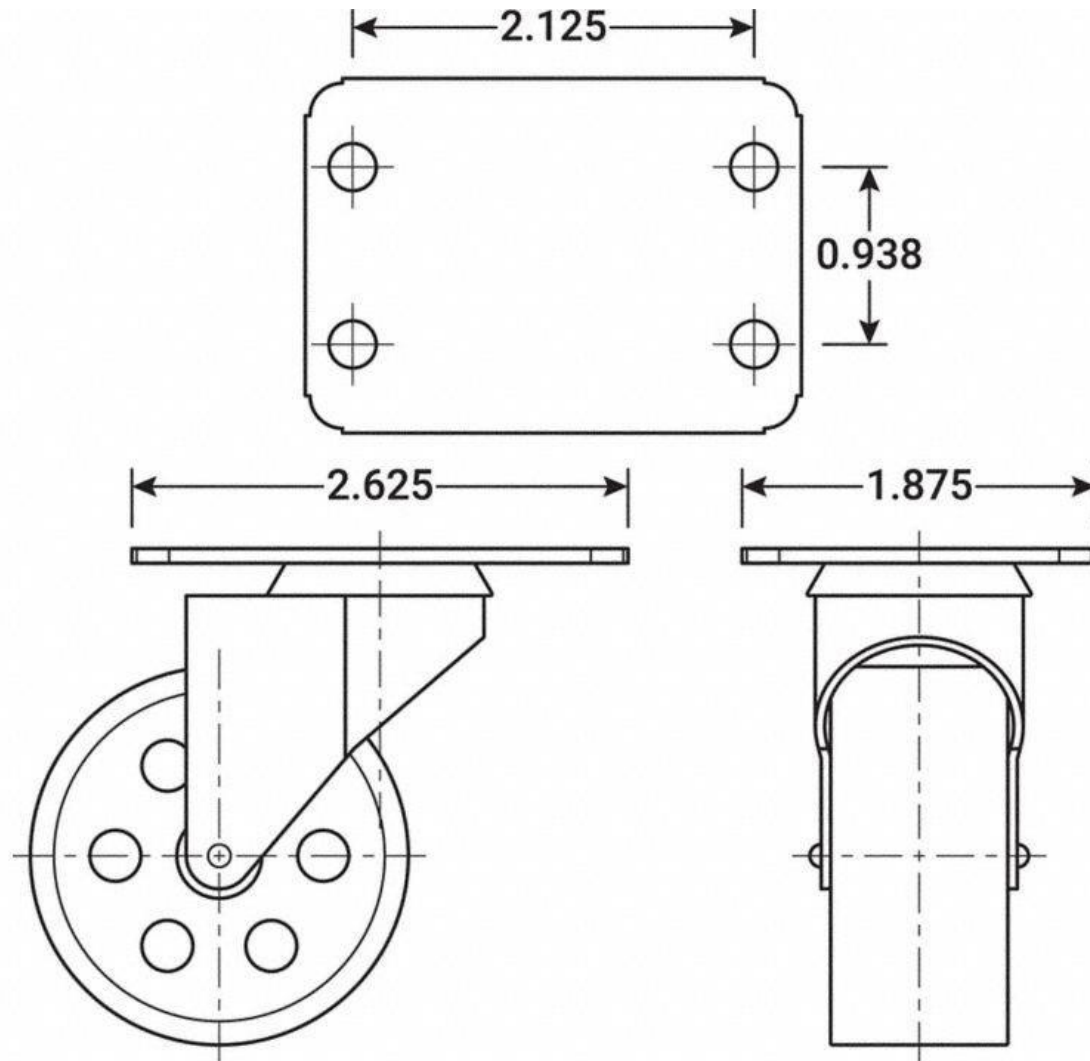
TITLE:		
Ramp Assembly		
SIZE	DWG. NO.	REV
A	418	
SCALE: 1:10		SHEET 1 OF 1



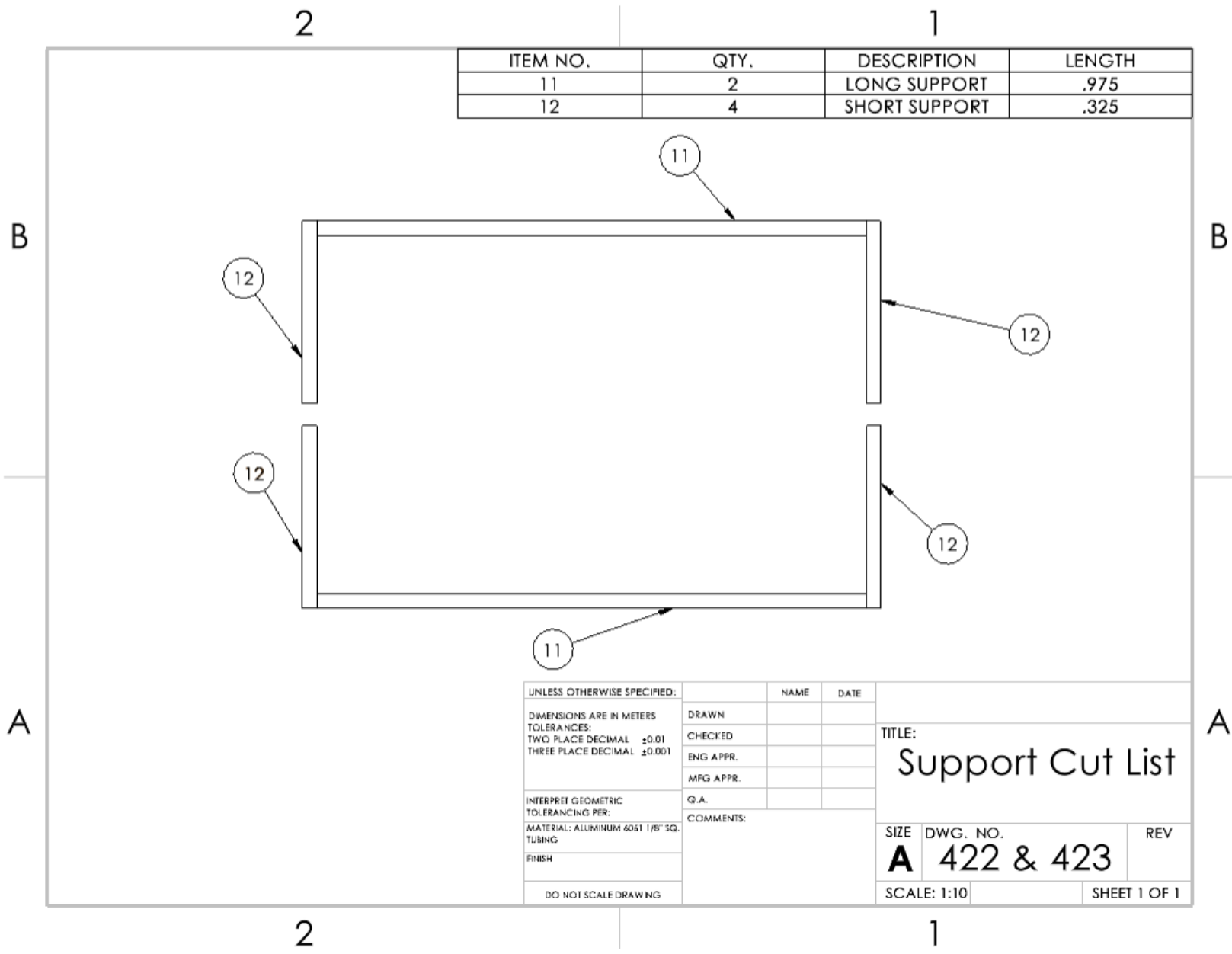
ITEM NO.	PART NUMBER	DESCRIPTION	QTY.
10	421	CASTER WHEELS	4
11	422	LONG SUPPORT	2
12	423	SHORT SUPPORT	4
13	424	CHANNEL	1
14	425	PLATE	1

TITLE:		
Exploded Payload Cart		
SIZE	DWG. NO.	REV
A	420	
SCALE: 1:18	SHEET 1 OF 1	

Part Number 421



Mounting Plate Bolt Hole Pattern D
Mounting Hole Diameter: 1/4"



ITEM NO.	QTY.	DESCRIPTION	LENGTH
11	2	LONG SUPPORT	.975
12	4	SHORT SUPPORT	.325

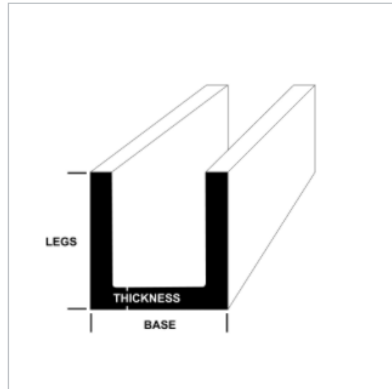
UNLESS OTHERWISE SPECIFIED:		NAME	DATE
DIMENSIONS ARE IN METERS	DRAWN		
TOLERANCES:	CHECKED		
TWO PLACE DECIMAL ±0.01	ENG APPR.		
THREE PLACE DECIMAL ±0.001	MFG APPR.		
INTERPRET GEOMETRIC TOLERANCING PER:	Q.A.		
MATERIAL: ALUMINUM 6061 1/8" SQ. TUBING	COMMENTS:		
FINISH			
DO NOT SCALE DRAWING			

TITLE:		
Support Cut List		
SIZE	DWG. NO.	REV
A	422 & 423	
SCALE: 1:10		SHEET 1 OF 1

Part Number 424

Cut to a length of 1.5m

Aluminum Architectural Channel 6063-T52 has excellent corrosion resistance, good formability, and light weight. 6063 is more easily formable and much more corrosion resistant than 6061, but it is only about half as strong. 6063-T52 is typically used in applications where corrosion resistance and aesthetic are more important than strength, such as piping, furniture, and decorative applications.



Dimension Name	Specification
Alloy	6063
Temper	t52
Production Method	extruded
Shape Type	architectural
Base	2
Legs	2
Thickness	0.125
Max Length	192
MTR Availability	Yes
Material	aluminum
Shape	channel
Custom Cut Warehouse	1

Material Specifications

This material meets the following specs:
ASTM -B221, AMS -QQ-A-200/9

Weight/Lineal Foot

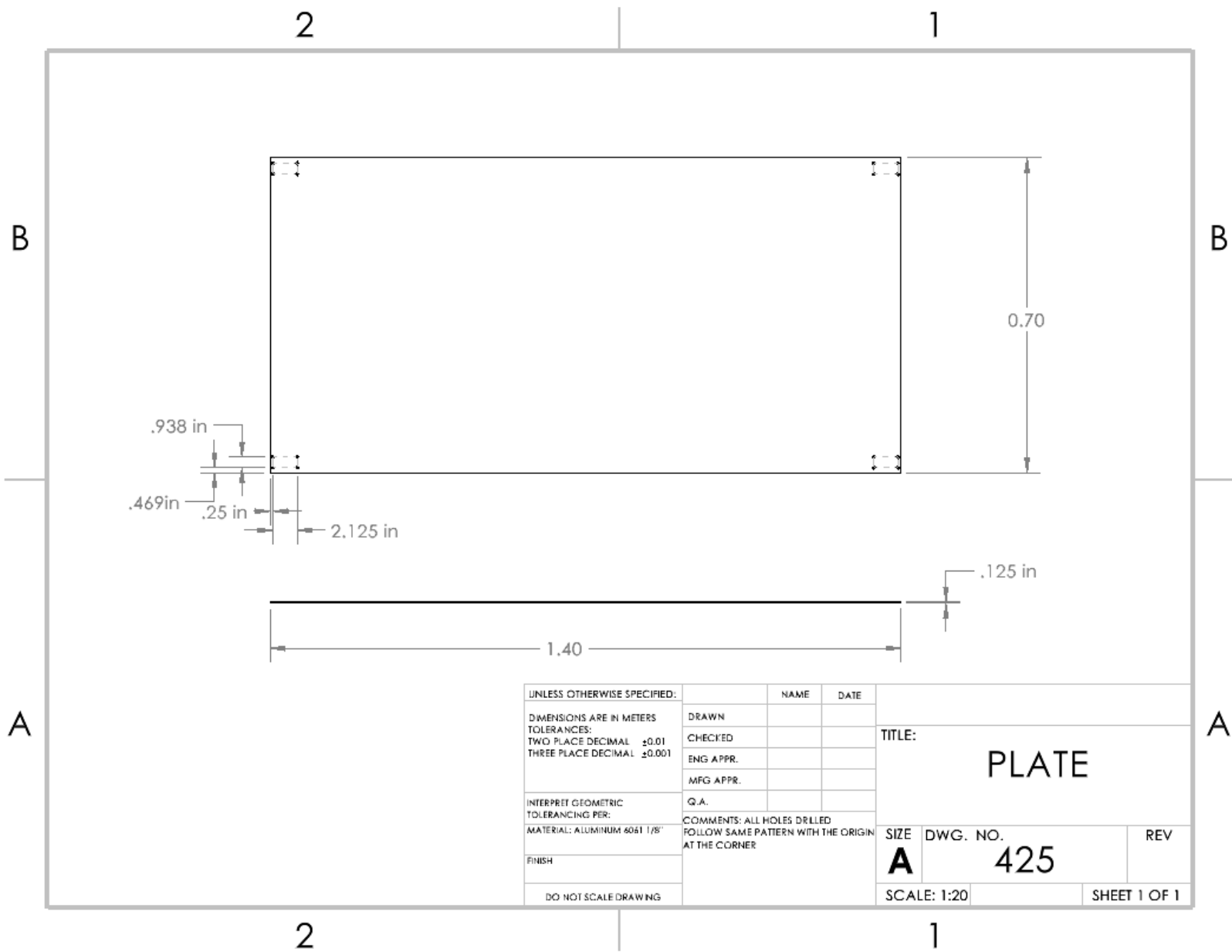
0.87 pounds

Please note that this data is to be used ONLY FOR REFERENCE, NOT FOR DESIGN, and by using it, you agree that any decisions you make regarding materials for your project are at your own discretion.

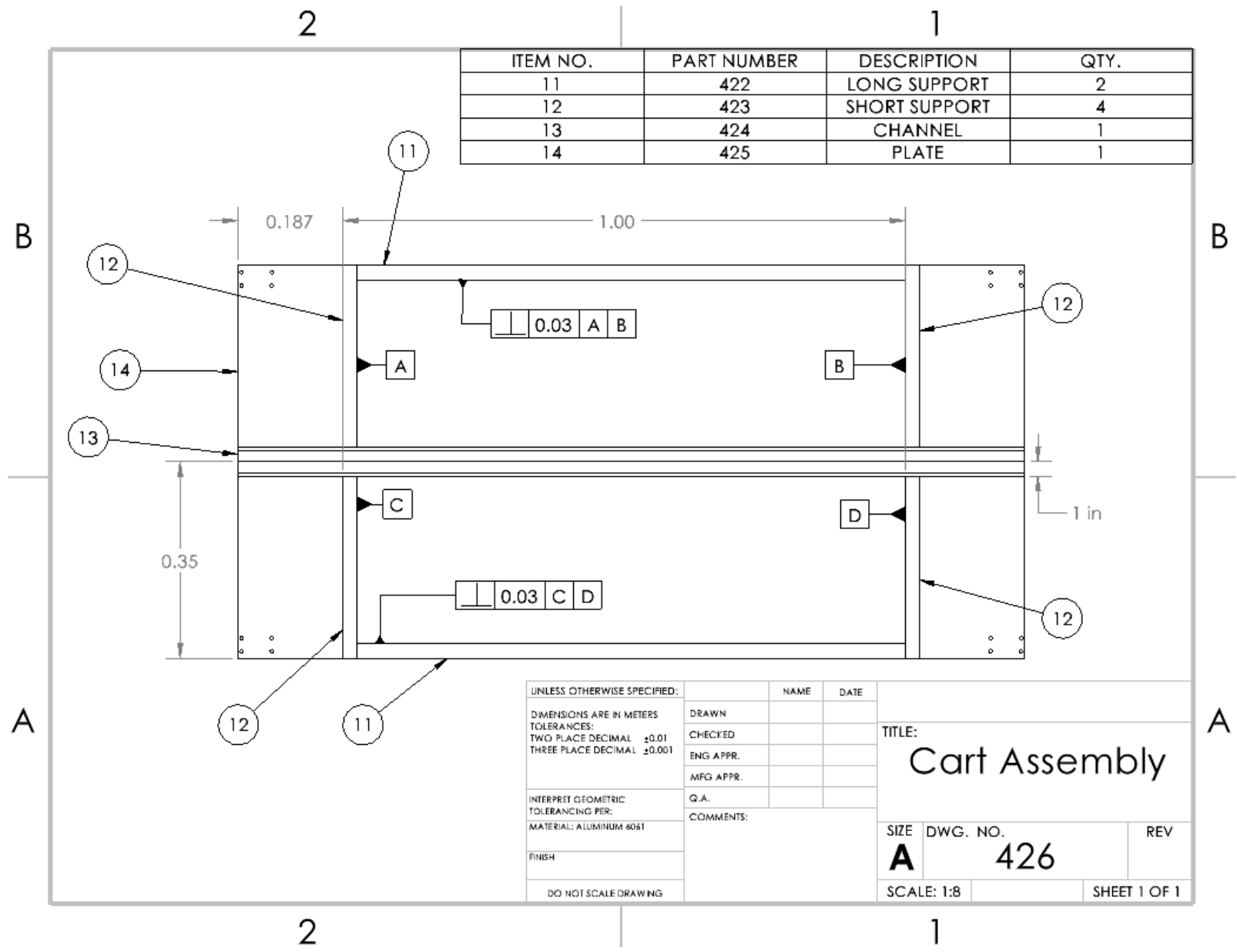
Mechanical Properties	
Property	Value
Brinell hardness	60 min
Elongation % in 2 inches	12
Endurance limit KSI	10
Modulus of Elasticity KSI x 10 ³	10
Ultimate KSI	27
Ultimate shear strength KSI	17
Yield KSI	21

Chemistry Information: 6063 Aluminum

Element	Percentage
Cu	0.1 max
Al	98.9
Cr	0.1 max
Fe	0.35 max
Mg	0.45 - 0.9
Mn	0.1 max
Si	0.2 - 0.6
Ti	0.1 max
Zn	0.1 max



UNLESS OTHERWISE SPECIFIED:		NAME	DATE		
DIMENSIONS ARE IN METERS	DRAWN			TITLE: PLATE	
TOLERANCES:	CHECKED				
TWO PLACE DECIMAL ±0.01	ENG APPR.				
THREE PLACE DECIMAL ±0.001	MFG APPR.				
INTERPRET GEOMETRIC TOLERANCING PER:	Q.A.			SIZE DWG. NO. REV A 425	
MATERIAL: ALUMINUM 6061 1/8"	COMMENTS: ALL HOLES DRILLED FOLLOW SAME PATTERN WITH THE ORIGIN AT THE CORNER				
FINISH				SCALE: 1:20 SHEET 1 OF 1	
DO NOT SCALE DRAWING					



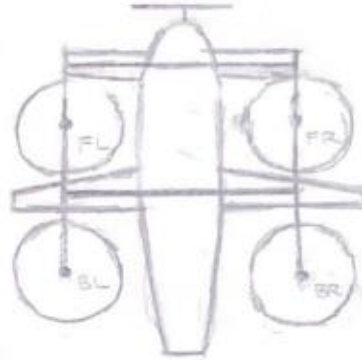
ITEM NO.	PART NUMBER	DESCRIPTION	QTY.
11	422	LONG SUPPORT	2
12	423	SHORT SUPPORT	4
13	424	CHANNEL	1
14	425	PLATE	1

UNLESS OTHERWISE SPECIFIED:		NAME	DATE
DIMENSIONS ARE IN METERS		DRAWN	
TOLERANCES:		CHECKED	
TWO PLACE DECIMAL ±0.01		ENG APPR.	
THREE PLACE DECIMAL ±0.001		MFG APPR.	
INTERPRET GEOMETRIC TOLERANCING PER:		Q.A.	
MATERIAL: ALUMINUM 6061		COMMENTS:	
FINISH			
DO NOT SCALE DRAWING			

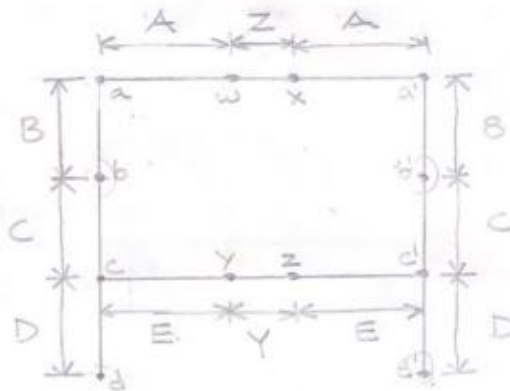
TITLE: Cart Assembly		
SIZE A	DWG. NO. 426	REV
SCALE: 1:8		SHEET 1 OF 1

Appendix I: Wing and Rotor Frame Loads

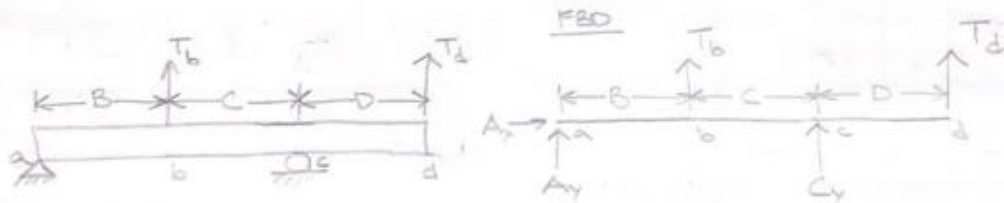
PROPULSION STRUCTURE



FRAME



BEAM a-b-c-d



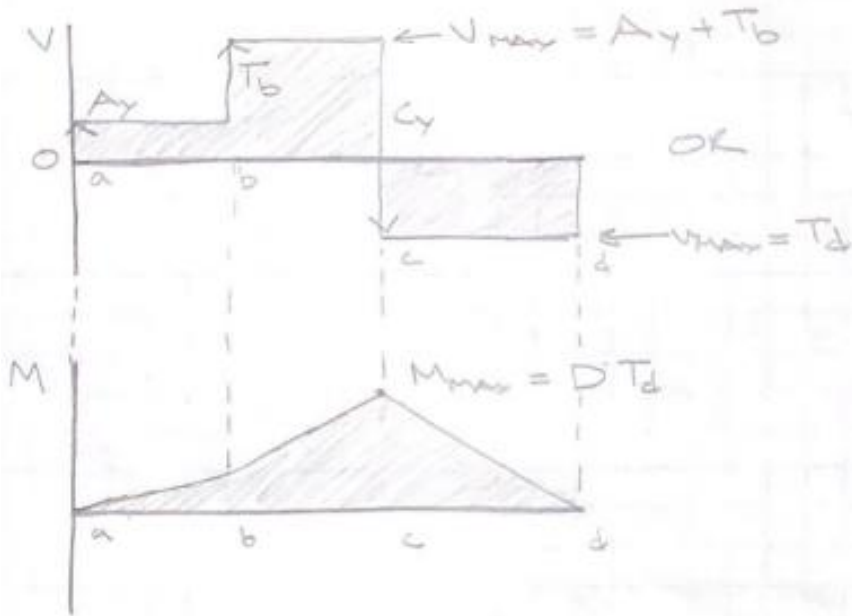
$$\sum F_y = 0: A_y + C_y + T_b + T_d = 0$$

$$\sum M_a = 0: B T_b + (B+C) C_y + (B+C+D) T_d = 0$$

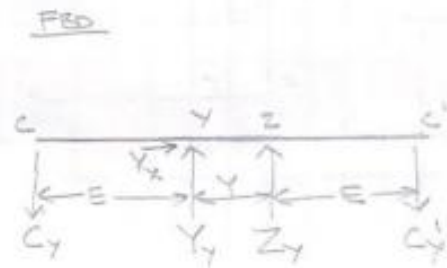
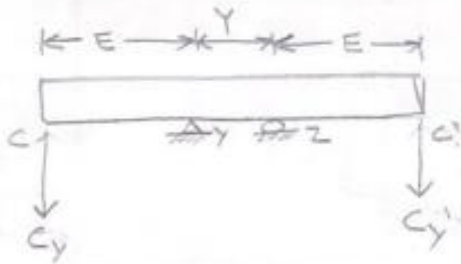
$$C_y = \frac{-(B+C+D) T_d - B T_b}{B+C}$$

$$A_y = -(T_b + T_d) + \frac{(B+C+D) T_d + B T_b}{B+C}$$

BEAM a-b-c-d: SHEAR/MOMENT



BEAM c-y-z-c'



$$\sum F_y = 0: -C_y - C_{y'} + Y + Z = 0$$

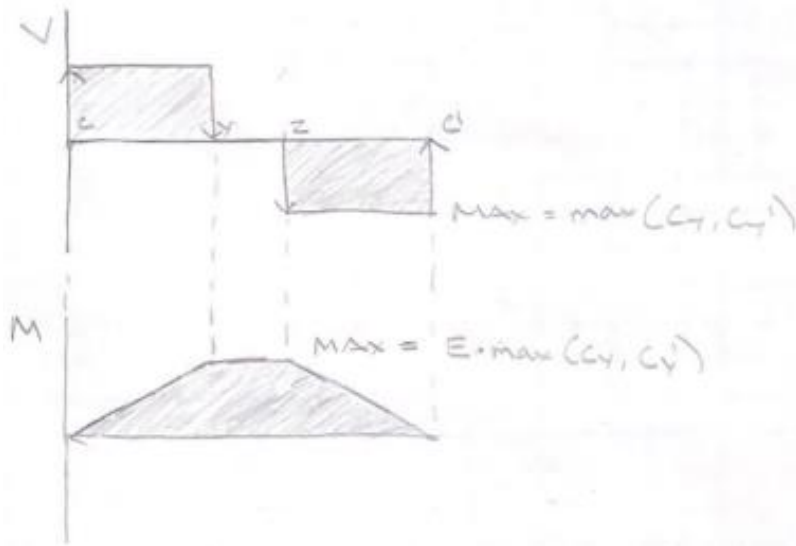
$$Y + Z = C_y + C_{y'}$$

$$\sum M_y = 0: E C_y + Y Z - (Y + E) C_{y'} = 0$$

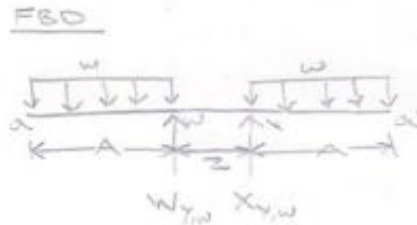
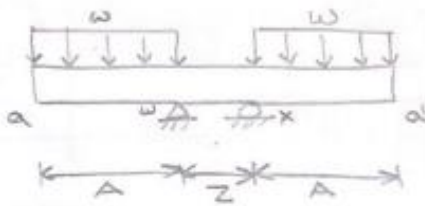
$$Z = \frac{(Y + E) C_{y'} - E C_y}{Y}$$

$$Y = C_y + C_{y'} - \frac{(Y + E) C_{y'} - E C_y}{Y}$$

BEAM C-Y-Z-C' : SHEAR/MOMENT



BEAM a-w-x-a'



$$\sum F_y = 0: W_{Y,w} + X_{Y,w} - wA - wA = 0$$

$$W_{Y,w} + X_{Y,w} = 2wA$$

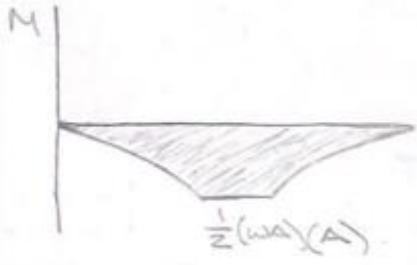
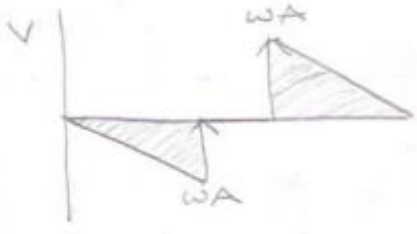
$$\sum M_o = 0: z X_{Y,w} + \frac{A}{2}(wA) - (z + \frac{A}{2})(wA) = 0$$

$$X_{Y,w} = \frac{(z + \frac{A}{2})(wA) - \frac{A}{2}(wA)}{z} = \frac{z w A + \frac{A^2}{2} w - \frac{A^2}{2} w}{z}$$

$$\boxed{X_{Y,w} = wA} \Rightarrow \boxed{Y_{Y,w} = w_c E}$$

$$\boxed{W_{Y,w} = wA} \Rightarrow \boxed{Z_{Y,w} = w_c E}$$

BEAM a-w-x-a'



Appendix J: Design Verification Plan and Test Procedure

DVPR

DVP&R - Design Verification Plan (& Report)									
Project:	F56 UAV			Sponsor:					
TEST PLAN									
Test #	Specification	Test Description	Measurements	Acceptance Criteria	Required Facilities/Equipment	Parts Needed	Responsibility	TIMING	
								Start date	Finish date
1	11 (thrust and lift analysis)	Attach rotor to motor and power motor at expected power available. Create triangle test stand. Use scale to calculate lift force in kg.	weight to convert to thrust	125kg	Machine Shops to build a test stand to hold Motor and scale	Scale, Electric Motor, Power Source for electric Motor	Brandon	April 6th, TBD	TBD
2	Power Drain	Test various power drains at varying RPMs	Power	Produce a cruve	Machine Shops to build a test stand to hold Motor and scale	Current Sensor, Voltage Sensor	Richard	April 6th, TBD	TBD

Test Procedure

Test Name: Small-Scale UAV Model Wind Tunnel Test

Purpose: Measure the drag coefficient of two small-scale UAV models when subjected to horizontal air flow at a range of air speeds. This test will attempt to simulate the drag on the full-scale UAV in forward flight and compare the drag performance of two fuselage designs.

Scope: The scope of the test is to build a general understanding of how wind tunnels are used to observe the interactions between air and flying aircraft.

Equipment:

1. Wind tunnel
2. 3D-printed scaled down UAV model
3. Test Stand
4. Load Cell

Hazards:

- Improperly attached model in wind tunnel
- Lack of structural integrity in model

PPE Requirements:

- Safety glasses
- No loose clothes or accessories
- Hair tied-up
- Sleeves rolled up
- Ear plugs
- Long pants
- Closed-toed shoes

Appendix K: Uncertainty Analysis

$$U_{C_{D0}} = \pm \left[\left(\frac{\partial C_{D0}}{\partial F} U_F \right)^2 + \left(\frac{\partial C_{D0}}{\partial \rho} U_\rho \right)^2 + \left(\frac{\partial C_{D0}}{\partial S} U_S \right)^2 + \left(\frac{\partial C_{D0}}{\partial V} U_V \right)^2 \right]^{1/2}$$

$$\frac{\partial C_{D0}}{\partial F} = \frac{1}{0.5 \rho S V^2} \quad U_F = \pm 0.5$$

$$\frac{\partial C_{D0}}{\partial \rho} = \frac{-F}{0.5 \rho^2 S V^2} \quad U_\rho = \pm 0.01$$

$$\frac{\partial C_{D0}}{\partial S} = \frac{-F}{0.5 \rho^2 S^2 V^2} \quad U_S = \pm 0.02$$

$$\frac{\partial C_{D0}}{\partial V} = \frac{-F}{0.25 \rho S V^3} \quad U_V = \pm 0.1$$

$$\frac{\partial C_{D0}}{\partial F} \cdot U_F = \frac{0.5}{0.5 (0.0715) \left(\frac{1}{32.2} \right) (32.8^2)} = 0.39$$

$$\frac{\partial C_{D0}}{\partial \rho} \cdot U_\rho = \frac{-0.01 (4.09)}{0.5 (0.0715^2) \left(\frac{1}{32.2} \right) (32.8^2)} = 0.418$$

$$\frac{\partial C_{D0}}{\partial S} \cdot U_S = \frac{-0.02 (4.09)}{0.5 (0.0715) \left(\frac{1^2}{32.2} \right) (32.8)^2} = 0.064$$

$$\frac{\partial C_{D0}}{\partial V} \cdot U_V = \frac{-0.1 (4.09)}{0.25 (0.0715) \left(\frac{1}{32.2} \right) (32.8)^3} = 0.0195$$

$$U_{C_{D0}} = \pm \sqrt{(0.39)^2 + (0.418)^2 + (0.064)^2 + (0.0195)^2} = \boxed{0.58}$$